Desulphurization and Deoxidation in a 300 ton Ladle

A Thesis Submitted

In Partial Fulfillment of the Requirements

for the Degree of

Master of Technology

By

Arghya Dey

Roll No: Y220602

Under The Guidance of Dr. Brahma Deo

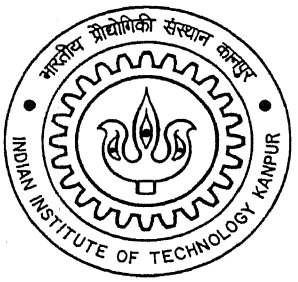

Department of Materials and Metallurgical Engineering

Indian Institute of Technology, Kanpur

December 2004

CERTIFICATE

This is to certify that the work contained in the thesis entitled **"Desulphurization and Deoxidation in a 300 ton Ladle"** *by* **Arghya Dey (Roll No. Y220602)** *has been carried out under my supervision and to the best of my knowledge this work has not been submitted elsewhere for a degree.*

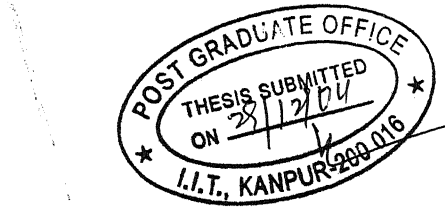

Dr. Brahma Deo

Professor

Department of Materials & Metallurgical Engineering

December, 2004

Indian Institute of Technology, Kanpur, India

ACKNOWLEDGMENT

I would like to express my heartfelt thanks and gratitude to my thesis supervisor Prof. Brahma Deo for his expert guidance, support and encouragement throughout my post graduate study at IIT Kanpur.

I am thankful to Dr. Mats Söder, Scientist, Royal Institute of Technology, Sweden, for allowing me to consult his thesis related to inclusion formation and floatation.

My time in the process control lab was enriched by the interaction with my fellow students. I specially wish to thank Ashish, Satish, Pramod and Ajay Shukla.

I must acknowledge the support provided by my loving parents and my wife Gouri. I could not have come so far without their unconditional love and care.

Last but not the least, I express my gratitude to all the staff of Materials and Metallurgical Engineering department, who helped me on many occasions.

December, 2004 Arghya Dey

IIT, Kanpur

ABSTRACT

Process control models can be developed by using both conventional and AI approaches. The conventional approaches include regression models and process kinetic models. The artificial intelligence (AI) approaches are based on artificial neural nets (ANN), genetic algorithm (GA) and fuzzy rule based expert systems (FRBES). Plant data on hot metal desulphurization, carried out by injecting calcium carbide in 400 ton torpedo ladles, is analyzed to test and tune different types and combinations of models and then evaluate their relative performance. While the control models based on process fundamentals provide a fillip to the new ideas for technological developments and improvements, the combination of conventional and AI approaches may be a better option for process control on the shop floor. It is advisable to first develop and test all models and then decide about the best strategy of using them.

The phenomenon of nitrogen and oxygen pickup by the liquid steel from the atmosphere, during tapping into a ladle, is described first. The results of the absorption model are fed into the model for inclusion control. The kinetic model for inclusion control (prediction of inclusion size, size distribution and amount) is based on mixed mass transfer of dissolved aluminum and dissolved oxygen in the bath, collision mechanisms (Brownian motion, Stoke's collision, and turbulent collision), and simultaneous assimilation of inclusions by the top slag. The model also predicts the amount of aluminum needed to achieve a desired level of dissolved oxygen in the final steel. In the user-friendly model developed in this work, an output window has been created to view all the predictions in the form of graphic displays. Computation time has been optimized by applying genetic algorithm.

The model has been tested for the case of 300 ton ladles at Bokaro Steel Plant. The SEM observation of the inclusions in the samples collected at Bokaro Steel Plant show that most inclusions, in absence of bottom stirring of ladle are of size 15 microns or smaller. Model predictions agree well with this result. Further, according to the models developed in this work, only a maximum of 8% of the inclusions may get removed during a holding/transfer time of 45 minutes. Gas stirring in the ladle at the rate of 2 liters/ton/min, soon after tapping, would greatly help in the floatation of inclusions by more than 50% during the time of transfer to ladle treatment station.

LIST OF FIGURES

LIST OF TABLES

LIST OF SYMBOLS

a_o, a	Radius of stream at the tap hole exit and at the distance Z from the tap hole exit
A_f	Area of slag metal interface
A_h	Area of the stream of liquid metal at a small length Δh at height h
Al_i	Initial Al addition into the bath
A_S	Area of slag metal interface
C(i,m)	Number of collisions per unit volume per unit time between inclusions with radius r_i and r_m
d_b	Average bubble diameter
d_k	Average diameter of the entrained bubbles
d_n	Diameter of the tap hole
d_p	Average particle diameter
E_{gr}	Collision efficiency due to a velocity gradient in liquid steel
E_{Stk}	Collision efficiency due to Stokesian rise
f	Fraction of particles entrapped in the bubbles
F_l	Area of the Gas-metal interface
Fr	Froude number
g	Acceleration due to gravity
G	Average velocity gradient
Ga, Gp	Average velocity gradient in axial and peripheral region
G_T	Total gas volume entrained

h	Distance from the surface of liquid steel in the converter to the inlet of tap hole
h_i	Depth of injection of CAD
H	Height of the converter
I_R	Rate of injection of the desulfurizing agent
k	Boltzmann constant
k_{Al}	Average diffusivity of [Al] in molten steel
k_b	Sulfur partition coefficient between bubble
k_f	Sulfur transfer coefficient through the metal slag
kg	Mass transfer coefficient in gas phase
ko	Average diffusivity of [O] in molten steel
k_p	Sulfur transfer coefficient at particle melt boundary layer
k_s	Constant in Stokes' equation
l	Distance in the longitudinal direction from the bottom of the converter
l_o	Length of the tap hole
L_g^p	Sulfur partition coefficient between particles and melt respectively
L_s^g	Sulfur partition coefficient between particles entrapped in the bubble and melt
L_s^{ts}	Sulfur partition coefficient between top slag and melt
M_{CaC2}	Molecular mass of CaC_2
M_L	Weight of metal
M_s	Molecular mass of sulfur
$M_{ts(t=0)}$	Mass of carry over slag
L	Height of ladle
L_H	Height of the metal bath in ladle

m	Mass of the protuberant portion of the stream
$m^{/}$	Mass of liquid steel displaced by an inclusion
m_i	Mass of inclusion formed in steel
m_N	Mass transfer coefficient of nitrogen in the liquid phase
m_O	Mass transfer coefficient of oxygen in the liquid phase
No	Initial no of particle
$[\%N_2^{air}]$	Nitrogen present in the air by mass percent
$\dot{N}_{0_2}, \dot{N}_{N_2}$	Rates of mass transfer in the liquid phase and the chemical reaction at the interface, respectively
$N(r_m)$	Number of inclusions with radius r_m per unit volume of liquid steel
$\Delta[\bar{N}]_{TS}, \Delta[\bar{N}]_{bbl}$	Average nitrogen absorbed from the entrained gas bubbles and through the surface of the tapping stream
$[O]^b, [O]^i$	Oxygen content in bulk of liquid steel in falling stream and at the metal-atmosphere interface, respectively
$[O]_i$	Initial Oxygen level
$[\%O_2^{air}]$	Oxygen present in the air by mass percent
$\Delta[\bar{O}]_{TS}, \Delta[\bar{O}]_{bbl}$	Average oxygen absorbed from the entrained gas bubbles and through the surface of the tapping stream
P_o	Average pressure in side the bubble
P_{02}, P_{02}^i	Oxygen partial pressure and its value at the interface
P_r	Average reference pressure
p(i,m)	Frequency of collisions per unit time of an inclusion with radius r_i with inclusion r_m
$\Delta p/L$	Pressure gradient

r	Radius of an inclusion r
r_i	Radius of i^{th} inclusion
r_{max}	Radius of the largest inclusion in steel
R	Universal gas constant
R_C	Radius of the cavity
Re	Reynolds number
R_L	Radius of the ladle
Q	Gas flow rate
[%S]	Instantaneous concentration of sulfur in the metal bulk
S_f	Final Sulphur content
$[\%S]_i$	Instantaneous concentration of sulfur at top slag- metal interface (metal side)
$[\%S]_o$, S_i	Initial sulfur concentration in the melt
Stk	Stokes number = $\frac{\rho_s.\mathrm{Re}}{9.\rho}$
t	Total time of a process
trp, τ	Particle residence time
trb	Bubble residence time
T	Temperature of the liquid steel
u_r, u_z	Velocity of an inclusion in r and z direction
U_o, U	Flow velocity at the tap hole exit and its value at the distance Z from the tap hole exit
v_r, v_z	Average fluid velocities in r, z directions
V	Volume of an inclusion
V_{cr}	Volume of the ladle

V_{gr}	Collision volume per unit time for an inclusion with radius r_i and r_m under a velocity gradient
V_g^o, V_g	Rates of the gas entrainment of the vertical stream and of the tilting stream, respectively
V_h	Volume of the stream of liquid metal at a small length Δh, at a height h
V_l	Rate of tapping
V_m	Volume of metal
ρ_L	Specific weight of melt
ρ_p	Specific weight of particle
We	Weber number
W_i	Initial mass of the liquid steel in the converter
W_L	Mass of the liquid steel in the ladle at time t
W_m	Weight of the liquid steel in the converter at time t
Z_t, Z_f	Tapping height and it's final value
Z_F	The distance between top of the ladle and bottom of converter
Z_L	The height of metal pool in the ladle
α	Collision efficiency
θ, θ'	the angle of BOF with the horizontal axis and incident angle of the tapping stream to the liquid steel pool in the ladle, degrees
μ	Viscosity of steel
μ_{Fe}	Average viscosity of iron
η_{Al}	Aluminum recovery
$\eta_{O_2}^b$, $\eta_{N_2}^b$	Absorption efficiency at the bubble-liquid interface of oxygen and nitrogen respectively

$\varepsilon, \varepsilon_o$	Amplitude of disturbance present on surface of stream at a distance Z and at the tap hole exit, respectively
ε_e	Energy dissipated per unit time per unit mass
λ	Wave length of the ripples at the surface of liquid steel
ρ, ρ_{Fe}	Density of liquid steel
ρ_L	Specific weight of melt
ρ_p	Specific weight of particle
ρ_s	Density of liquid steel and inclusion, respectively
ν	Kinematic viscosity of steel
σ_{s-a}	Surface tension at air and liquid steel interface
σ_{s-i}	Surface tension at steel and inclusion interface

TABLE OF CONTENTS

kinetics. The present work focuses on comparing the efficacy of different control models that can be developed for a given plant situation and the strategy that should be adopted in a plant environment.

We shall first describe, briefly, various models, namely an empirical (regression) model (section 2.1.1), a simple kinetic model based on second order chemical reaction control (section 2.1.2), a sophisticated kinetic model based on the assumption of mass transfer (first order) control (section 2.1.3), ANN models (section 2.1.4), fuzzy rule based expert systems (FRBES) model (section 2.1.5), and GA optimized model (section 2.1.6) to control/predict desulphurization of hot metal. Then we shall compare their efficacy in terms of the success to predict the final sulphur content of the hot metal. For the sake of a just comparison, the same set of data (section 2.2) is used to validate different models because the main point here is the importance of comparative performance of the models for a given plant situation.

The liquid steel, at the end of heat in a basic oxygen furnace (BOF), may contain 400-900 ppm dissolved oxygen, 2-4 ppm dissolved hydrogen, 40-60 ppm dissolved nitrogen, and the temperature of metal varies in the range 1873-1973K. During tapping from BOF, the falling stream of liquid metal as well as the turbulent surface of liquid steel in the ladle promotes absorption of additional oxygen, hydrogen and nitrogen from the ambient atmosphere into the melt. After the tapping operation is over, deoxidizers like coke, Fe-Si, Fe-Mn, Al may be added during the tapping operation and at the steel refining unit (SRU). For example, the steel may be subjected to argon stirring at argon rinsing station (ARS), or steel may be reheated to a desired temperature in the ladle furnace (LF) and thereafter subjected to further deoxidation treatment by aluminum and calcium. During the time of tapping and the time of transfer of ladle to SRU, the deoxidation reactions, growth of deoxidation products in

size due to mass transfer and collisions, and assimilation of deoxidation products into top slag take place continuously. The liquid steel in the BOF, during tapping and transfer to SRU, continuously looses heat by radiation and convection. The slag lying on top of metal can react with metal and with the lining of the ladle. For a better process control, it is necessary to understand the thermodynamics and kinetics occurring at various stages of steel processing.

The product of deoxidation by aluminum, when aluminum is added to liquid steel during the tapping operation, is solid alumina. The presence of solid alumina in liquid steel above a certain level is undesirable, because alumina can clog the nozzle in tundish. Retention of solid alumina, as inclusions in the solidified product, is also harmful because it decreases cleanliness of the steel and affects the final mechanical properties of the product. It is necessary to control both the amount of size range of inclusions in liquid steel. During their residence time in liquid, the oxides in solid or liquid state, can grow in size by several mechanisms [2.13-2.16], such as growth by mass transfer, Oswald ripening, and collision. The bigger inclusions (10-100 microns) can float up whilst the smaller inclusions (<10 microns) may get recirculated with the convection streams present in the liquid metal. As a thumb rule, the inclusions of size greater than 50 microns should be completely avoided in flat products because they act as the sites for crack initiation. In thin sheets, as a precautionary measure, the total amount of inclusions should be less than 30 ppm.

The present study focuses on killed steels made in 300 ton BOFs at Bokaro steel plant. In the operating practice followed at Bokaro Steel Plant, the liquid steel is deoxidized in the ladle during tapping by adding deoxidizers such as carbon in the form of coke, ferro-silicon, ferro-manganese and aluminum. The amount of deoxidizer(s) to be added is decided by the aim dissolved oxygen content of liquid

steel after tapping from BOF. Coke is added in the very initial stages of tapping so as to remove part of the dissolved oxygen as CO gas. While the CO gas escapes from liquid metal almost instantaneously, the oxide products (SiO_2, MnO, Al_2O_3) may take finite time to float up. Chapter 3 describes the absorption of nitrogen and oxygen gases during tapping, and thermodynamic aspects of deoxidation by aluminum are discussed first, followed by the kinetic model of growth of alumina inclusions.

It is reported in literature that the growth of inclusions may take place by several mechanisms like mass transfer, Brownian motion, turbulent collision and Stokes collision. In this work, different models of inclusion growth have been developed and subjected to sensitivity analysis. A model, with a user friendly interface, is presented for the situation at Bokaro Steel Plant with the help of which it is possible to predict:

- Pickup of nitrogen and oxygen from ambient atmosphere during the tapping operation (section 3.5.1),
- Initial amount of deoxidant to be added for a given composition and temperature of steel (section 3.5.2),
- Size distribution and amount of inclusion present in liquid steel as a function of time (section 3.5.4 and 3.5.5).

Chapter - 2

2. Strategies for Development of Process Control Models for Hot Metal Desulphurization: Conventional and AI techniques

2.1 Different models for prediction of final sulphur content of the bath

There have been several studies[2.1-2.21] in the last decade to develop control/prediction models for hot metal desulphurization on the basis of metallurgical kinetics [2.1-2.9], statistics (regression models) [2.7], artificial neural nets (ANN) [2.10], genetic algorithms (GA)[2.11], and fuzzy rule based expert systems (FRBES) [2.7]. The set of computational techniques comprising of ANN, GA and fuzzy logic (including their combinations like Fuzzy-GA, GA-ANN, Fuzzy-ANN, etc.) are now known as 'soft computing techniques'. The different models are described below

2.1.1 Statistical analysis of data and development of regression models

The first step in model development should be to study the mean, variance, normal distribution, variance-covariance and correlation matrices, eigen values and eigen vectors followed by principal components analysis so as to decide the possibility of dimensionality reduction and check the presence of clusters in the data. Each column of data (for 229 heats, typical data set given in Table 2.1) was checked for normal

distribution. By observing the magnitude of the off-diagonal correlations in the correlation matrix (given below) it was concluded that the variables (1) treatment time, (2) mass of hot metal, (3) initial sulphur content and (4) CAD injection rate, assumed to be independent, were only weakly correlated..

Correlation Matrix

Treatment time	Mass of hot metal	Initial S content	CaD injection rate	Final S content
1.0000	0.2304	0.4160	-.2021	-.6712
0.2304	1.0000	0.0008	-.0797	-.0519
0.4160	0.0008	1.0000	-.0207	0.2052
-.2021	-.0797	-.0207	1.0000	-.0685
-.6712	-.0519	0.2052	-.0685	1.0000

On analyzing the eigen values, eigen vectors followed by principal components analysis, it was found that there were no clusters in the data. The dimensionality of the problem could not be reduced because the scree curve (Fig. 2.1) did not show any rocky debris or flat portion at tail end. Multiple linear regression analysis was, therefore, carried out with final sulfur content as the dependent variable and the other four (described above) as independent variables. The standard error of estimate was 0.0018 and multiple correlation coefficient (R) was 0.91 (R squared = 0.8229, corrected R squared =0.8202).

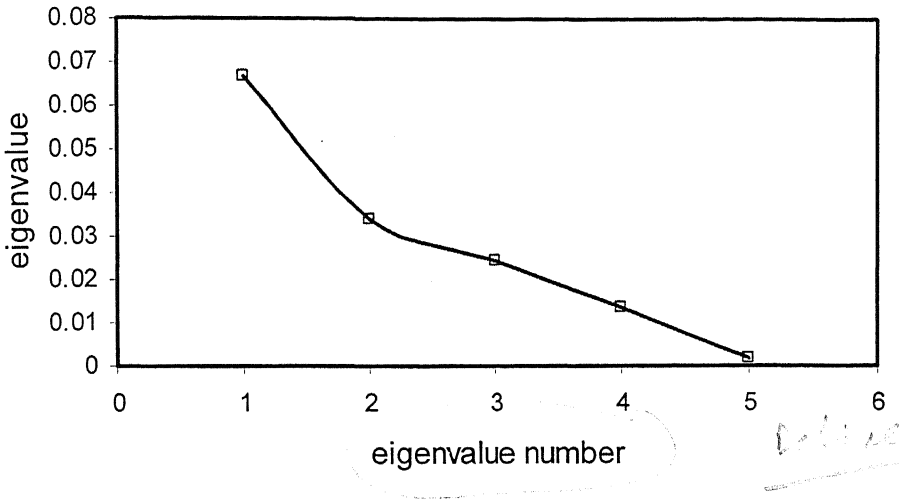

Fig. 2.1: Scree-cruve: eigen value vs. eigen value number; variable 1: Treatment time, 2. Mass of metal, 3. Initial Sulphur content, 4. CaD injection rate, 5. Final Sulphur content.

Several modifications can be made in the choice of input (independent) variables to be used in a regression model. In order to account for any possible non-linear correlation, the independent variables can be suitably modified. In the case of desulphurization of hot metal, for example, the independent variables can be suitably modified and selected on the basis of process fundamentals. As will be discussed later, according to kinetic fundamentals, the injection rate is expected to be dependent on initial and final sulphur in the form $\ln\left(\frac{S_i}{S_f}\right)$. A linear regression model, called a ballistic model, was developed at Sollac, France, according to which the amount of powder injected, Q_{CaD}, was calculated from

$$Q_{CaD} = X_1 + W_m \text{ x } \ln\left(\frac{S_i}{S_f}\right) \text{x } \{X_2 + X_3 \text{ x } S_i + (X_4 + X_5 \text{ x } I_R) \text{ x } S_f + X_6 \text{ x } I_R\} \qquad (2.1)$$

Where, X_1 ..... X_6: Constants, W_m: Hot metal weight, S_i : Initial sulfur content, S_f: Final sulfur content, I_R: Injection flow rate, Q_{CaD}: Mass of calcium carbide needed.

2.1.2 Model based on second order chemical reaction

In this model the desulphurization is assumed a priori to be controlled by second order chemical reaction and the governing equation is:

$$\frac{dS}{dt} = -KS_tC \qquad (2.2)$$

Where, C is the concentration of desulphurizer at time t, S_t is concentration of sulphur

at time t and K is the chemical rate constant for desulphurizer. It is further assumed that the residence time (τ) of any desulphurizer particle is short, relative to the total injection time, and during this injection time the hot metal sulphur content remains approximately constant. Upon integration of equation (2.2) final expression is obtained in terms of the injection rate Q' (kg of powder/metric ton of hot metal) as

$$Q' = \frac{(S_i - S_f)}{MPf + \frac{MPf}{K\tau(S_i - S_f)}\left[e^{-K\tau S_i} - e^{-K\tau S_f}\right]} \qquad (2.3)$$

Where, $M = \frac{M_S}{M_{CaC2}} \times 0.1$, M_S and M_{CaC2} are molecular mass of sulfur and desulphurizer respectively, P is the component purity, F is the blend fraction, S_i: initial sulfur content, S_f: sulfur content in the hot metal after time t. From the plot of actual versus predicted sulphur, on using the value of K as 8.33 and $\tau = 1$ s, the value of R^2 is obtained as 0.80. In this kinetic model no separate treatment is incorporated to account for the specific contributions of transitory reaction (while the particle is traveling in the metal) and the permanent contact reaction (when the particle has joined the top slag reactions).

2.1.3 Model based on mass transfer (first order), including the transitory and permanent reactions

A detailed kinetic model, considering the specific contributions of the transitory and the permanent contact reactions, assuming mass transfer as rate controlling step, is described in detail elsewhere [2.5]. This model was further improved by Sheshadri et al [2.6]. According to this model the desulphurization process is divided into three parts:

contribution of individual powder particles while they are rising independently in the liquid metal, R_p, contribution of the powder particles which are captured in the rising carrier gas bubbles, R_b, and the contribution of particles when they join the top slag, R_{ts}. The overall rate equation is

$$\frac{-M_L}{M_S}\frac{d[\%S]}{dt} = R_{ts} + R_p + R_b \qquad (2.4)$$

$$\text{Where } R_{ts} = \frac{K_f A_{S-M} \rho_L}{M_s 100} \times \left([\%s] - \frac{M_L([\%S]_o - [\%s]) + M_{ts(t=0)}(\%S)_o}{L_S^{ts}(M_{ts(t=0)} + I_R t)} \right)$$

$$R_p = \frac{(1-f) I_R L_s^p}{M_s 100} \left[1 - \exp\left(- \frac{6 K_p \rho_L trp}{L_s^p d_p \rho_p} \right) \right] [\%S]$$

$$R_b = \frac{f.I_R L_s^g}{M_s 100} \left(1 - \exp\left(- \frac{2.38 K_b \rho_L trbQT}{273 d_b I_R L_s^g f} \times \frac{P_o}{P_r} \right) \right) \times [\%S]$$

2.1.4 ANN Model

A detailed discussion of the application of neural nets to the desulphurization problem is explained elsewhere [2.10]. The artificial neural nets, similar to the regression models, can be directly applied to raw data without any prior knowledge of the process fundamentals. The sigmoidal function used for training ANN is able to automatically account for any nonlinearity present between the independent and dependent variables, and there is no need to hunt for a specific relationship similar to equation (2.2). However, better results can be obtained if the selection of the input and output variables is guided by prior process knowledge.

The list of various symbols and their values used in equation (2.4) is given below.

Symbol		Value
A_{S-M}	Area of slag-metal interface (m^2)	40
d_b	Average bubble diameter (m)	Variable
d_p	Average particle diameter (m)	15×10^{-5}
f	Fraction of particles entrapped in the bubbles	0.3
h_i	Depth of injection of CAD (m)	1.8
I_R	Rate of injection of the desulfurizing agent (kg/s)	0.45 – 1.5
k_b	Sulfur partition coefficient between bubble	2.36×10^{-3}
k_f	Sulfur transfer coefficient through the metal slag	8.70×10^{-4}
k_p	Sulfur transfer coefficient at particle melt boundary layer	2.36×10^{-3}
L_g^p	Sulfur partition coefficient between particles and melt, respectively.	2000
L_s^g	Sulfur partition coefficient between particles entrapped in the bubble and melt.	2000
L_s^{ts}	Sulfur partition coefficient between top slag and melt	2000
M_{CaC2}	Molecular mass of CaC_2 (g/mol)	64
M_L	Weight of metal (Ton)	280 -370
M_s	Molecular mass of sulfur (g/mol)	32
$M_{ts(t=0)}$	Mass of carry over slag (kg)	5
P_o	Average pressure in side the bubble (atm)	1.0
P_r	Average reference pressure (atm)	Variable
Q	Gas flow rate (Nm^3/s)	0.033
[%S]	Instantaneous concentration of sulfur in the metal bulk	Variable

	(%wt)	
S_f	Final Sulphur content (%wt)	0.002-0.02
$[\%S]_i$	Instantaneous concentration of sulfur at top slag- metal interface (metal side) (%wt)	Variable
$[\%S]_o$, S_i	Initial sulfur concentration in the melt (%wt)	0.0015-0.07
t	Total time for desulphurization treatment (s).	500-3400
trp, τ	Particle residence time (s)	Variable
trb	Bubble residence time (s)	Variable
ρ_L	Specific weight of melt (kg/m^3)	7000
ρ_p	Specific weight of particle (kg/m^3)	1740

In the ANN model, a multidimensional surface is represented by a complex combination of terms, for example exponential equations when a sigmoidal function used for training. It is necessary that enough data is available to train the net for each part of the multidimensional surface, other wise in the regions where data is scarce the predictions can become very erroneous. This does not usually happen with other models described above which are based on fundamental considerations of process thermodynamics and kinetics. For this reason, it is advised to use ANN models for interpolation and not for extrapolation.

The popular back propagation method was used in the present work for the training by employing a sigmoidal function, with momentum factor $\alpha = 0.5$, training rate $\beta = 0.5$, and logistic $T = 1.0$. The training set consisted of 91 data and test set contained 79 data. The training was terminated when the learning curve became nearly flat (visually); maximum iterations needed were less than 5000. Several net architectures were tried. The R^2 values obtained from the plot of actual versus predicted sulphur for some of nets, which yielded good results, were: for three layer (4-5-1 net) 0.87, three layer (4-6-1 net) 0.81, four layer (4-6-3-1 net) 0.80, and four layer (4-5-3-1) net 0.86, respectively.

It is our experience that for most iron and steel making processes (viz. blast furnace, basic oxygen furnace, RH degasser, etc) if there are, say, n input variables and one out put variable, then a simple three layer net of n+1, n-1, n+2 or n-2 middle layer neurons usually gives the best results. The minimum number of training data needed may vary from 20n to 40n, but it should be properly distributed over the entire multidimensional domain.

2.1.5 Fuzzy rule based expert system (FRBES) model

In principle, the fuzzy rule based expert system models are normally used when the fundamental knowledge of the process is poor, the relationship between the variables is complex and some of the process variations are stochastic. With regard to the desulphurization treatment, the ambiguity or imprecision in information is usually present in the measurement of input and output data coupled with stochastic variations in particle shape, size and composition, and fluid flow patterns with in the metal. For example, the concentration of sulphur measured at one location is not representative of the other parts of the same system. The concentration at the top of bath is different from that at the bottom due to improper mixing. Thus, even though concentration has been measured to an accuracy of ±1%, the system is fuzzy (or dizzy) with regard to the concentraton in different parts of the same system. As the vessel size changes, viz due to erosion of refractory, the flow patterns also change and process performance drifts. In the FRBES approach, an attempt is made to divide the multidimensional surface of the input and out put variables into a number of regions demarcated by process and plant specific fuzzy decision rules so as to capture the process behavior. In our case, the output variable is final sulphur content of hot metal and the input variables are (1) treatment time, (2) mass of hot metal, (3) initial sulphur content of hot metal and (4) CAD injection rate. A lot of practical experience or expertise is required in framing the rules, and hence they can vary from person to person and from one plant to another. The obvious disadvantage is that a slight change in the operating conditions may call for the review of the whole set of rules framed to predict the output. On the other hand, an advantage of the fuzzy systems is that they can produce a nonlinear functional mapping just as the algorithms do.

In the FRBES model developed in the present work, treatment time is fuzzified into five classes, CAD injection rate into four classes, hot metal weight into five classes, initial sulphur content into five classes, and final sulphur content into five classes. The linguistic labels used are: Very low (VL), Low (L), Medium (M), High (H) and Very high (VH). Symmetrical, normal, triangular membership functions with 50% overlap are assigned for each fuzzy subset. The symbol μ is used to represent the membership value. A typical example of the mathematical description of membership function of treatment time and its validity range is given in Table 2.2. The eleven fuzzy rules, given below, were arrived at after hundreds of trials with respect to A: treatment time, B: hot metal mass, C: initial mass % of sulphur, D: CAD flow rate, and E: final mass % sulphur in hot metal.

1. IF A is VL and B is M and C is M and D is VH THEN E is VH.
2. IF A is VH and B is L and C is M and D is VH THEN E is VL.
3. IF A is VH and B is M and C is L and D is VH THEN E is VL.
4. IF A is VL and B is M and C is VL and D is H THEN E is L.
5. IF A is H and B is VH and C is M and D is VH THEN E is L.
6. IF A is H and B is H and C is M and D is H THEN E is M.
7. IF A is VL and B is M and C is L and D is H THEN E is H.
8. IF A is M and B is M and C is M and D is VH THEN E is H.
9. IF A is M and B is VH and C is H and D is H THEN E is VH.
10. IF A is VL and B is L and C is L and D is VH THEN E is VH.
11. IF A is VL and B is VL and C is VL and D is H THEN E is M.

The plot of actual versus predicted sulphur for one of five classes yielded highest R^2 value of 0.94.

2.1.6 Optimization by GA

GA works with a population of solutions, and during the iterations it continually updates the population according to the set objective function, throwing away poorer solutions and replacing them with improved solutions [2.22]. GA is, no doubt, computer time and memory intensive but that is not a limitation at all with small optimization problems discussed in this work. In fact GA is now accepted as one of the most powerful techniques of evolutionary search and optimization in process metallurgy.

2.2 Plant data

The plant data used in this work relates to 400 ton torpedo ladles (for details see [2.7, 2.10, 2.11]) in which desulphurization was carried out by injecting calcium carbide powder through a submerged twin-whole lance. Nitrogen (2 m^3/min) was used as a carrier gas. A typical plant data set is shown in Table 2.1. Data for 229 heats was collected, and the range of variation of each parameter was as follows: treatment time (473-1719 ± 20 seconds), hot metal weight (250-379 ±5 tons), initial sulphur content (90-440 ppm ± 5 ppm), CaD injection rate 45.0-71.0 ± 1.5 kg/min), and final sulphur content (13-180ppm ± 2 ppm).

2.3 Results and discussion

A typical set of data for a sample calculation by different models is given below,

	Symbol	units	Value
Treatment time	t_{Total}	sec	1808
Weight of hot metal	W_m	ton	334
Initial sulphur content of bath	S_i	mass %	0.033
Injection rate of CaC_2	I_R	kg/min	51
Final sulphur content of bath	S_f	mass %	0.004

The models described in sec 2.3 are applied to predict the final sulphur content of hot metal.

2.3.1 Application of models

(a) Application of regression model to predict the required mass of calcium carbide for desulphurization

The regression model developed from the stastical analysis (Eqn 2.1) may be used to predict the required mass of calcium carbide needed for desulphurization, Q_{CaD}, to achieve a desired final sulphur content of the bath.

The following model, known as Ballistic model, is used

$$Q_{CaD} = X_1 + W_m \text{ x } \ln\left(\frac{S_i}{S_f}\right) \text{x } \{X_2 + X_3 \text{ x } S_i + (X_4 + X_5 \text{ x } I_R) \text{ x } S_f + X_6 \text{ x } I_R\} \quad (2.1)$$

Where, X_1 ..... X_6: Constants, W_m: Hot metal weight, S_i: Initial sulphur content, S_f: Final sulphur content, I_R: Injection flow rate, Q_{CaD}: Mass of calcium carbide needed. For the data set used in the present work, the values of the estimated parameters obtained by multiple linear regression are: $X_1 = 103.12$, $X_2 = 4.7 \times 10^{-4}$, $X_3 = 0.014$, $X_4 = 0.076$, $X_5 = -0.081$, $X_6 = 0.0012$.

Thus, the predicted value of the required mass of calcium carbide for desulphurization, Q_{CaD}, can be calculated by using Eqn (2.1).

$$Q_{CaD} = X_1 + W_m \times \ln\left(\frac{S_i}{S_f}\right) \times \{X_2 + X_3 \times S_i + (X_4 + X_5 \times I_R) \times S_f + X_6 \times I_R\}$$

$$= 103.12 + 334 \times 10^3 \times \ln\left(\frac{0.033}{0.004}\right) \times \{4.7 \times 10^{-4} + 0.014 \times 0.033 + (0.076 - 0.081 \times 0.85) \times 0.004 + 0.0012 \times 0.85\}$$

$$= 1492.95 \text{ kg}$$

From the data the actual required mass of calcium carbide for desulphurization, Q_{CaD}, is Actual, $Q_{CaD} = t_{Total} \times I_R$

$$= \left(\frac{1808}{60}\right) \times 51 = 1567.8 \text{ kg}$$

The plot of actual versus predicted mass of calcium carbide is shown in Fig. 2.2. It is possible to back calculate the final sulphur content of hot metal (S_f) from Eqn (2.1) and from the plot of actual versus predicted sulphur, the value of $R^2 = 0.87$ was obtained. This R^2 value is marginally higher than the value of $R^2 = 0.82$, as determined in the earlier regression model (in which no logarithmic relationship was assumed between S_i and S_f). It demonstrates that if the process fundamentals are properly understood then it is easier to select the regression parameters for improving the accuracy of prediction.

(b) Application of the model based on second order chemical reaction to predict the final sulphur content of the bath

The model based on second order chemical reaction (Eqn 2.3) may use to predict the final sulphur content of the bath

$$Q' = \frac{(S_i - S_f)}{MPf + \frac{MPf}{K\tau(S_i - S_f)}\left[e^{-K\tau S_i} - e^{-K\tau S_f}\right]} \qquad (2.3)$$

Where, $M = \frac{M_S}{M_{CaC2}} \times 0.1$, M_S and M_{CaC2} are molecular mass of sulphur and desulphurizer respectively, P is the component purity, F is the blend fraction, S_i: initial sulphur content, S_f: sulphur content in the hot metal after time t.

The values of different parameters used in Eqn (2.3) are: M = 0.05, P = 1.0, f = 1.0, K = 8.33, and τ = 1 sec

$$\text{Thus, } \frac{1567.8}{334} = \frac{(0.033 - S_f)}{0.05\times1\times1 + \frac{0.05\times1\times1}{8.33\times1\times(0.033 - S_f)}\left[e^{-8.33\times0.033} - e^{-8.33\times0.004}\right]}$$

From the above relationship the value of final sulphur content of the bath, S_f, is calculated by iteration, and S_f = 0.0037; the actual sulphur content observed in this heat was 0.004%, and the two values (actual and predicted) agree well.

Results for all the heats are plotted in Fig. 2.4 and it can be seen that the overall R^2 value is 0.80. In this kinetic model no separate treatment is incorporated to account for the specific contributions of transitory reaction (while the particle is traveling in metal) and the permanent contact reaction (when the particle has joined the top slag reactions).

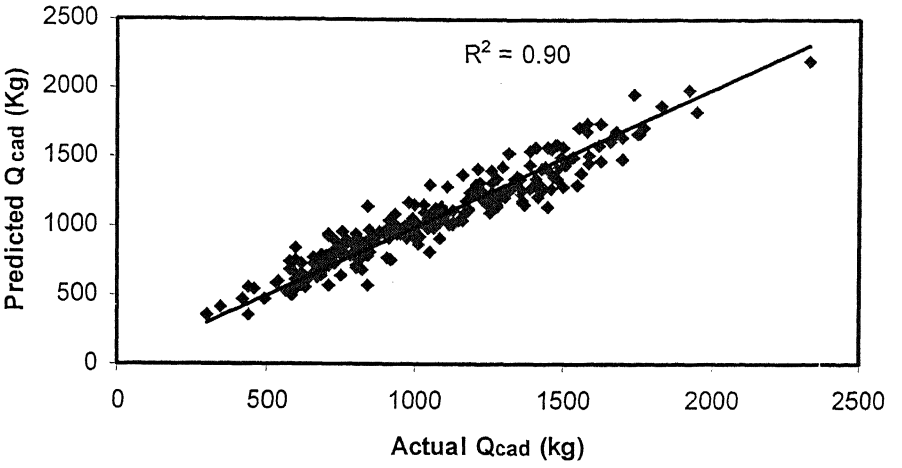

Fig. 2.2: Actual versus predicted Q_{CaD} by regression model

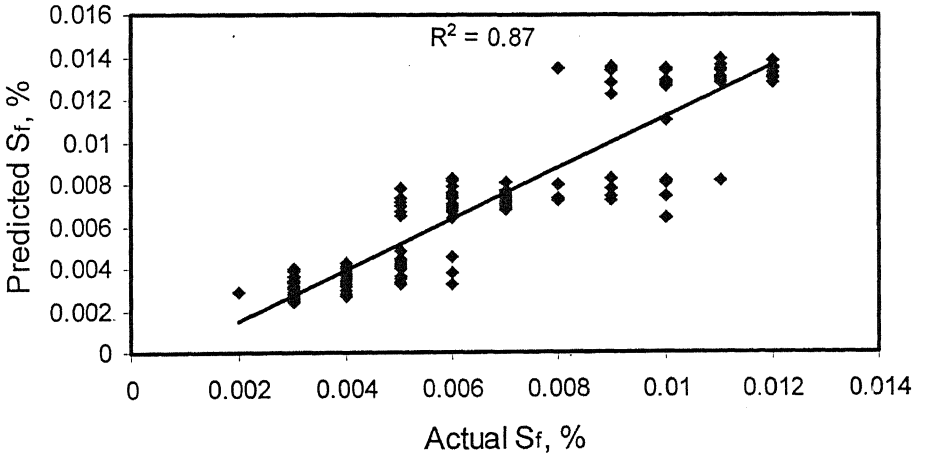

Fig. 2.3: Actual versus predicted S_f by regression model

(c) Application of the model based on mass transfer (first order), including the transitory and permanent reactions

The model based on second order chemical reaction (Eqn 2.4) may use to predict the final sulphur content of the bath

$$\frac{-M_L}{M_S}\frac{d[\%S]}{dt} = R_{ts} + R_p + R_b$$

Where, R_p is the contribution of individual powder particles while they are rising independently in the liquid metal, R_b is the contribution of the powder particles which are captured in the rising carrier gas bubbles, and R_{ts} is the contribution of particles when they join the top slag.

For a small time step $\Delta t = 0.1$ sec the values of R_{ts}, R_p, R_b can be calculated by,

$$R_{ts} = \frac{K_f A_{S-M} \rho_L}{M_s 100} \times \left([\%s] - \frac{M_L([\%S]_o - [\%s]) + M_{ts(t=0)}(\%S)_o}{L_S^{ts}(M_{ts(t=0)} + I_R t)} \right)$$

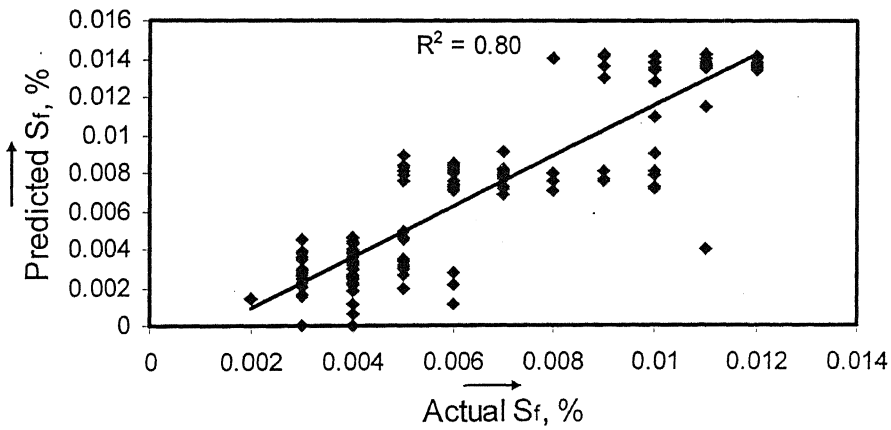

Fig. 2.4: comparison of the actual versus predicted sulphur for the second order chemical kinetics model [2.1]

The list of various symbols and their values used in the above equations is given in Table 2.4. By putting the values in the above equation,

$$R_{ts} = \frac{8.70\times10^{-4}\times40\times7000}{32\times100}\times\left(0.033-\frac{334\times10^{3}(0.033-0.033)+5\times0}{2000\times(5+0.85\times1)}\right) = 0.0392$$

$$R_p = \frac{(1-f)I_R L_s^p}{M_s 100}\left[1-\exp\left(-\frac{6k_p\rho_L trp}{L_s^p d_p \rho_p}\right)\right][\%S]$$

The list of various symbols and their values used in the above equations is given in Table 2.4. By putting the values in the above equation,

$$R_p = \frac{(1-0.3)\times0.85\times2000}{32\times100}\left[1-\exp\left(-\frac{6\times2.36\times10^{-3}\times7000}{2000\times15\times10^{-5}\times1740}\right)\right]\times[0.033]$$

$$= 0.045$$

$$R_b = \frac{f.I_R L_s^g}{M_s 100}\left(1-\exp\left(-\frac{2.38K_b\rho_L trbQT}{273d_b I_R L_s^g f}\times\frac{P_o}{P_r}\right)\right)\times[\%S]$$

The list of various symbols and their values used in the above equations is given in Table 2.4. By putting the values in the above equation,

$$R_b = \frac{0.3\times0.85\times2000}{32\times100}\left(1-\exp\left(-\frac{2.38\times2.36\times10^{-3}7000\times7.13\times0.033\times1473}{273\times0.02\times0.85\times2000\times0.3}\times1\right)\right)\times[0.033]$$

$$= 0.0053$$

Finally, the decrease in sulphur content of metal small time step, Δt, is

$$\Delta[\%S] = (R_{ts}+R_p+R_b)\frac{M_L}{M_S}\Delta t \qquad = (0.0392+0.0405+0)\times\frac{32}{334\times10^{3}}\times0.01$$

$$= 3.92 \text{ x } 10^{-6}$$

For the total time the predicted value of the final sulphur content of the bath, S_f, is 0.039 %

The results obtained for all the heats are plotted in Fig. 2.5. The value of $R^2 = 0.84$ (obtained from the plot of actual versus predicted sulphur) is higher than that of the second order chemical kinetics model ($R^2 = .80$) but lower than the two regression models discussed earlier. This first order mass transfer model, even though more sophisticated in approach to account for transitory and permanent contact reactions, is based on several assumptions and has some parameters which can be tuned or optimized. The advantages of optimization of this model by GA will be discussed later. The results of some other models based on first order mass transfer are discussed elsewhere [2.12-2.17].

(d) Application of ANN models to predict the final sulphur content of the bath

Results of the three typical ANN models are presented in Fig. (2.6-2.8) for three layer (4-5-1 net), three layer (4-6-1 net), and four layer (4-6-3-1 net), respectively. Simple back propagation method was used for training by using a sigmoidal function, with momentum factor $\alpha = 0.5$, training rate $\beta = 0.5$, and logistic $T = 1.0$. The training set contained 91 data and test set contained 79 data.

The $R^2 = 0.86$ is obtained for the case of simple net 4-5-1. The other two nets also gave the R^2 values close to 0.85.

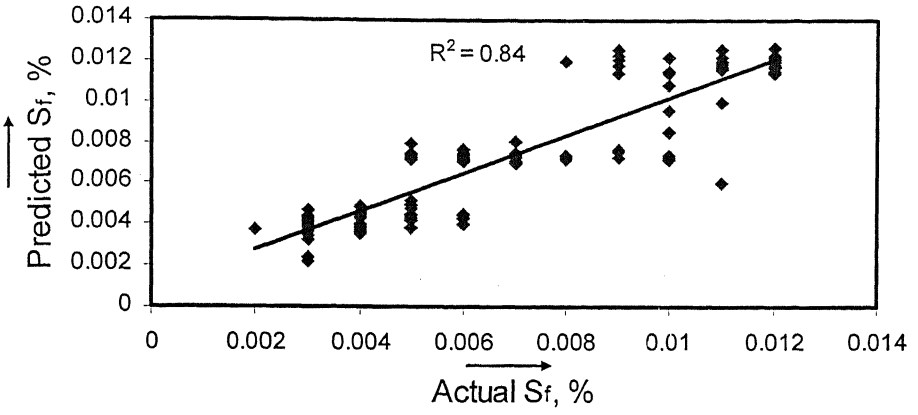

Fig. 2.5: Actual versus predicted S_f by mass transfer model [2.5]

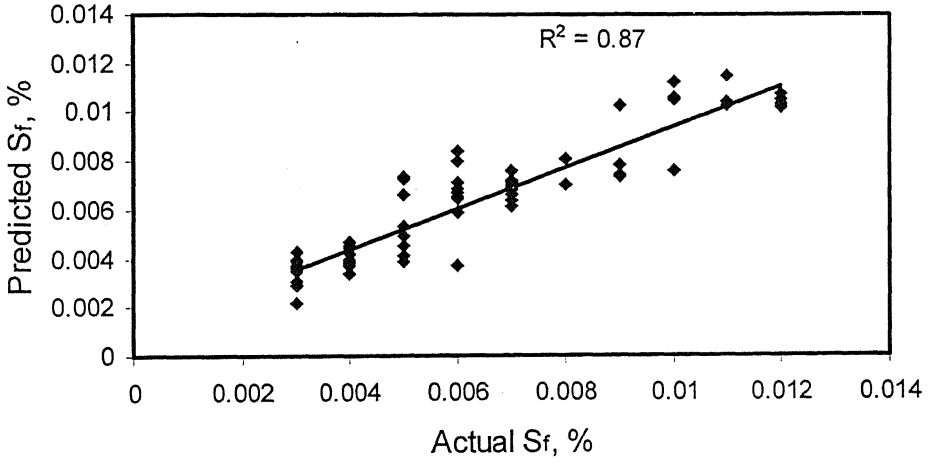

Fig. 2.6: Actual versus predicted S_f by ANN 4-5-1 net

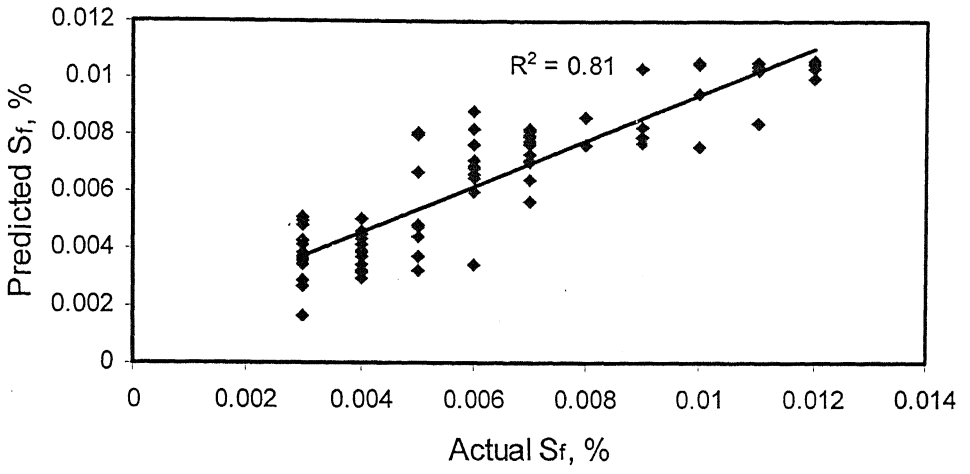

Fig. 2.7: Actual versus predicted S_f by ANN 4-6-1 net

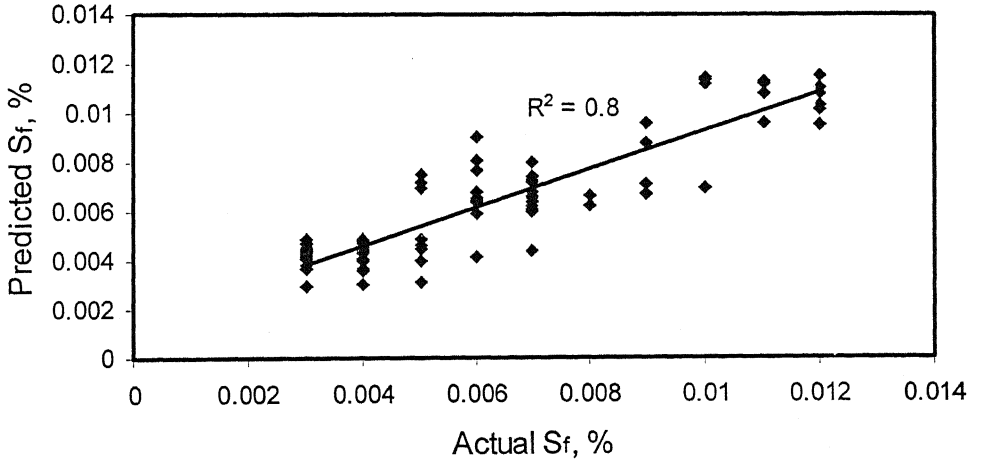

Fig. 2.8: Actual versus predicted S_f by ANN 4-6-3-1 net

(e) **Application of Fuzzy rule based expert system (FRBES) model to predict the final sulphur content of the bath**

The plot of actual versus predicted sulphur (for the data set given in the Table 2.1) is shown in Fig. 2.9.

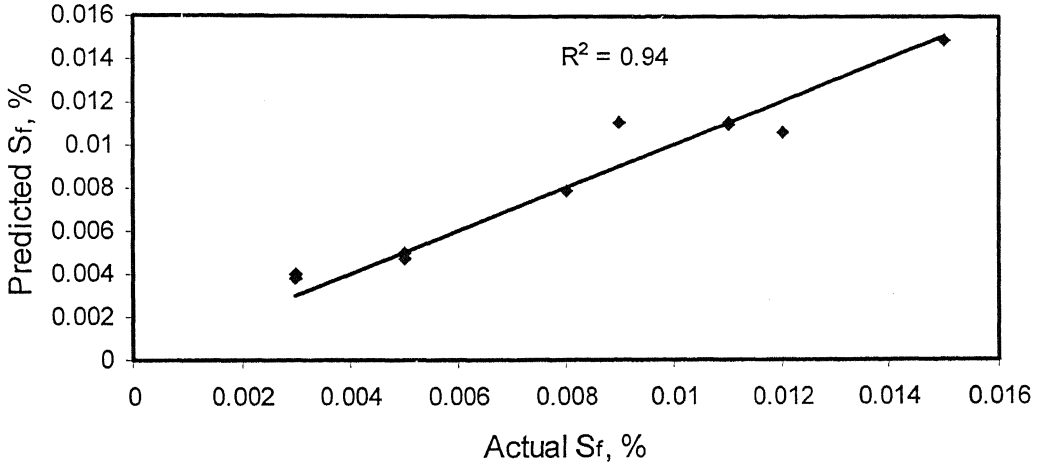

Fig. 2.9: Actual versus predicted S_f by fuzzy rule based expert system (FRBES) model

(f) Application of genetic algorithm (GA) to predict the final sulphur content of the bath

In an earlier work the model based on mass transfer was optimized [2.11] by using GA. A simple genetic algorithm (SGA) was employed with Roulette Wheel Selection, crossover probability ranging from 0.7-0.85, and mutation was less than 0.01. The relative contributions of powder particles (see equation (2.4)) rising independently in the liquid metal (R_p), powder particles captured in the rising carrier gas bubbles (R_b), and the powder particles when they join the top slag (R_{ts}) were investigated. It was shown that the contribution of particles captured in rising gas bubbles should be neglected. This significant result could not be obtained by the application of a regression technique even after optimizing the coefficients R_p, R_b, and R_{ts} in equation (2.4) [2.11]. The result predicted by the combined GA-kinetic model has been found to be in agreement with the experimental observations that there is a critical limit to the ratio of mass of powder to the mass of gas injected per unit time at which the utilization of desulphurization agent is optimal with respect to desulphurization time and the cost of reagent injected. In the final GA-optimized model the kinetic term R_b was dropped altogether [2.11]. The GA optimization further revealed that the contribution of top slag (R_{ts}) was nearly 1.5 times of the contribution of particles independently rising in the metal (R_p). The optimization of the exponent of R_p and R_{ts} improved the predictions further and from the plot of actual versus predicted sulphur the R^2 value obtained was 0.80. The benefit of optimizing the mass transfer model by using GA was two fold: better understanding of the process kinetics and an improved kinetic model based on process fundamentals.

2.4 Comparison of modeling strategies

The results of both conventional and AI techniques demonstrated in this work are summarized in Table 2.3, in terms of average error, mean square error and the square of the product-moment correlation coefficient (R^2) for actual versus predicted final sulphur content. To start with, the experimental data was selected for a wide range of final sulphur content, 0.005- 0.018 %. It was, however, observed that in all the models, in the range of final sulphur lying between 0.010-0.018 mass %, the predicted out put was almost independent of the actual out put. For example, from the results of multiple linear regression analysis of the two above mentioned data sets, for final sulphur content < 0.010 and 0.01-0.018 mass % respectively, a considerable decrease in standard error of estimate was observed for the first set but for the second set, 0.01-0.018 mass %, the R^2 value dropped to 0.0217. This suggested that the process data should be split in two parts for prediction purposes namely, 0.005- 0.012% and 0.01-0.018%, respectively. In the present work the results are presented for the former case when final sulphur content is less than 0.012%. It is advisable to tune or optimize a model to experimental data in specific ranges if that helps to increase the predictability. The process characteristics can change in different regions.

The plus point of a kinetic model based on process fundamentals is that as the process understanding improves it becomes possible to make further modifications in the design/technology. For example, having learnt from GA optimization experiments that the contribution of powder particles rising in the bubbles was nearly zero, the lance nozzle design was improved to inject powder deeper into the melt and also increase residence time of the particle freely rising in the melt. This led to a significant improvement in process efficiency.

If we compare only the numerical values of R^2 for conventional models, both the multiple regression models ($R^2 = 0.87$) and second order chemical kinetics model (($R^2 = 0.80$) have performed well. The process knowledge gained with these models can however be misleading at times. The same is true for ANN model ($R^2 = 0.88$). A major limitation of using ANN models in a plant environment is that in certain regions of the multidimensional space, wherein enough training data is not available, the predictions can become totally unreliable. The fuzzy rule based expert system model appears to give the best result ($R^2 = 0.94$) because it was possible to make specific rules based on actual plant data and then focus on a small class. For example, in the case of the data in the range of 0.01-0.018 mass %S, the base of the triangular membership function for final sulphur was increased as the final sulphur content increased. In spite of better prediction of final sulphur content, FRBES model does not provide any additional information or insight into the process. The rule base in FRBES also needs to be updated frequently in a plant environment and this is not a simple exercise. From the point of view of practical convenience, therefore, only when no other suitable model is available, one should try the FRBES approach.

Besides a high R^2 value, the other selection criteria of a good model is that both average error and mean square error should be as small as possible (given in Table 2.3), and the spread of error should be uniform over the entire range of predicted variable. The residual error plots for different models are compared in Fig. 2.12. The spread of error is almost uniform in the case of ANN model followed by GA-kinetic model. The second order chemical kinetics model shows the worst spread followed by Sheshadri/Deo kinetics model, ballistic model and the second order chemical kinetics model.

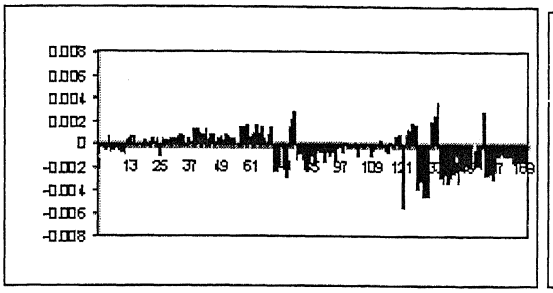

Ballastic (Linear Regression) Model

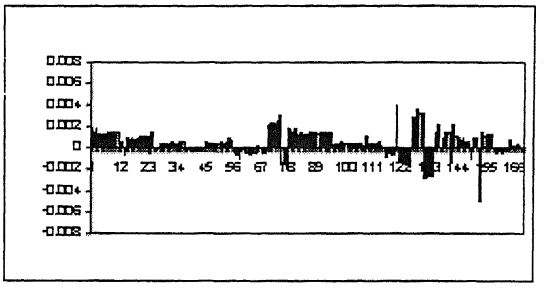

Sheshadri/Deo Model

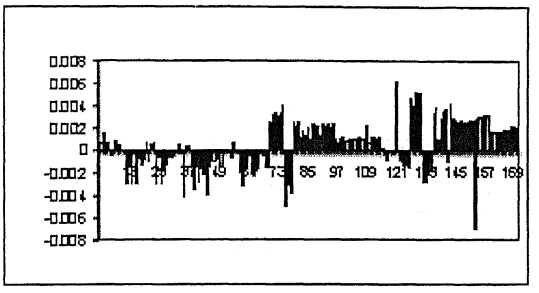

Second Order Chemical Kinetics Model

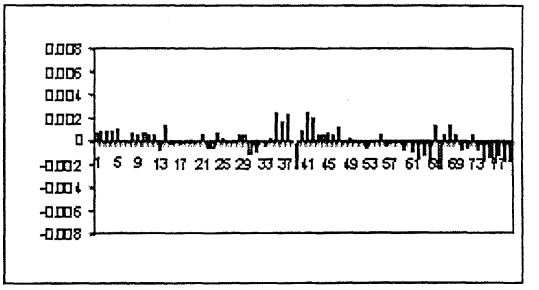

ANN 4-5-1 Net

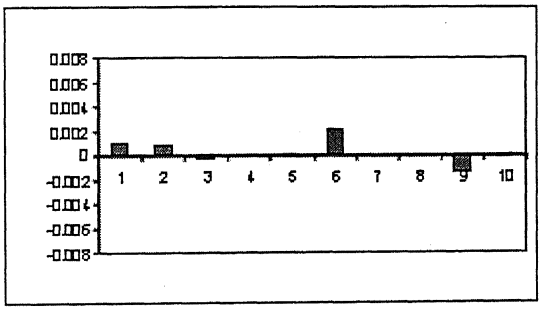

FRBES model

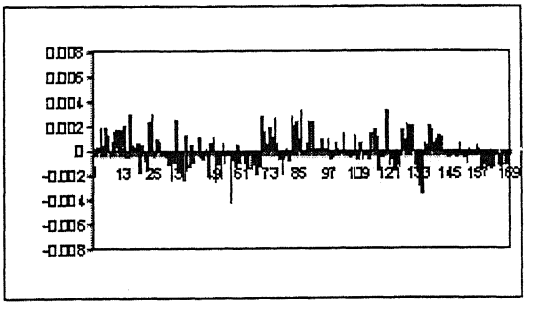

GA-kinetics model

Fig. 2.12: Plot of residual error (i.e., actual–predicted) versus heat number for different models

Table 2.1: Typical plant data set on desulphurization

Total no. of observations: 11				
Treatment time (Sec)	Hot Metal Weight (Tons)	Initial Sulphur (mass %)	CaD injection rate (kg/min)	Final Sulphur (mass %)
1404	280	0.026	67	0.003
1421	309	0.024	70	0.003
473	303	0.016	62	0.005
1161	362	0.030	73	0.005
1085	336	0.028	63	0.008
559	308	0.021	63	0.009
483	304	0.018	58	0.011
501	317	0.020	63	0.011
779	295	0.030	68	0.012
796	344	0.033	60	0.015
455	271	0.022	68	0.017

Table 2.2: Fuzzification details of treatment time

μ (VL)	1 (675 – X)/202 0	X ≤ 473 473 ≤ X ≤ 675 X = 675
μ (L)	(X-625)/67.5 1 (760-X)/67.5	625 ≤ X ≤ 692.5 X = 692.5 692.5 ≤ X ≤ 760
μ (M)	(X-725)/137.5 1 (1000-X)/137.5	725 ≤ X ≤ 862.5 X = 862.5 862.5 ≤ X ≤ 1000
μ (H)	(X-950)/225 1 (1400-X)/225	950 ≤ X ≤ 1175 X= 1175 1175 ≤ X ≤ 1400
μ (VH)	0 (X-1300)/419 1	X = 1300 1300 ≤ X ≤ 1719 X ≥ 1719

Table 2.3: Comparison of the performance of different models

MODELS	Average Error	Mean Square Error	R^2
Ballastic model (Linear Regression)	0.0016	1.21×10^{-3}	0.87
Second order chemical kinetics	0.0022	1.77×10^{-3}	0.80
Seshadri/B.Deo, mass transfer	0.0013	9.98×10^{-4}	0.84
ANN [4-5-1]	0.0044	1.26×10^{-5}	0.88
ANN [4-5-3-1]	0.0072	$1.6\,0x\,10^{-7}$	0.86
ANN [4-6-1]	0.0012	1.01×10^{-3}	0.81
ANN [4-6-3-1]	0.0040	1.27×10^{-5}	0.80
FRBES model*	0.0002	9.01×10^{-4}	0.94
Optimization by genetic algorithm	0.0014	1.09×10^{-3}	0.80

* best result obtained for one of the five data sets (class) in FRBES

Table 2.4: The list of various symbols and their values used in equation (2.4)

Symbol		Value
A_f	Area of slag metal interface (m^2)	40
d_p	Average particle diameter (m)	1.5×10^{-5}
f	Fraction of particles entrapped in the bubbles	0.3
h	Depth of injection (m)	1.8
I_R	Rate of injection of the desulfurizing agent (kg/s)	0.85
k_b	Sulfur partition coefficient between bubble	2.36×10^{-3}
k_f	Sulfur transfer coefficient through the metal slag	8.70×10^{-4}
k_p	Sulfur transfer coefficient at particle melt boundary layer	2.36×10^{-3}
L_g^p	Sulfur partition coefficient between particles and melt respectively.	2000
L_s^g	Sulfur partition coefficient between particles entrapped in the bubble and melt.	2000
L_s^{ts}	Sulfur partition coefficient between top slag and melt	2000
M_{CaC2}	Molecular mass of CaC_2 (g/mol)	64
M_L	Weight of metal (Ton)	334
M_s	Molecular mass of sulfur (g/mol)	32
$M_{ts(t=0)}$	Mass of carry over slag (kg)	5
P_o	Average pressure in side the bubble (atm)	1.0
Q	Gas flow rate (Nm^3/s)	0.033
S_f	Final Sulphur content (%wt)	0.004
$[\%S]_o$, S_i	Initial sulfur concentration in the melt (%wt)	0.033

t	Total time for desulphurization treatment (s).	500-3400
ρ_L	Specific weight of melt (kg/m^3)	7000
ρ_p	Specific weight of particle (kg/m^3)	1740

Chapter - 3

Theoretical and practical aspects of nitrogen and oxygen absorption, and inclusion engineering

3.1 Model of Oxygen and Nitrogen Absorption by Liquid Steel during Tapping

3.1.1 Introduction: Liquid steel, at the end of heat in a BOF, contains dissolved oxygen (400-900ppm), hydrogen (2-6 ppm), nitrogen (40-60 ppm) and the temperature of metal varies in the range 1873-1973K. During tapping of the liquid steel from BOF into a ladle, the falling stream of liquid steel is surrounded by the gaseous atmosphere (Fig. 3.1), which is rich in both N_2 and O_2. There is diffusion of N_2 and O_2 into the stream of liquid steel from the atmosphere and hence additional nitrogen and oxygen are picked up by the steel. Also, the metal bath in the ladle becomes turbulent during tapping due to of kinetic energy of falling stream and energy input due to bottom stirring and this leads to entrapment of gas bubbles in the metal. The gas bubbles may dissolve (partially or fully) and therefore further add to the dissolved nitrogen and oxygen content of steel.

The phenomenon of N_2 and O_2 pickup was studied in the past by several investigators [3.1-3.6]. The mathematical model of N_2 and O_2 pickup presented in this work has been

adapted [3.1-3.3] and further improved to incorporate the effect of absorption by tapping stream as well as absorption through the top surface of metal bath.

3.1.2 Description of the kinetic model of absorption

During tapping, the N_2 and O_2 dissolution in liquid steel occurs simultaneously by:

a) Diffusion through the surface of the falling stream

b) Diffusion through top surface of the molten metal pool in the ladle

c) Diffusion of oxygen and nitrogen from air bubbles, which are entrained in the molten pool.

Following assumptions have been made in the kinetic model developed in this work:

- The liquid steel in the ladle is uniformly mixed during tapping due to high amount of turbulence
- Temperature distribution is uniform throughout the system and almost constant during tapping
- Tilting angle of the BOF vessel changes such that metal flow rate remains steady (constant stream diameter) throughout the tapping operation
- All the oxygen in the entrapped bubble is completely absorbed, but nitrogen is absorbed only partially.

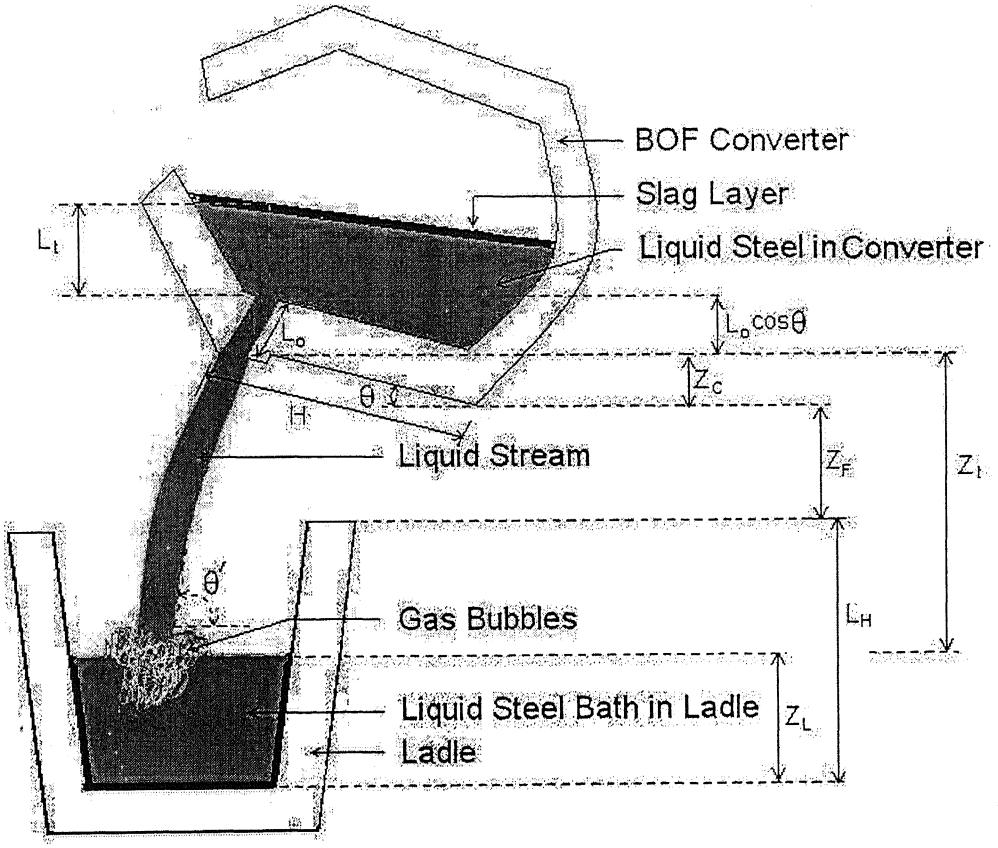

Fig. 3.1: Schematic diagram of tapping of liquid steel into a ladle

Different mechanisms of absorption of nitrogen and oxygen have been discussed below

(a) Absorption of nitrogen and oxygen by diffusion through the surface of the falling stream

The equilibrium constant for oxygen dissolution in liquid steel is

$$\tfrac{1}{2}(O_2)_g = 2\,[O] \qquad K_O = \left(\frac{([O]^i)^2}{p_{O2}}\right) = 10^{\left[-\frac{11370}{T} + 3.645\right]} \tag{3.1}$$

Where, K_o is the equilibrium constant, p_{O_2} is the partial pressure of oxygen in the ambient atmosphere, $[O]^i$ is the concentration of oxygen at the air-stream interface within a small height Δh, and T is the temperature of metal. Since the chemical reaction of oxygen dissolution is extremely fast [3.5], the oxygen absorption by the liquid steel stream surface is assumed to be controlled by mass transfer of oxygen in the metal phase. From Eqn (3.1), if we know the values of p_{O_2} and T, the interfacial concentration of oxygen at the metal surface can be calculated. The increase in oxygen content, $\Delta[\bar{O}]_{TS}$, during the time step Δt can be calculated from

$$\Delta[\bar{O}]_{TS} = \sum_{h=o}^{Z_R} k_O \frac{A_h}{\Delta V_h}([O]^i - [O]^b)\Delta t \tag{3.2}$$

Where, $[O]^b$ is the concentration of oxygen in a small volume, ΔV_h of height Δh of the liquid stream, A_h is the area of the small volume exposed to the atmosphere, and k_o is the coefficient of mass transfer of oxygen in the stream of liquid metal.

The equilibrium constant for nitrogen dissolution in liquid steel is

$$N_2(g) = 2\,[N] \qquad K_N = \left(\frac{([N]^i)^2}{p_{N2}}\right) = 10^{\left[-\frac{371.9}{T} - 2.5\right]} \tag{3.3}$$

Where, K_N is the equilibrium constant for the dissolution of nitrogen by liquid steel, p_{N_2} is the partial pressure of nitrogen in the ambient atmosphere, $[N]^i$ is the concentration of nitrogen at the air-stream interface within a small height Δh. The phenomenon of absorption of nitrogen by the surface of metal stream, similar to that for oxygen, is also assumed to be controlled by mass transfer of nitrogen in the metal phase. From Eqn (3.3), for known values of p_{N_2} and T, the equilibrium concentration of nitrogen at the metal surface can be calculated and the rate of nitrogen absorption can therefore be calculated from

$$\Delta[\bar{N}]_{TS} = \sum_{h=o}^{Z_R} k_N \frac{A_h}{\Delta V_h}([N]^i - [N]^b)\Delta t \tag{3.4}$$

Where, $[N]^b$ is the concentration of nitrogen in a small volume, ΔV_h of height Δh at the liquid stream. A_h is the area of the small volume exposed to the atmosphere. k_N is the coefficient of mass transfer of nitrogen in the stream of liquid metal.

The procedure adopted for oxygen and nitrogen pickup (flow chart given in Fig. 3.2) is as follows:

Within a small time step Δt the increase in oxygen and nitrogen content of the stream of liquid metal for a small stream length, Δh, can be calculated from Eqns (3.2) and (3.4), respectively. The increase in $[O]^b$ and $[N]^b$ within the small stream length, Δh, is continuously updated.

$$[O]^b = [O]^b + \Delta[\bar{O}]_{TS}\big|_{t=\Delta t} \tag{3.5}$$

$$[N]^b = [N]^b + \Delta[\bar{N}]_{TS}\big|_{t=\Delta t} \tag{3.6}$$

The new values of $[O]^b$ and $[N]^b$, thus obtained, are used for calculating the $[O]^b$ and $[N]^b$ values over the following small stream length (i.e. Δh to $2\Delta h$). This iteration process continues until the total stream length equals to the stream height, Z_t, i.e. when the stream joins the metal pool of ladle. The total oxygen and nitrogen pickup due to absorption through the entire surface of the stream, over a small time step Δt is therefore,

$$\Delta[O]_{Stream} = \sum_{h=0+\Delta t}^{Z_R} \Delta[\bar{O}]_{TS} \tag{3.7}$$

$$\Delta[N]_{Stream} = \sum_{h=0+\Delta t}^{Z_R} \Delta[\bar{N}]_{TS} \tag{3.8}$$

The total stream height, Z_t, changes as a function of time because of the filling up of the ladle and the change in tilt angle of the BOF vessel. The value of Z_t, at any given time, is

$$Z_t = (L_H - Z_L) + Z_F + Z_C \tag{3.9}$$

Where, L_H is the height of the ladle, Z_L is the height of the metal pool of the ladle, Z_F is the distance between top of the ladle and the bottom of the converter, Z_C is the distance between the position of the tap hole of the converter and the ladle (see Fig. 3.1) at the horizontal state and that during tapping. The height of the metal pool of the ladle, Z_L, can be calculated from

$$Z_L\big|_{t+\Delta t} = \left[Z_L + \frac{\Delta V_{Fe}}{A_L} \right]_t \tag{3.10}$$

Where, $[O]^{i}_{bath}$ is the interfacial concentration of oxygen at the metal pool and the atmosphere, $[O]^{bulk}_{bath}$ is the average bulk concentration of oxygen in the liquid bath, A_L is the area of the surface of liquid pool, k_O is the coefficient of mass transfer of oxygen at the pool of liquid steel.

The equilibrium constant for oxygen dissolution is given by Eqn (3.3). The phenomenon of absorption of nitrogen by the surface of metal stream is also assumed to be controlled by mass transfer in the metal phase. From Eqn (3.3), for known values of p_{N_2} and T, equilibrium concentration of nitrogen at the metal surface can be calculated and the rate of nitrogen absorption can be calculated from

$$\Delta[\bar{N}]_S = k_N \frac{A_h}{\Delta V_h}([N]^{i}_{bath} - [N]^{bulk}_{bath})\Delta t \qquad (3.12)$$

Where, $[N]^{i}_{bath}$ the concentration of nitrogen at the metal pool-air interface, $[N]^{bulk}_{bath}$ is the average bulk concentration of nitrogen at the liquid bath, A_L is the area of the surface of liquid pool, k_N is the coefficient of mass transfer of nitrogen at the pool of liquid steel.

(c) Absorption of nitrogen and oxygen from gas bubbles entrained in liquid steel

The rate of gas entrainment by a stream of liquid steel into a pool of liquid steel, V_g, as described by Choh et al [3.1-3..3], is

$$V_g = \frac{V_g^{\circ}}{\sin\theta'} \qquad (3.13)$$

Where, V_g^o is the rate of the gas entrainment of the vertical component of the stream and θ' is the incident angle of the tapping stream with respect to the liquid steel pool in the ladle. V_g^o can be calculated from

$$V_g^o = 0.02 V_l \left[\frac{R_c - a}{a_o} \right]^3 \qquad (3.14)$$

Where R_c radius of the cavity of the region in which the falling stream impinging on metal surface, a_o and a are the radius of stream at the tap hole exit and at distance Z from the tap hole exit. R_c can be calculated from

$$R_c = \left[\left(1.14 + 8.9 \times 10^{-4} E_1 \right)^{0.5} - 1.067 \right]^{0.5} \qquad (3.15)$$

Where E_1 is the kinetic energy of the stream of liquid just before it heats the liquid pool.

$$E_1 = \tfrac{1}{2} m U^2 \qquad (3.16)$$

Where U is the velocity of the stream of liquid metal just before it heats the liquid pool. The mass of the protuberant portion of the stream, W_m, and can be calculated from,

$$m = \pi \rho \lambda \left[2a\varepsilon - \frac{\varepsilon^2}{2} \right] \qquad (3.17)$$

Where, λ is the wavelength, $\varepsilon, \varepsilon_o$ are the amplitude of the surface disturbance of stream at the distance Z and at the tap hole exit, respectively. The radius of stream at a distance Z from the tap hole exit can be calculated from

$$a = a_o \xi^{-2} \qquad (3.18)$$

Where, ξ is the function of ratio of total energy to kinetic energy ($\xi \geq 1$), Z and velocity of the stream at exit of the nozzle, U_o. The value of ξ can be calculated by

$$\xi = \left[\frac{2gZ}{U_o^2} + 1\right]^{1/8} \tag{3.19}$$

The wave length of ripples on the surface of metal can be calculated from,

$$\lambda = 8.38\ a \tag{3.20}$$

The velocity of the stream, U, of liquid metal just before it heats the liquid pool can be calculated from

$$U = U_o \xi^4 \tag{3.21}$$

Amplitude of the surface disturbance of stream when the stream heats the metal pool, ε is given by

$$\varepsilon = \varepsilon_o \exp\left[\left(\frac{2}{7}\right)(\xi^7 - 1) \times Fr \times We^{0.35}\right] \tag{3.22}$$

Where, Fr is Froude number $Fr = \frac{U^2}{d_n g}$, d_n is the diameter of the nozzle at exit, g is the acceleration due to gravity. The weber number, *We*, is defined as

$$We = \frac{U^2 \rho_{Fe} d_n}{\sigma_{s-a}}$$

Where, ρ_{Fe} is the density of liquid steel, $\sigma_{s\text{-}a}$ is the surface tension of the liquid.

Amplitude of the disturbance (ripple) on the surface of stream at the exit of nozzle, ε_o, is given by

$$\varepsilon_o = a_o \exp\left[-44.3\left(\frac{L_o}{d_n}\right)^{-0.75} Re^{-0.1}\right] \tag{3.23}$$

Where, L_o is Length of the nozzle, and Re is the Reynold's number of the stream defined as

$$Re = \frac{\rho_{Fe} U d_n}{\mu_{Fe}}$$

Where, μ_{Fe} is viscosity of the liquid steel.

The incident angle of tapping stream with respect to liquid steel pool in the ladle, θ', can be calculated from the following equation,

$$\theta' = \tan^{-1}\left[\frac{(2gZ + U_O^2 \cos^2\theta)^{1/2}}{U_O \sin\theta}\right] \tag{3.24}$$

Where, as before, θ is the exit angle of liquid metal stream through the nozzle. The increase in nitrogen content during the small time step Δt is,

$$\Delta[\bar{N}]_{bbl} = \frac{\eta^b_{N_2}[\%N_2^{atm}]\rho_{air} V_g}{W_L}\Delta t = \frac{0.0144\eta^b_{N_2} V_g}{W_L}\Delta t \tag{3.25}$$

Similarly, the increase in oxygen content during a small time step Δt can be calculated from

$$\Delta[\bar{O}]_{bbl} = \frac{\eta^b_{O_2}[\%O_2^{atm}]\rho_{air} V_g}{W_L}\Delta t = \frac{0.00437\eta^b_{O_2} V_g}{W_L}\Delta t \tag{3.26}$$

With the help of relationships (3.13)-(3.26) it is possible to calculate N_2 and O_2 pickup due to the bubbles entrained in the metal. The details of calculations are provided in section 3.5.

(d) Total increase in dissolved nitrogen and oxygen content of the bath

The total increase in nitrogen content during the small time step Δt can be calculated from

$$\Delta[\bar{N}]_t = \Delta[\bar{N}]_{TS} + \Delta[\bar{N}]_S + \Delta[\bar{N}]_{bbl} \tag{3.27}$$

Hence, the total increase in nitrogen content of the liquid metal during tapping is

$$\Delta[\bar{N}] = \sum_{t=o}^{t} \Delta[\bar{N}]_t \qquad (3.28)$$

Similarly, the total increase in oxygen content during the small time step Δt can be calculated from

$$\Delta[\bar{O}]_t = \Delta[\bar{O}]_{TS} + \Delta[\bar{O}]_S + \Delta[\bar{O}]_{bbl} \qquad (3.29)$$

Hence, the total increase in oxygen content of the liquid metal during tapping is

$$\Delta[\bar{O}] = \sum_{t=o}^{t} \Delta[\bar{O}]_t \qquad (3.30)$$

The different symbols, used for calculation of oxygen and nitrogen pickup, are listed in Table 3.1. The symbols are in CGS units as discussed in the original work [3.3].

Table 3.1: List of symbols used for calculation in the absorption model

Symbol	Meaning
a_o, a	Radius of stream at the tap hole exit and at the distance Z from the tap hole exit, cm
A_h	Area of the stream of liquid metal at a small length Δh at height h, cm^2
d_k	Average diameter of the entrained bubbles, cm
d_n	Diameter of the tap hole, cm
F_I	Area of the Gas-metal interface (cm^3)
Fr	Froude number
G_T	Total gas volume entrained, cm^3
h	Distance from the surface of liquid steel in the converter to the inlet of tap hole, cm
H	Height of the converter, cm
Kg	Mass transfer coefficient in gas phase, cm/sec
m_N	Mass transfer coefficient of nitrogen in the liquid phase, cm/sec
m_O	Mass transfer coefficient of oxygen in the liquid phase, cm/sec
l	Distance in the longitudinal direction from the bottom of the converter, cm
l_o	Length of the tap hole, cm
m	Mass of the protuberant portion of the stream, g
$[\%N_2^{air}]$	Nitrogen present in the air by mass percent, %
$\dot{N}_{0_2}, \dot{N}_{N_2}$	Rates of mass transfer in the liquid phase and the chemical reaction at the interface, respectively, mol/(cm^2.sec)
$\Delta[\bar{N}]_{TS}, \Delta[\bar{N}]_{bbl}$	Average nitrogen absorbed from the entrained gas bubbles and through the surface of the tapping stream, %
$[O]^b$,$[O]^i$	Oxygen content in bulk of liquid steel in falling stream and at the metal-atmosphere interface, respectively, %
$[\%O_2^{air}]$	Oxygen present in the air by mass percent, %
$\Delta[\bar{O}]_{TS}, \Delta[\bar{O}]_{bbl}$	Average oxygen absorbed from the entrained gas bubbles and through the surface of the tapping stream, %

P_{02}, P_{02}^{i}	Oxygen partial pressure and its value at the interface
R_C	Radius of the cavity, cm
Re	Reynolds number
R_L	Radius of the ladle, cm
T	Temperature of the liquid steel, K
U_o, U	Flow velocity at the tap hole exit and its value at the distance Z from the tap hole exit, cm/sec
V_g^o, V_g	Rates of the gas entrainment of the vertical stream and of the tilting stream, respectively, cm^3/sec
V_h	Volume of the stream of liquid metal at a small length Δh, at a height h
V_l	Rate of tapping, cm^3/sec
We	Weber number
W_i	Initial mass of the liquid steel in the converter, g
W_L	Mass of the liquid steel in the ladle at time t, g
W_m	Weight of the liquid steel in the converter at time t, g
Z_t, Z_f	Tapping height and it's final value, cm
θ, θ'	the angle of BOF with the horizontal axis and incident angle of the tapping stream to the liquid steel pool in the ladle, degrees
$\eta_{O_2}^b, \eta_{N_2}^b$	Absorption efficiency at the bubble-liquid interface of oxygen and nitrogen respectively
$\varepsilon, \varepsilon_o$	Amplitude of disturbance present on surface of stream at a distance Z and at the tap hole exit, respectively, cm
λ	Wave length of the ripples at the surface of liquid steel, cm
$\sigma_{s\text{-}a}$	Surface tension at air and liquid steel interface, dyn/cm
ρ_{Fe}	Density of liquid steel, g/cm^3

3.2 Thermodynamics of deoxidation by aluminum

The amount of aluminum reacted to obtain a given dissolved oxygen content, at a particular temperature can be calculated as follows

$$2[Al] + 3[O] \rightarrow [Al_2O_3] \quad (3.31)$$

Let the initial conc:	X	Y	0
Let the final conc:	X-2x	Y-3x	x

Let the initial moles of iron present be Z. The total number of moles of iron, aluminum and oxygen at equilibrium is Z+X+Y-5x

The equilibrium concentrations of Al and O in bulk are related to the equilibrium constants, K_e,

$$K_e = \frac{a_{Al_2O_3}}{(h_{Al})^2 (h_O)^3} \quad (3.32)$$

$$\text{Where } \log K_e = \frac{58473}{T} - 17.74, \quad (3.33)$$

and $h_{Al} = f_{Al}(\text{mass\%Al})$, $h_O = f_O(\text{mass\%O})$

The equilibrium mass percentage of aluminum, $[Al]_e$, can be calculated from

$$[Al]_e = \frac{(X-2x)*27*100}{27*(X-2x)+16*(Y-3x)+56*Z} \quad (3.34)$$

The equilibrium mass percentage of oxygen, $[O]_e$, can be calculated from

$$[O]_e = \frac{(Y-3x)*16*100}{27*(X-2x)+16*(Y-3x)+56*Z} \quad (3.35)$$

On substitution to Eqn (3.32),

$$K_e = \frac{1}{\left[\frac{f_{Al}*27*(X-2x)*100}{27*(X-2x)+16*(Y-3x)+56*Z}\right]^2\left[\frac{f_O*16*(Y-3x)*100}{27*(X-2x)+16*(Y-3x)+56*Z}\right]^3} \quad (3.36)$$

In our calculations activity coefficients of aluminum, (f_{Al}), and oxygen, (f_O), and the activity of alumina, ($a_{Al_2O_3}$), are assumed to be unity for the shake of simplicity. The non-linear Equation (3.36) can be solved for one unknown x since the values, K_e, X, Y, Z, f_{Al}, f_o are already known.

The decrease in oxygen content of the bath due to deoxidation, ΔO_T, is

$$\Delta O_T = -([O]_i - [O]_e)\frac{W_m}{100} \text{ kg} \quad (3.37)$$

Where, $[O]_i$ and $[O]_e$ are the initial and equilibrium mass percent of oxygen in the bath, and W_m is the weight of the liquid steel.

The increase in aluminum content in the bath is ΔAl_T

$$\Delta Al_T = ([Al]_i - [Al]_e)\frac{W_m}{100} \text{ kg} \quad (3.38)$$

Where, $[Al]_i$ and $[Al]_e$ are the initial and equilibrium mass percent of aluminum in the bath.

Now, theoretically 1.125 kg aluminum is needed for removal of 1kg oxygen. Hence, theoretical aluminum needed for deoxidation, T_{Al}, is

$$T_{Al} = 1.125\,|\Delta O_T| + \Delta Al_T \quad (3.39)$$

In a practical situation, a part of aluminum charged into the steel may burns or react with the atmosphere. If the efficiency of aluminum utilization is η_{AL} then the amount of aluminum needed to be charged is

$$Al_{Charge} = \eta_{Al} T_{Al} \quad (3.40)$$

Aluminum, the deoxidizer, is usually charged into the liquid steel during tapping in the form of aluminum ingots (20 kg blocks, at Bokaro steel plant). The aluminum blocks dissolve rapidly into the steel due to the turbulence created by the tapping stream. The calculations of efficiency of aluminum utilization (recovery) for the situation of Bokaro Steel Plant are discussed in sec 3.5.3

3.3 Nucleation and growth of alumina particles in the melt

The deoxidation reaction (of dissolved aluminum with dissolved oxygen) proceeds through the following steps

1. Nucleation of the solid alumina particles
2. Subsequent growth of inclusions by mass transfer
3. Growth of inclusions by collision with other inclusions (Brownian motion, Stokes' collision, laminar shear etc.)
4. Assimilation of inclusions by top slag

Nucleation of alumina particles is discussed first (section 3.3.1), followed by development of the kinetic model and its application to 300 ton ladle (section 3.5). The phenomenon of growth and also removal of inclusions is reviewed in section 3.3.2-3.4.4, followed by application of different models in section 3.5.

3.3.1 Nucleation of solid alumina particles in molten steel

According to the classical theory of homogeneous nucleation, the solid alumina inclusions may start to nucleate from the parent phase (melt) when the change in the Gibbs free energy for the deoxidation reaction (Eqn 3.31) is negative. At equilibrium,

$$\frac{d\Delta G}{dr} = 0 \qquad (3.41)$$

Where, r is the radius of the nucleous. The shape of the nucleating particles may be spherical, planar, cylindrical or star shaped. For the sake of simplicity, we assume the shape of the nuclei to be spherical. In the case of spherical particles, the sum of volume of free energy and the surface energy created owing to the formation of new surfaces is given by,

$$\Delta G = \frac{4}{3}\pi r^3 \Delta G_v + 4\pi r^2 \sigma \qquad (3.42)$$

Where, ΔG_v is the change in free energy per unit volume, and $\sigma_{s\text{-}i}$ is the surface tension between Al_2O_3 particle and liquid steel.

On solving equation (3.41) and (3.42)

$$\Delta G_v = -\frac{2\sigma_{s-i}}{r_C} \qquad (3.43)$$

The value of ΔG_v is given by:

$$\Delta G_v = -\frac{RT}{V_m}\ln \Pi \qquad (3.44)$$

The super saturation, Π, is the ratio of the actual and the equilibrium concentrations

$$\Pi = \frac{C_t}{C_{eq}} \qquad (3.45)$$

Assuming that Al_2O_3 is pure, $a_{Al2O3} = 1$. Thus,

$$\frac{C_t}{C_{eq}} = \frac{K}{K_e} = \frac{([mass\%Al]_b)^2([mass\%O]_b)^3}{K_e} \tag{3.46}$$

Where, $[mass\%Al]_b$ is the mass percentage of aluminum in bulk, $[mass\%O]_b$ is the mass percentage of oxygen in bulk. The value of K_e can be calculated from Eqn (3.33). From equations (3.44), (3.45) and (3.46), the following expression is obtained for the critical radius, r_c ,of the nucleous:

$$r_C = \frac{2\sigma V_m}{RT \ln \Pi} = \frac{2\sigma V_m}{RT \ln\left(\frac{([mass\%Al]_b)^2([mass\%O]_b)^3}{K_e}\right)} \tag{3.47}$$

The critical radius is defined as the minimum radius of a nucleus for which the thermodynamic conditions are satisfied, and, therefore, nucleation can occur only when $r > r_c$. From equation (3.47) we can easily see that the critical radius of a nucleus decreases with increase of super saturation and with decrease of surface tension. Also, since super saturation changes both with time and temperature during the deoxidation process, the critical radius also changes accordingly.

The value of the critical radius is the starting radius of each inclusion. Subsequent increment to radius (i.e. growth of nucleous) takes place by mass transfer.

3.3.2 Growth of nucleous:

Once a stable nucleous has formed, it begins to grow by diffusion of [Al] and [O] to Al_2O_3

$2[Al] + 3[O] \rightarrow [Al_2O_3]$

Aluminum and oxygen dissolved in the melt combine at the interface of the inclusion to form Al_2O_3. A boundary layer develops at the surface of the inclusion and metal, as shown in the diagram (Fig. 3.2). Diffusion of any one or both the elements (Al and O) across the boundary layer may be considered as the rate determining step.

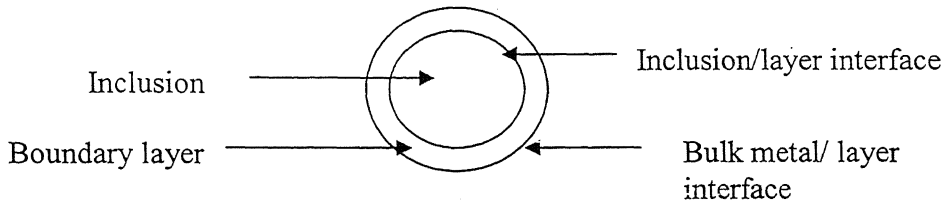

Fig. 3.2: The boundary layer formed at the surface of the inclusion and metal

3.3.3 Calculation of interfacial concentrations of oxygen and aluminum

(a) Calculation of interfacial concentration oxygen

Similar to the method discussed at section 3.2 the equilibrium mass percentages of aluminum and oxygen can be calculated from Eqns (3.34) and (3.35).

The equilibrium constant, K_e, of reaction (3.31) from the Eqn (3.33). At the inclusion-liquid steel interface the value of K_e is given by

$$J_O = k_O(C_O^b - C_O^i) \tag{3.52}$$

Flux balance of the mixed mass transfer controlled reaction is

$$\frac{1}{2}\frac{d[Al]}{dt} = \frac{1}{3}\frac{d[O]}{dt} = \frac{d[Al_2O_3]}{dt} \tag{3.53}$$

From Eqns (3.51-3.53), the equation for the interfacial concentration of aluminum at the particle-bulk interface, C_{Al}^i, can obtained

$$C_{Al}^i = \frac{3.k_{Al}.C_{Al}^b - 2k_O(C_O^b - C_O^i)}{3.k_{Al}} \tag{3.54}$$

Where, C_{Al}^b is the concentration of aluminum in bulk, C_O^i is the concentration of oxygen at interface, C_O^b is the concentration of oxygen in bulk, k_{Al}, k_O are mass transfer coefficients of aluminum and oxygen, respectively.

From Eqn (3.54) the value of C_{Al}^i can be calculated for a particular time step if the values of C_{Al}^b, C_O^i, C_O^b, k_{Al}, k_O are known. The value of C_{Al}^i and C_O^i can be calculated by iterative method by using Eqns (3.50) and (3.54).

A function formed by using Eqn (3.54) is

$$F(C_{Al}^i) = C_{Al}^i - \frac{3.k_{Al}C_{Al}^b - 2k_O(C_{Al}^b - C_O^i)}{3.k_{Al}}$$

$$\text{Or, } F(C_{Al}^i) = C_{Al}^i - \left[C_{Al}^b - \frac{2k_O}{3.k_{Al}} \left\{ C_O^i - \left(\frac{\rho_{Fe}}{\rho_O}\right) \times \sqrt[3]{\frac{1}{K_e\left[C_{Al}^i \times \left(\frac{\rho_{Al}}{\rho_{Fe}}\right)\right]^2}} \right\} \right] \tag{3.55}$$

The function $F(C_{Al}^i)$ (Eqn 3.55) can be solved by using different starting values of C_{Al}^i. At the correct value of interfacial concentration the value of the function would

be zero. The corresponding value of C_O^i can be calculated by using C_{Al}^i, obtained from the iteration, in Eqn (3.50).

The bulk composition of dissolved aluminum is given by

$$C_{Al}^b = [mass\%Al^b]\frac{\rho_{Fe}}{100 \times M_{Al}} \tag{3.56}$$

Where, M_{AL} is the molecular weight of aluminum.

The composition of dissolved oxygen in the bulk is given by

$$C_O^b = [mass\%O^b]\frac{\rho_{Fe}}{100 \times M_O} \tag{3.57}$$

It can be seen from Eqn (3.54) that the interfacial concentrations of aluminum and oxygen will continuously change with time as the bulk concentrations change continuously.

3.3.4 Increase in radius of inclusion

The total initial volume of an inclusion of radius r is

$$Vol = \frac{4}{3}\pi * r^3 * n \tag{3.58}$$

Where, n = number of inclusions present in the liquid steel.

The increase in radius of an inclusion can be calculated as follows.

$$\frac{dn_{Al_2O_3}}{dtA} = J_{Al_2O_3} = \frac{1}{2}J_{Al}$$

$$\text{Or, } \frac{dn_{Al_2O_3}}{dtA} = \frac{1}{2}k_{Al}(C_{Al}^b - C_{Al}^i)$$

$$\text{Or, } \frac{dw_{Al_2O_3}}{dt \times 102} = \frac{1}{2}Ak_{Al}(C_{Al}^b - C_{Al}^i)$$

$$\text{Or, } \frac{d(\frac{4}{3}\pi r^3)\rho_{\ldots}}{dt} - \frac{1}{2}102 \times 4\pi r^{\cdot} \times k_{Al}(C_{Al} - C_{Al})$$

$$\text{Or, } \frac{4}{3}\pi\rho_{Al_2O_3} \times 3r^2 \frac{dr}{dt} = \frac{102}{2} \times 4\pi r^2 \times k_{Al}(C^b_{Al} - C^i_{Al})$$

$$\text{Or, } \frac{dr}{dt} = \frac{51}{\rho_{Al_2O_3}} k_{Al}(C^b_{Al} - C^i_{Al})$$

Density of inclusion, $\rho_{Al_2O_3}$, is 4000 kg/m^3. Therefore,

$$\frac{dr}{dt} = \frac{51}{4000} k_{Al}(C^b_{Al} - C^i_{Al})$$

$$\text{Or, } \frac{dr}{dt} = 0.01275 k_{Al}(C^b_{Al} - C^i_{Al}) \qquad (3.59)$$

From equation (3.59), the increment in radius, dr, can be calculated during each time step dt. After each time step, the bulk concentrations of oxygen and aluminum are updated. Growth of nuclei will occur untill equilibrium concentration is achieved in bulk.

3.3.5 Change in bulk concentration of aluminum and oxygen in the bath

From the flux balance the change in aluminum and oxygen in a small time step dt can be calculated by

$$\frac{d[Al_2O_3]}{dt} = \frac{1}{2}\frac{d[Al]}{dt} \text{ and } \frac{d[Al_2O_3]}{dt} = \frac{1}{3}\frac{d[O]}{dt}$$

Change in mass of alumina in the bath in a small time step dt is

$$d[Al_2O_3] = N_0 \frac{4}{3}\pi\{[r + dr]^3 - r^3\}\rho_{Al2O3} \qquad (3.60)$$

Where, N_0 is the number of inclusion present at time t. r and (r + dr) are the radius of particles at time t and (t + dt), respectively.

$$d[mass\%Al] = \frac{2 \times d[Al_2O_3]}{W_m} \times 100 \quad (3.61)$$

$$d[mass\%O] = \frac{3 \times d[Al_2O_3]}{Wm} \times 100 \quad (3.62)$$

The change in bulk concentrations of aluminum and oxygen is updated and can be use for the next time step.

3.4 Growth of inclusion by collision mechanisms

As mentioned above, the size of nuclei increases initially due to the diffusion of aluminum and oxygen towards the nucleus-steel interface (as discussed in Section 3.3.4). The inclusions can also grow in size by simultaneous contribution of one or more of the following mechanisms, depending upon the flow/mixing/stirring conditions present in the ladle [3.13-3.16]

- Ostwald ripening (diffusion coalescence)
- Brownian motion
- Stokes collision
- Turbulent collision
- Laminar shear

3.4.1 Ostwald ripening

In Ostwald ripening, small inclusions, which form in a system initially, slowly disappear because they combine (by diffusion coalescence) with larger crystals. The smaller crystals thus act as "nutrients" for the bigger crystals. As the larger crystals grow, the area around them is depleted of smaller ones. It has been reported that the relative contribution of Ostwald ripening to inclusion growth is almost negligible [3.9, 3.14] because it is a very slow process (atomic diffusion over short distances).

3.4.2 Growth of inclusions by collisions caused by Brownian motion

Collision of inclusions due to Brownian motion has been described by the Stoke-Einstein equation and the collision volume is given by [3.13-3.16]

$$W_{ij}^{B} = \frac{2KT}{3\mu_{Fe}}\left(\frac{1}{r_i}+\frac{1}{r_j}\right)\left(r_i + r_j\right) \qquad (3.63)$$

Where, k is the Boltzmann constant, and T is the temperature. In principle, the contribution of Brownian motion to inclusion growth should be limited to small particles (of approximately 1 micron) because only they can move randomly in a fluid. Further, for the contribution of Brownian motion to inclusion growth to be significant, the difference in inclusion sizes must also be large. For example, if $r_i = r_j$ in Eqn (3.63) the value of W_{ij}^{B} increases only by a factor of 4 but if $r_i = 100r_j$ then the value of W_{ij}^{B} increases by factor of 100. Collision volume for Brownian motion nearly attains a constant value after approximately 1 μm (Fig. 3.3)

3.4.3 Growth of inclusions by Stokes' collision

The inclusions rise through the steel bath because of the difference in density between steel and the oxide (alumina). The rising velocity (governed by Stokes' law) increases with increasing size. Large inclusions rise at a faster rate than the small inclusions. Thus, during their rise large inclusions can collide with the smaller inclusions (called Stokes' collision) and grow in size.

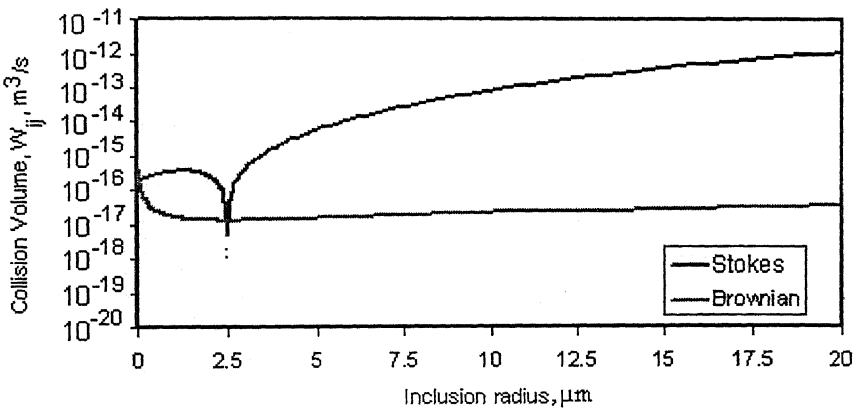

Fig. 3.3: Collision volumes of different mechanisms (for an inclusion with a 2µm radius) as a function of radius of the other inclusions

The collision volume of inclusions formed by Stokes' collisions, as suggested by Lindborg and Torssell [3.7],

$$W_{ij}^{s} = \frac{2\pi g(\rho_{Fe} - \rho_i)}{9\mu_{Fe}}(r_i + r_j)^3 \mid r_i - r_j \mid \qquad (3.64)$$

Where g is the gravitational acceleration, μ is the dynamic viscosity, and ρ_{fe} and ρ_i are the densities of the steel and the inclusion, respectively. It has been reported that for an inclusion of 2μm radius the contribution of Stokes' collision to inclusion growth is significant only for inclusions of size grater than 5μm. The variation of collision volume with inclusion size is shown in Fig. 3.3; it is clear that only after 5μm microns the collision volume increases [3.14].

3.4.4 Growth of inclusions by turbulent collision

The inclusions can collide with each other due to the influence of the turbulent eddies present in liquid bath. Saffman and Turner [3.10] described a model for growth of rain drops by turbulent collision. The same model has been adopted for the case of inclusions in liquid steel [3.10]. The equation for the collision volume created due to turbulent collision is

$$W_{ij}^{T} = 1.3\pi^{1/2}\alpha(r_i + r_j)^3\sqrt{\frac{\varepsilon}{\nu_{Fe}}} \qquad (3.65)$$

Where ε is the turbulent energy dissipation, ν_{Fe} is the kinematic viscosity of steel, and α is the collision efficiency. In literature, α is reported to vary between 0.27-0.65 for alumina inclusions in liquid steel. The effect of turbulent collisions is found to be most prominent on inclusions which are above 1-2 μm in size.

3.4.5 Growth of inclusions by laminar shear

The inclusions can move along with the different laminar streams in the metal bath. The laminar streams may form by stirring, due to temperature gradient or due to metal flow during teeming. An inclusion moving in a fast streamline can collide with an inclusion moving in a slower streamline. The collision volume of inclusions formed by collision due to laminar shear, W_{ij}^{L}, as suggested by Smoluchowski [3.3], is given by

$$W_{ij}^{L} = \frac{4}{3}\left(r_i + r_j\right)^3 \frac{du}{dx} \qquad (3.66)$$

Where, $\frac{du}{dx}$ is the velocity gradient in the direction where laminar flow exists.

3.4.6 Decrease in the number of inclusions due to collision

Let the initial inclusion size, after the attainment of deoxidation equilibrium, be r_o and the number of inclusions present in the metal be n_o. Now, some of the inclusions can collide with each other (collision mechanism) and form bigger sized particles. If two n_o sized particles, in a small time step Δt, collide and form a new inclusion of size r_1 then,

$$r_1 = \sqrt[3]{r_o^3 + r_o^3} = \sqrt[3]{2}.r_o \qquad (3.67)$$

Again, after a small time step Δt, some of the newly formed particles (of radius r_1) can collide with other inclusions present in the bath. If particles of radius r_1 and r_0 collide with each other then the resultant radius would be $\sqrt[3]{3}.r_o$. For the collision between two particles of same diameter, r_1 the resultant radius would be $\sqrt[3]{4}.r_o$, and so on. The general expression for r_n can, therefore, be written as

$$r_n = \sqrt[3]{m}.r_o \tag{3.68}$$

where, n and m are integers. The growth process may continue in this manner till solidification. The total number of inclusions present in the bath decreases due to merging of inclusions by collision mechanisms, and the rate of decrease of the number of particles can be calculated by the general equation

$$-\frac{dn_{ij}}{dt} = \sum_{K=S}^{T,B} W_{ij}^{K} N_i N_j \tag{3.69}$$

Where N_i and N_j are the number of inclusions, respectively, of two different sizes, and W_{ij}^{K} is the collision volume of the particular mechanism (such as stokes, turbulent etc.).

3.4.7 Decrease in the number of inclusions due to assimilation by top slag

When an inclusion reaches the top surface of metal it can get assimilated into top slag. For a given bath height H, the decrease in the number of inclusions due to assimilation can be calculated from

$$-\frac{dn_i}{dt} = \frac{2g}{9\mu}(\rho_{Fe} - \rho_i) r_i^{\,2} \frac{N_i}{H} \tag{3.70}$$

It may be noted that the processes of decrease in number of inclusions by collision and due to assimilation by top slag go on concurrently.

3.4.8 Growth of inclusions by simultaneous action of two or more mechanisms

Different mechanisms of inclusion growth, as described above, can occur simultaneously. Lindborg and Torssell Model [3.7] suggested in 1968 a model in which only Stokes and gradient collision were considered to act simultaneously. Iyengar and Philbrook[3.8] suggested, in 1972, a model in which Stokes and turbulent collision were considered simultaneously. In fact, since 1970, there have been many studies to predict the growth and removal of inclusions in liquid steel. These studies[3.13-3.16] are not limited to the case of a ladle stirred by natural convection, but also extended to removal of inclusion to the slag, removal of inclusion to the refractory surfaces, removal of inclusion by gas purging (attachment of inclusions to bubbles: Bubble flotation models), removal of inclusion due to induction stirring, floatation of inclusions in tundish, etc. Most of these studies make use of the work by Lindborg – Torssell, and by Iyengar - Philbrook these two models are described in this section.

(a) Lindborg and Torssell Model [3.7]:

According to this model, the rate of change of radius of inclusion, before the attainment of deoxidation equilibrium, is obtained from flux equation based on mass transport control,

$$\frac{dr}{dt} = \left[\frac{D}{r} \frac{C_\infty(t) - C_0}{C_p - C_0} \right] \qquad (3.71)$$

Where,

C_∞ is the time-dependent solute concentration at a large distance from the particle, C_0 is the solute concentration adjacent to the particle, C_p is the concentration of solute inside the particle itself.

$$C_\infty(t) = C_\infty(0) - N\left[\frac{3}{4.\pi}\right] r^3(t)(C_p - C_0) \tag{3.72}$$

The radius of the final particle, at equilibrium, can be calculated from

$$r_f = \left[\frac{3}{4.\pi.N}\frac{C_\infty(0) - C_0}{C_p - C_0}\right]^{1/3} \tag{3.73}$$

Only Stokes and gradient collisions are considered in this model. The effect of turbulent eddies in the collision mechanism has been neglected. Also, the effect of Brownian motion has been neglected for the large size of inclusions.

If the inclusions in the steel bath have a density function f(r) then the volume of the inclusions is

$$\mathrm{I} = \int f(r)\frac{4}{3}\pi.r^3 dr \tag{3.74}$$

Now, according to Eqn (3.67), if two particles with radius r_1 and r_2 collide, the resultant size is $R = \sqrt[3]{r_1^3 + r_2^3}$, Because of collision there is a decrease in the density function $f(r_1)$ and $f(r_2)$ and an increase in f(R). The rate of change in $f(r_1)$ will be the sum over all particles raidus r_1 colliding during time step dt

$$\frac{df(r_1)}{dt} = -f(r_1)\int_0^\infty f(r_2).W(r_1, r_2)dr_2 \tag{3.75}$$

Where $W(r_1,r_2)$ is the collision volume which can be calculated for an assumed mechanism (Eqns 3.63-3.66). There is also formation of particle of radius r_1 due to collision of particles having radius smaller than r_1. A single generalized formula has been obtained to calculate the change in density function as follows

$$\frac{df(r)}{dt} = \frac{1}{2}\int_0^r f(r_1).W(r_1,r_2).f(r_2)\left(\frac{r_1}{r_2}\right)^2 dr_1 - f(r_1)\int_0^\infty f(r_2).W(r_1,r_2)dr_2 \qquad (3.76)$$

Finally, a decrease in the value of f(r) takes place due to the assimilation of inclusions in the slag phase. The rate of change of f(r) due to this process is

$$\frac{df(r)}{dt} = -f(r_1)\frac{u_r}{h} \qquad (3.77)$$

Where, u_r is the upward velocity of inclusions according to Stokes' law and h is the height of the melt. The overall value of rate of change of f(r) with time is obtained by adding Eqns (3.76) and (3.77).

(b) Iyengar and Philbrook Model[3.8]:

The motion of inclusions in a laminar flow due to natural convection in the r and z directions of a cylindrical coordinate system is given by

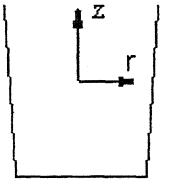

$$m\frac{du_r}{dt} = 6.\pi.\mu.r.(u_r - v_r)$$

$$m\frac{du_z}{dt} = (m - m').g + 6.\pi.\mu.r.(u_z - v_z)$$

Here z axis is in the vertical direction and r is radial direction from the centre of the ladle.

If u_z and u_r are the velocity of the inclusion int the upward and radial directions, respectively, then the displacement of an inclusion particle from its initial position can be calculated from the following equations,

$$\frac{dr}{dt} = u_r \text{ and } \frac{dz}{dt} = u_z$$

According to Smoluchowski[3.9], if Brownian motion and fluid dynamic interaction between the particles are neglected then the probability of collision between the r_i and r_m sized particle is

$$p(i,m) = \frac{4}{3}\pi.G.(r_i + r_m)^3 N(r_m) = V_{gr} N(r_m) \quad (3.78)$$

The particle collision frequency, p(i,m), due to turbulent flow field inside the steel bath[3.10] is

$$p(i,m) = \frac{4}{3}\pi.\left(\frac{\varepsilon}{v}\right)^{1/2} (r_i + r_m)^3 N(r_m) \quad (3.79)$$

If there are $N(r_i)$ inclusions per unit volume with radius r_i and $N(r_m)$ inclusions per unit volume with radius r_m, then according to Smoluchoski[3.9] , the number of collisions per second between these two species of inclusions is,

$C(i,m) = Vgr\ N(r_m)\ N(r_i)$

If the collision efficiency in a convective flow is E_{gr} (value less than unity), then we can modify the above equation as

$$C(i,m) = Vgr\ N(r_m)\ N(r_i)\ E_{gr} \quad (3.80)$$

Where Vgr is the collision volume per unit time for an inclusion with radius r_i and r_m under a velocity gradient

The contribution to Vgr comes from two sources:

1. Collision in the peripheral or annular region (G_p)
2. Collision in the axial or pipe region (G_a)

$$\text{Therefore, } V_{gr} = \frac{4}{3}\pi(r_i + r_m)^3 (G_p + G_a) \quad (3.81)$$

$$\text{And } C(i,m) = N(r_i)N(r_m)\frac{4}{3}\pi(r_i + r_m)^3 (G_p + G_a)E_{gr}$$

Adding the contribution of Stokes' collision to the above,

$$C(i,m) = N(r_i)N(r_m)\pi(r_i + r_m)^3\left\{\frac{4}{3}(G_n + G_n)E_{..} + |r_i + r_m|k.E_{..}\right\} \qquad (3.82)$$

The values of E_{gr} [3.11-3.12] and E_{stk} can be calculated from the following equations,

$$E_{gr} = \left(1 + \frac{0.75 \times \ln(2.Stk)^{-2}}{Stk - 1.214}\right) + \left(1 + \frac{r_m}{r_i}\right)^2 - \frac{3}{2}\left(1 + \frac{r_m}{r_i}\right) + \frac{1}{2.\left(1 + \frac{r_m}{r_i}\right)} \qquad (3.83)$$

Where $r_m < r_i$ and,

$$E_{Stk} = \left(\frac{0.0625\left(r_m / r_i\right)^2}{\left(1 + r_m / r_i\right)^2}\right) \qquad (3.84)$$

Finally, the expression for rate of change in the number of inclusions with radius r_i is[3.8]

$$\frac{dN(r_i)}{dt} = \frac{1}{2}\int_{r_m=0}^{r_i}\int_{r_i=0}^{r_i} C(l,m_i)dr_m dr_l - \int_0^{r_{max}} C(i,m_i)dr_m - f(s) \qquad (3.85)$$

The meanings of different symbols, used in this section, are described in Table. 3.2.

Table 3.2: List of Symbols used in section 3.5.8

Symbol	Meaning	Symbol	Meaning
C(i,m)	Number of collisions per unit volume per unit time between inclusions with radius r_i and r_m	r_{max}	Radius of the largest inclusion in steel
E_{gr}	Collision efficiency due to a velocity gradient in liquid steel	Re	Reynolds number for the larger inclusion
E_{Stk}	Collision efficiency due to Stokesian rise	Stk	Stokes number = $\frac{\rho_s.\mathrm{Re}}{9.\rho}$
G	Average velocity gradient	t	Time
Ga, Gp	Average velocity gradient in axial and peripheral region	u_r, u_z	Velocity of an inclusion in r and z direction
g	Acceleration due to gravity	v_r, v_z	Average fluid velocities in r and z directions
k_s	Constant in Stokes' equation	V	Volume of an inclusion
L	Height of ladle	V_{gr}	Collision volume per unit time for an inclusion with radius r_i and r_m under a velocity gradient
m_i	Mass of inclusion	V_{cr}	Volume of the ladle
m′	Mass of liquid steel displaced by an inclusion	r	Radial direction
$N(r_m)$	Number of inclusions with radius r_m per unit volume of liquid steel	z	Vertical direction

$p(i,m)$	Frequency of collisions per unit time of an inclusion with radius r_i with inclusion r_m	ε_e	Energy dissipated per unit time per unit mass
$\Delta p/L$	Pressure gradient	ρ, ρ_s	Density of liquid steel and inclusion, respectively
r	Radius of an inclusion r	μ	Viscosity of steel
r_i	Radius of inclusion i; i = i, m, l	ν	Kinematic viscosity of steel

3.5 Results and Discussion: Application to 300 ton BOF at Bokaro Steel Plant

3.5.1 Prediction of nitrogen and oxygen pickup from ambient atmosphere during the tapping operation

A user friendly computer program has been developed to calculate the pickup of nitrogen and oxygen by molten metal stream during tapping. Flow chart of the algorithm is shown in Fig. 3.4 and various steps of calculation are as follows

Step 1: Enter relevant input through user friendly interface, and save to input file "Data.txt

Step 2: Set initial time, t_o, is zero i.e., $t = 0$ and the time step Δt is 0.01 sec (say).

Step 3: Calculate the total bath height Z_t at time t by Eqn (3.9)

Step 4: Set the distance from tap hole, h, of a volume, ΔV of liquid metal corresponding to small height, Δh, as zero, i.e., $h = 0$

Step 5: Calculate the interfacial nitrogen and oxygen concentrations i.e. concentrations at the interface of air-tapping stream, by using Eqns (3.1) and (3.3)

Step 6: Calculate the increase in dissolved nitrogen and oxygen content of the small volume ($\Delta[\bar{N}]_{TS}$ and $\Delta[\bar{O}]_{TS}$, respectively), due to absorption through the surface of the tapping stream, in time Δt by using Eqn (3.2) and (3.4)

Step 7: Increase in the nitrogen and oxygen content of the bulk in ΔV in Δt is calculated by using Eqns (3.5) and (3.6)

Step 8: The value of h is incremented by Δh. If $h < Z_t$ then go to Step 3, else continue

Step 9: Calculate the total increase of nitrogen and oxygen of steel by the tapping stream, from Eqns (3.7) and (3.8)

Step 10: Calculate the nitrogen and oxygen concentrations at the interface of air-metal bath by using Eqns (3.1) and (3.3)

Step 11: Calculate the increase in nitrogen and oxygen content of the metal bath ($\Delta[\bar{N}]_S$ and $\Delta[\bar{O}]_S$, respectively) in time step Δt, due to absorption from atmosphere, by using Eqns (3.11) and (3.12)

Step 12: Calculate the increase in nitrogen and oxygen content of the bath, due to dissolution of the entrained gas bubbles ($\Delta[\bar{N}]_{bbl}$ and $\Delta[\bar{O}]_{bbl}$, respectively) in time step Δt, by using Eqns (3.25) and (3.26). The parameters used in Eqn (3.25) and (3.26) can be calculated from Eqns (3.13–3.24)

Step 13: Calculate the total increase in nitrogen and oxygen content of the bath during the small time step Δt by using Eqns (3.27–3.29)

Step 14: The value of t is now incremented by Δt. If $t <$ total tapping time then go to Step 3, else continue

Step 15: Calculate increase in total nitrogen and oxygen content of the bath ($\Delta[\bar{N}]$ and $\Delta[\bar{O}]$, respectively) during tapping period by using Eqns (3.28) and (3.30)

Step 16: Display the results of total nitrogen and oxygen pickup within the tapping time in the output window

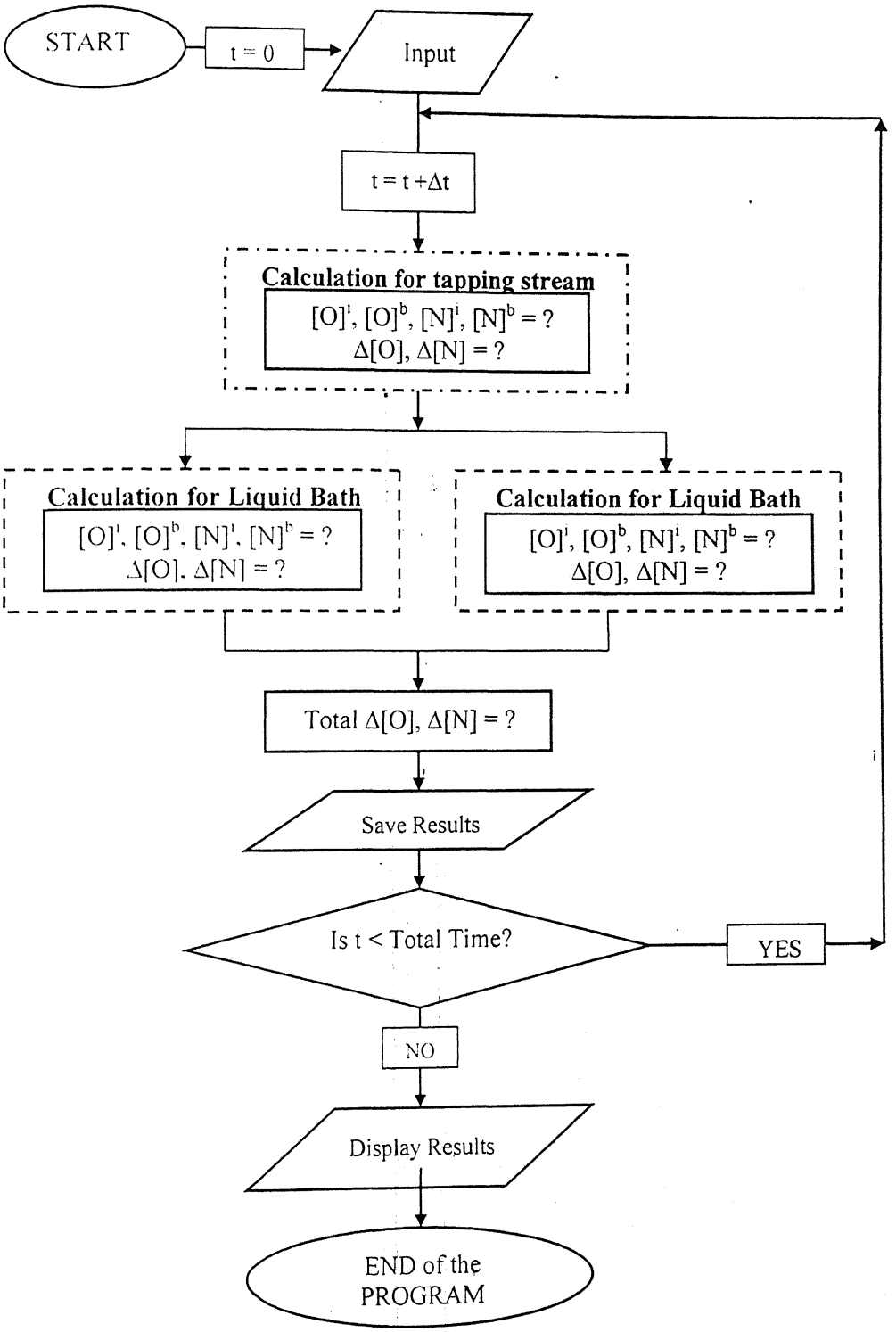

Fig. 3.4: Flow chart of oxygen and nitrogen absorption during tapping of liquid steel

It is assumed that all the nitrogen and oxygen gas present in the bubble is dissolved in the bath (i.e. 100% dissolution of the gas into the bath) and the other parameters/conditions (assumed in case of 300 ton BOF) are given below

Symbol	Meaning of the symbol	Numerical value
d_n	Diameter of the exit nozzle of the converter	14 cm
h	Height of steel above the inlet of tap hole in the converter	100 cm
H	Height of the converter	600 cm
K_N	Mass transfer coefficient of nitrogen in the liquid phase	0.0025 cm/s
K_O	Mass transfer coefficient of oxygen in the liquid phase	0.0025 cm/s
l_o	Length of the exit nozzle of the converter	100 cm
T	Temperature of liquid steel	1923 K
t_T	Total tapping time	12 min
Z_F	The distance between top of the ladle and bottom of converter	400 cm
Z_L	The height of metal pool in the ladle	600 cm
Z_t	tapping height	1479 cm
$\theta_{initial}$	Initial Angle of ejection of the liquid metal through the nozzle exit of the converter. θ decreases linearly with tapping time	15 °
ρ_{Fe}	Density of liquid steel	7 gm/cm^3
μ_{Fe}	Viscosity of liquid steel	0.05 g/cm.s
σ_{s-a}	Surface tension between air and liquid steel interface	5 dyn/cm

Δt	Small time step	0.1 sec

(a) Magnitude of nitrogen and oxygen pickup through the surface of falling stream

The increase in oxygen content, $\Delta[\bar{O}]_{TS}$, during the time step Δt can be calculated from Eqn (3.2)

$$\Delta[\bar{O}]_{TS} = \sum_{h=o}^{Z_R} K_O \frac{A_h}{\Delta V_h}([O]^i - [O]^b)\Delta t$$

Where, A_h and V_h are the exposed surface area and volume, respectively, of a small length of the tapping stream, Δh. The value of Δh is calculated by dividing the total stream length into 500 equal segments (decided a priori)

$$\Delta h = \frac{Z_t}{500}$$

The value of Z_t for the first time step, $\Delta t = 0.1$ sec, can be calculated from Eqn (3.9)

$Z_t = (L_H - Z_L) + Z_F + Z_C$

Where, L_H is the height of the ladle, Z_L is the height of the metal pool of the ladle, Z_F is the distance between top of the ladle and the bottom of the converter, Z_C s the distance between the position of the tap hole of the converter and the ladle

Now, $L_H = 600$, $Z_L = 0$, $Z_F = 400$, $Z_C = H \cos\theta - L_o$, $H=600$, $\theta = 15°$, $L_o = 100$

Hence, $Z_t = (600 - 0) + 400 + [600 \cos(15°) - 100]$

$= 1479.56$ cm

Therefore, the value of Δh is 2.96 cm

The interfacial mass % of oxygen can be calculated from Eqn (3.1)

$$K_O = \left(\frac{([O]^i)^2}{p_{O2}}\right) = 10^{\left[-\frac{11370}{T} + 3.645\right]}$$

$$\text{Or, } [O]^i = \sqrt{p_{O2} \cdot 10^{\left[\frac{11370}{-} + 3.645\right]}}$$

Since the temperature of steel T = 1923K and $p_{O2} = 0.21$, hence

$$[O]^i = \sqrt{0.21 \times 10^{\left[-\frac{11370}{1923} + 3.645\right]}}$$

$$= 0.0337\ \%$$

The initial mass % of oxygen in the bulk is 0.07%

The increase in oxygen content, $\Delta[\bar{O}]_{TS}$, during the time step Δt for a small length of the tapping stream, Δh, is

$$\Delta[\bar{O}]_{TS} = k_O \frac{A_h}{\Delta V_h}([O]^i - [O]^b)\Delta t$$

$$= k_O \frac{1}{\Delta h}([O]^i - [O]^b)\Delta t$$

Since $[O]^i = 0.0337$, $[O]^b = 0.07$, we get

$$\Delta[\bar{O}]_{TS} = 0.0025\frac{1}{2.96}(0.0337 - 0.07) \times 0.1$$

$$= 3.14 \times 10^{-6}\ \%$$

Similarly, the increase in the nitrogen content, $\Delta[\bar{N}]_{TS}$, during the time step Δt can be calculated from Eqn (3.4)

$$\Delta[\bar{N}]_{TS} = \sum_{h=o}^{Z_R} k_N \frac{A_h}{\Delta V_h}([N]^i - [N]^b)\Delta t$$

The interfacial mass % of oxygen can be calculated from Eqn (3.3)

$$K_N = \left(\frac{([N]^i)^2}{p_{N2}}\right) = 10^{\left[-\frac{371.9}{T} - 2.5\right]}$$

$$\text{Or, } [N]^i = \sqrt{p_{N2} \times 10^{\left[-\frac{371.9}{T} - 2.5\right]}}$$

Since in air $p_{N2} = 0.79$, we get

$$[N]^i = \sqrt{0.79 \times 10^{\left[-\frac{371.9}{1923} - 2.5\right]}}$$

$$= 0.0405\ \%$$

The initial mass % of nitrogen in the bulk is 0.005%. Hence the increase in nitrogen content, $\Delta[\bar{N}]_{TS}$, during the time step Δt for a small length of the tapping stream, Δh, is

$$\Delta[\bar{N}]_{TS} = k_N \frac{A_h}{\Delta V_h}([N]^i - [N]^b)\Delta t$$

$$= k_N \frac{1}{\Delta h}([N]^i - [N]^b)\Delta t$$

On substitution of the values calculated above,

$$\Delta[\bar{N}]_{TS} = 0.0025\frac{1}{2.96}(0.0405 - 0.005) \times 0.1$$

$$= 2.99 \times 10^{-6}\ \%$$

A typical profile of the increase in oxygen content caused by absorption through the surface of the tapping stream versus the distance from the exit of the tap hole of converter is shown in Fig. 3.5(a). Similar profile for nitrogen absorption is shown in Fig. 3.5(b).Total oxygen and nitrogen pickup, as indicated by the Figs. 3.5(a) and (b), is less than 2 ppm and can be ignored, when compared to absorption by other mechanisms (as discussed below)

(b) Magnitude of nitrogen and oxygen absorption through the surface of steel bath

Similar to the procedure followed in the previous section, the increase in oxygen content, $\Delta[\bar{O}]_{TS}$, during the time step Δt can be calculated from Eqn (3.11)

$$\Delta[\bar{O}]_S = k_O \frac{A_L}{\Delta V_L}([O]^i_{bath} - [O]^{bulk}_{bath})\Delta t$$

$$= k_O \frac{1}{L_H}([O]^i_{bath} - [O]^{bulk}_{bath})\Delta t$$

The value of height of the liquid in ladle, L_H, is 600 cm. The values of $[O]^i_{bath}$ and $[O]^{bulk}_{bath}$ can be obtained from Eqn (3.1) and (3.7). Hence,

$$\Delta[\bar{O}]_S = k_O \frac{A_L}{\Delta V_L}([O]^i_{bath} - [O]^{bulk}_{bath})\Delta t$$

$$= 0.0025 \frac{1}{600}(0.0337 - 0.0715) \times 0.1$$

$$= 1.51 \times 10^{-8} \%$$

The increase in nitrogen content, $\Delta[\bar{N}]_{TS}$, during the time step Δt can be calculated from Eqn (3.12)

$$\Delta[\bar{N}]_S = k_N \frac{A_h}{\Delta V_h}([N]^i_{bath} - [N]^{bulk}_{bath})\Delta t$$

For the liquid bath in a ladle, $\frac{A_h}{\Delta V_h} = L_H$. Therefore,

$$\Delta[\bar{N}]_S = k_N \frac{1}{L_H}([N]^i_{bath} - [N]^{bulk}_{bath})\Delta t$$

$$= 0.00025 \frac{1}{(\text{unit})} (0.0405 - 0.0066) \times 0.1$$

$$= 1.4125 \times 10^{-8} \%$$

(c) Magnitude of nitrogen and oxygen absorption due to dissolution of the entrained gas bubbles

The increase in oxygen content during the small time step Δt can be calculated from Eqn (3.26)

$$\Delta[\bar{O}]_{bbl} = \frac{0.00437 \eta_{O_2}^{b} V_g}{W_L} \Delta t$$

And, the increase in nitrogen content during the small time step Δt can be calculated by Eqn (3.25)

$$\Delta[\bar{N}]_{bbl} = \frac{0.0144 \eta_{N_2}^{b} V_g}{W_L} \Delta t$$

The different parameters which are needed so as to calculate $\Delta[\bar{O}]_{bbl}$ and $\Delta[\bar{N}]_{bbl}$ can be determined from the Eqns (3.13-3.24). Values of parameters used in the calculation are given below

Parameters	Calculated Value	Parameters	Calculated Value
Δt		m	1.57×10^4
U_o	3.87	E_1	3.43×10^{10}
U	2090.54	R_c	74.31
a_0	14	V_g	1.35×10^5
a	6.59	λ	55.19

We	2.93×10^6	θ'	86.76
Fr	10.89	ε	1.02
Re	7.58×10^5	$\eta_{O_2}^b$	1
W_L	4.167×10^4	$\eta_{N_2}^b$	1

Hence, the increase in oxygen content during the small time step Δt is

$$\Delta[\bar{O}]_{bbl} = \frac{0.00437\eta_{O_2}^b V_g}{W_L}\Delta t$$

$$= \frac{0.00437 \times 1 \times 1.35 \times 10^5}{4.167 \times 10^4} 0.1$$

$$= 1.416 \times 10^{-3}\ \% \ (\approx 14.16\ \text{ppm})$$

The increase in nitrogen content during the small time step Δt is

$$\Delta[\bar{N}]_{bbl} = \frac{0.0144\eta_{N_2}^b V_g}{W_L}\Delta t$$

$$= \frac{0.0144 \times 1 \times 1.35 \times 10^5}{4.167 \times 10^4} 0.1$$

$$= 4.665 \times 10^{-3}\ \% \ (\approx 46.65\ \text{ppm})$$

A typical profile of the increase in oxygen content caused by dissolution of the air bubbles entrained into the bath versus tapping time is shown in Fig. 3.6(a). Similar profile for nitrogen absorption is shown in Fig. 3.6(b). [O] and [N] absorption caused by dissolution of the air bubbles causes a significant increase in [O] and [N] contents in the liquid bath. It can be seen from the Eqn (3.9) that towards the end of tapping the total height of the falling stream is lower than that during the preceding time steps due to the filling up of the ladle and consequence decrease of Z_t. For this reason, the

entrainment of air bubbles also decreases with time. Figs. 3.6(a) and 3.6(b) show, therefore, a continuous decrease in the magnitude of nitrogen and oxygen pickup at different stages of tapping. The absorption caused by dissolution of the air bubbles entrained into the bath is significant; the total amount of oxygen pickup is approximately 13 ppm and that for nitrogen is 43 ppm (assuming 100% absorption efiiciency), for 12 minutes of tapping time for a case of 300 ton liquid steel at Bokaro steel plant.

A summary of nitrogen and oxygen pickup by different mechanism is given in Table 3.3 The total increase in bath oxygen is plotted as a function of time in Fig. 3.7(a) and the total increase in bath nitrogen is plotted as a function of time in Fig. 3.7(b).

It can be seen from Table 3.3 that approximately 90% of oxygen and nitrogen pickup is by the dissolution of gases in the entrained bubbles. The effect of tapping rate on total absorption is plotted in Fig. 3.8. As shown in the Fig. 3.8 the absorption of nitrogen and oxygen increases with increase in tapping rate. Absorption increase may be due to the extra turbulence induced in the metal stream and in metal bath owing to high tapping rate. There is an optimum tapping rate to balance temperature loss vis-à-vis gas pickup.

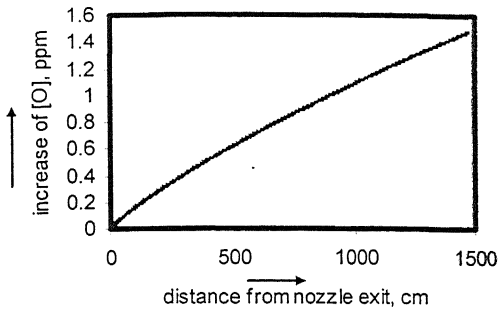

Fig. 3.5(a): Absorption of [O] through the surface of falling stream

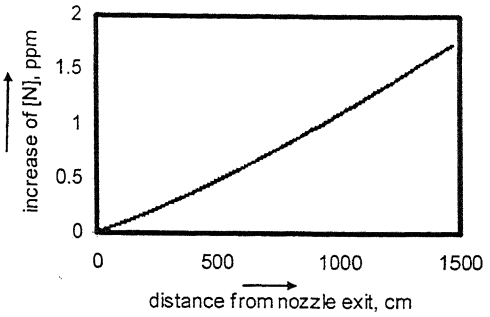

Fig. 3.5(b): Absorption of [N] through the surface of falling stream

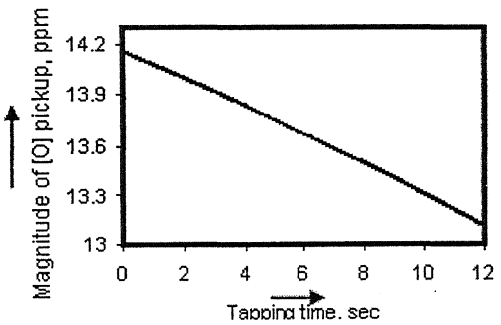

Fig. 3.6(a): Magnitude of [O] from entrained air bubbles at different tapping times of liquid steel

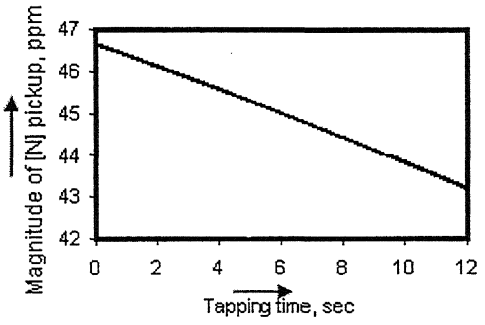

Fig.3.6(b): Magnitude of [N] from entrained air bubbles at different tapping times of liquid steel

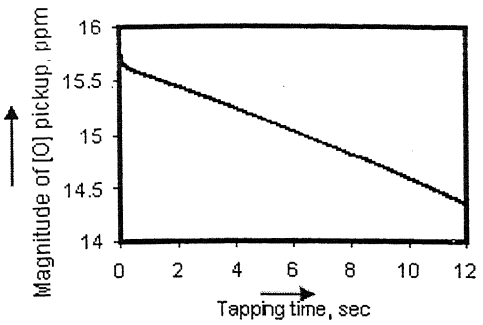

Fig. 3.7(a): Magnitude of [O] pickup by all mechanisms at different tapping times of liquid steel

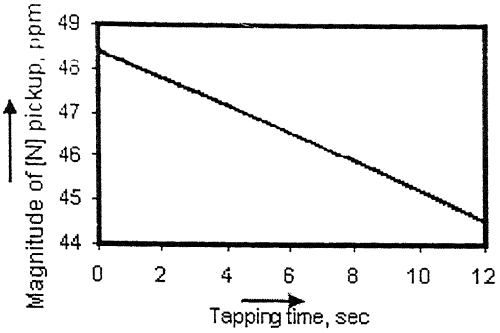

Fig. 3.7(b): Magnitude of [N] pickup by all mechanisms at different tapping times of liquid steel

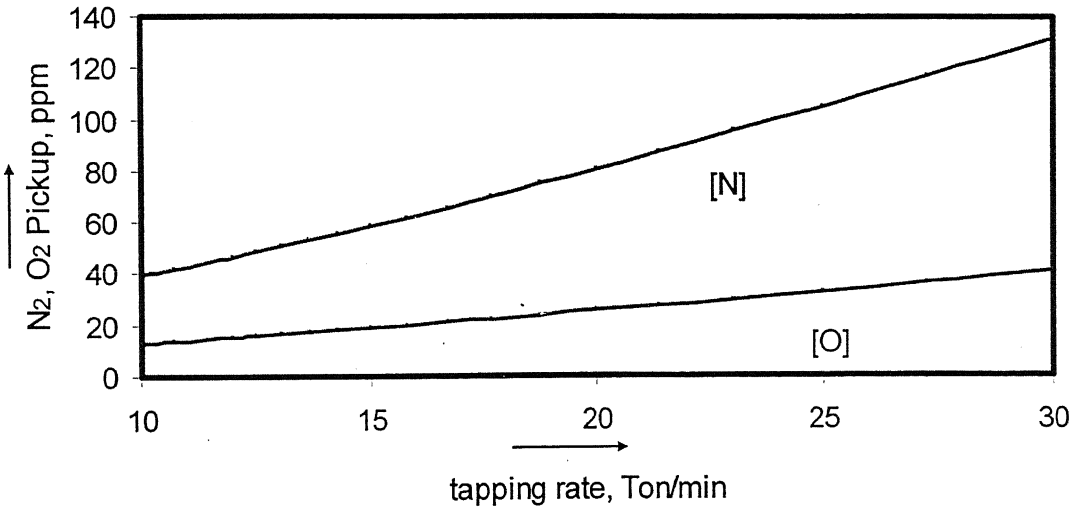

Fig. 3.8: Effect of tapping time on N_2 and O_2 pickup

Table 3.3: N_2 and O_2 pickup by different mechanisms

	Absorption Mechanisms	Extent of Absorption (ppm)	Percentage of Absorption
O_2 Pickup	Diffusion through tapping stream	1.48	10.17
	Diffusion through the surface of the metal pool	5.0×10^{-6}	3.45×10^{-7}
	Dissolution of Bubbles	13.07	89.83
N_2 Pickup	Diffusion through tapping stream	1.73	3.86
	Diffusion through the surface of the metal pool	2.0×10^{-6}	4.46×10^{-8}
	Dissolution of Bubbles	43.07	96.14

3.5.2 Calculation of initial amount of deoxidant to be added for a given composition and temperature of steel

In this study, our objective is to predict the amount of aluminum to be added to the ladle for known initial oxygen dissolved in the steel bath (in ppm). For the case of 300 ton liquid steel at 1923 K, initially containing 800 ppm dissolved oxygen, Table 3.4 shows the effect of aluminum addition on the final value of dissolved oxygen ([O]). This is for an ideal case when the recovery of aluminum added to the bath is assumed to be 100%.

A user friendly computer program has been developed to calculate the amount and size distribution of alumina inclusions formed by aluminum deoxidation. Flow chart of the algorithm has been shown in Fig. 3.9. Various steps of calculation are as follows

Step 1: Enter relevant input through user friendly interface, and save to input file "Data.txt"

Step 2: Set initial time as t_o zero i.e., $t = 0$ and the small time step as $\Delta t = 0.1$ sec (say).

Step 3: calculate the equilibrium concentrations of aluminum and oxygen by iteration of Eqns (3.34 – 3.36).

Step 4: Calculate the super-saturation of the bath by using Eqn (3.46)

Step 5: Calculate critical radius for nucleation of alumina by using Eqn (3.47)

Step 6: Calculate bath concentrations of aluminum and oxygen can be calculated by Eqn (3.56) and Eqn (3.57)

Step 7: Calculate interfacial concentration of aluminum, C^i_{Al}, by using Eqn (3.55)

Step 8: Calculate the increase in radius of alumina particles by mass transfer of aluminum and oxygen to the metal-alumina interface in the small time step Δt by using Eqn (3.59)

Step 9: Calculate the decrease in bulk concentration of aluminum and oxygen (C_{Al}^{b}, C_{O}^{b}, respectively) due to alumina formation, by using Eqns (3.61) and (3.62)

Step 10: Calculate the growth and removal of alumina particles by using Eqns (3.44), (3.53) and (3.54)

Step 11: Calculate the individual and total number of particle removed within time step Δt by different collision mechanisms and by assimilation in top slag, by using Eqns (3.49), (3.50), (3.53), (3.54)

Step 12: Store the data for the calculation of time, t, in different output files (see sec 3.6)

Step 13: Increment the value of t by Δt

Step 14: If $C_{Al}^{b} > C_{Al}^{e}$, then go to '**Step 4**' else continue

Step 15: If t < Total time, then go to '**Step 8**' else continue

Step 16: Display the results of inclusion size and amount, dissolved oxygen, nitrogen and aluminum, and maximum size of inclusion in the output window.

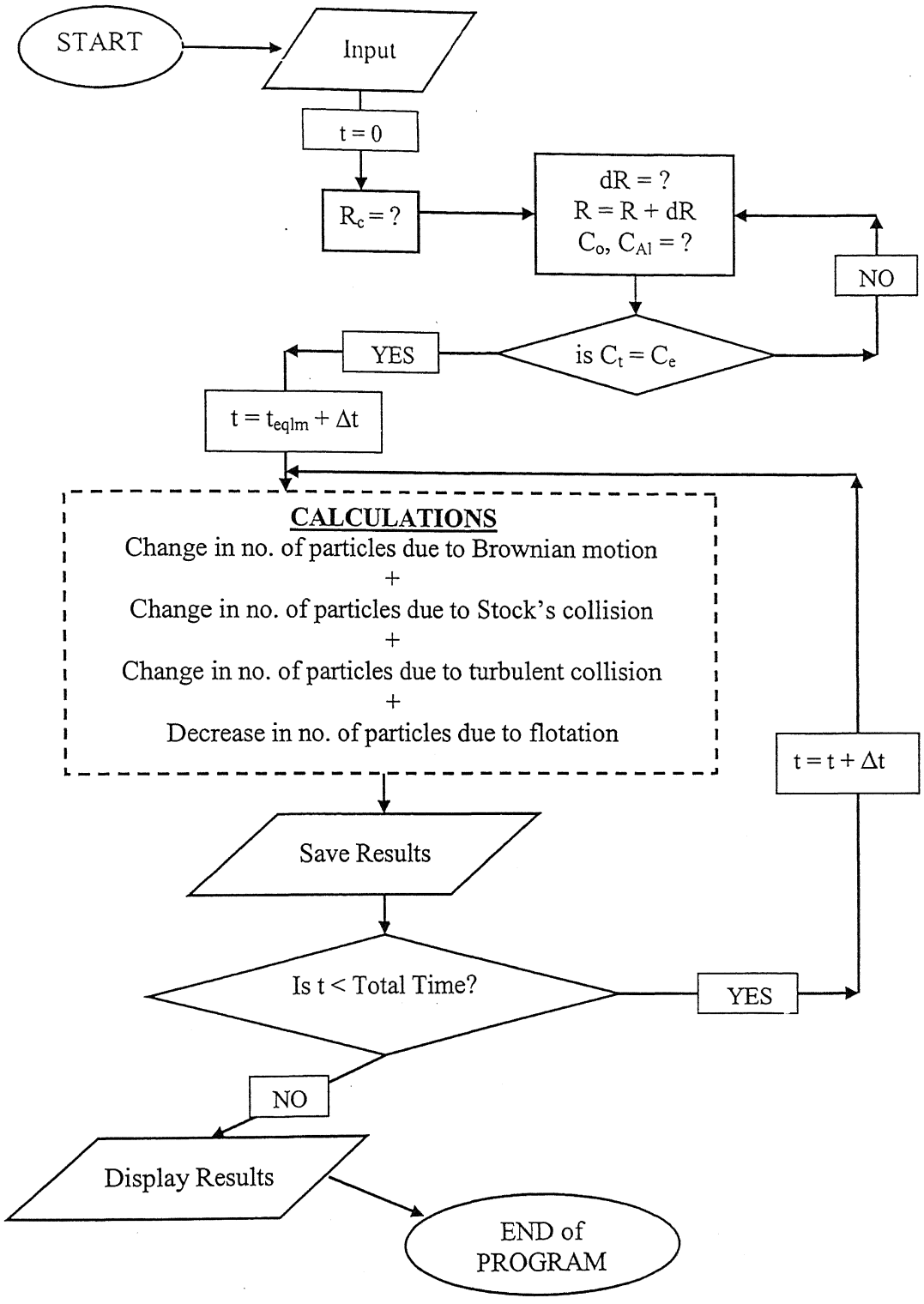

Fig. 3.9: Flow chart developed for calculation of critical radius of nucleus, growth of inclusions, and removal of alumina inclusions, during and after aluminum deoxidation

Table 3.4: $[O]_f$ and final $[Al]_f$ vs. Aluminum addition for 800ppm initial [O], Recovery 100%, temperature 1873 K

Sl. No.	Al added (kg)	final wt (ppm)	$[O]_f$ (ppm)
1	200	1.5	209.0
2	220	2.5	150.6
3	240	5	93.6
4	260	16	43.9
5	280	55	19.2
6	300	113	11.9
7	320	176	8.8
8	340	241	7.2
9	360	307	6.1
10	380	373	5.4
11	400	439	4.8
12	420	506	4.4
13	440	572	4.0
14	460	639	3.7
15	480	705	3.5
16	500	772	3.3

The final dissolved oxygen in ppm and final mass % aluminum dissolved into the bath after deoxidation versus aluminum addition in kg is plotted in Fig. 3.10. As seen from the Fig. 3.10, for the case of 800 ppm initial dissolved oxygen, with increasing the addition of aluminum the final amount of dissolved oxygen decreases initially at a rapid rate, but after 300 kg of aluminum addition (corresponding to equilibrium oxygen content of 7 ppm), further decrease in the dissolved oxygen is at a small rate. The final oxygen content of the metal bath versus aluminum added into the bath for different initial oxygen contents is also plotted in Fig. 3.10

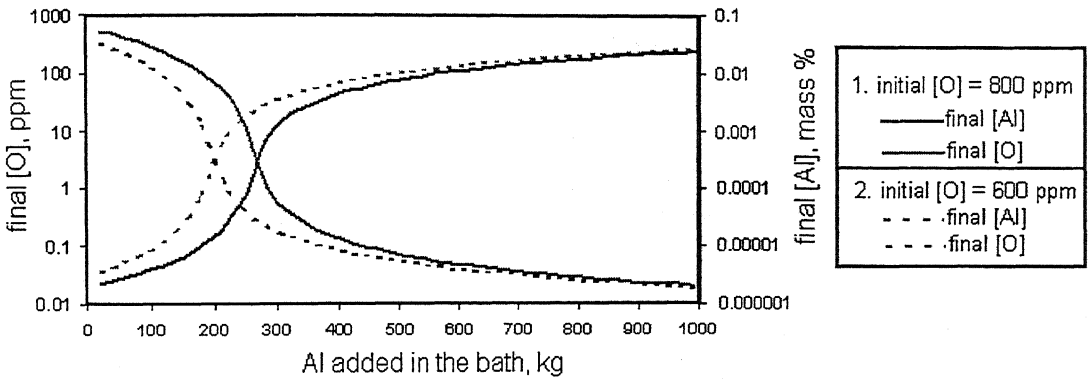

Fig. 3.10: Plot of Al used vs. final mass % of dissolved aluminum and oxygen

3.5.3 Recovery of aluminum during deoxidation

Percent recovery of aluminum is defined as

$$\% \text{ Recovary} = \frac{\text{Aluminum used for deoxidation} + \text{Aluminum dissolved in the metal bath}}{\text{Total aluminum charged into the bath}} \times 100$$

It is clear that aluminum reacting with FeO or O_2 in atmosphere is a loss.

(a) Calculation of Recovery of aluminum charged during tapping of steel at Bokaro steel plant (300 ton steel)

Heat No: 1442

Date: 27/2/2004

Venue: SMS-II, Bokaro Steel Plant

During Tapping:

Initial Oxygen in the bath $[O]_i = 506$ ppm (measured by Celox)

C charged = 300 kg

Al Charged = 460 kg

At SRU:

Final Oxygen in the bath $[O]_f$: < 3 ppm (measured by Celox)

Final Al in the bath $[Al]_f = 0.07$ %

Calculations:

300 kg C reduces 100 ppm [O] from the bath (approximately 10% reaction assumed).

Rest 406 ppm [O] was reduced by Al.

Hence [O] reduced by Al

$$= \frac{0.0403 \times 3 \times 10^5}{100} \text{ kg [O]}$$

=120.9 kg [O]

$$\text{Aluminum used} = \left(\frac{2 \times 27}{3 \times 16}\right) \times \frac{0.0406 \times 3 \times 10^5}{100}$$

= 136.013 kg

Suppose the initial aluminum content of bath is zero. When the ladle is brought to SRU the bath contained 0.07 % dissolved aluminum.

$$\text{Mass of aluminum dissolved in the metal bath} = \frac{0.07 \times 3 \times 10^5}{100} \text{ kg [Al]}$$

=210 kg [Al]

Total aluminum used in metal bath = (136.013 + 210) kg

=346.013 kg

Since total aluminum added was 460 kg, the percentage recovery of aluminum is

$$\text{Percentage recovery} = \frac{346.013}{460} \times 100$$

= 75.22 %

Such a high recovery is possible only when slag stopper is used in BOF to prevent transfer of slag from BOF to ladle and also coke is used for initial deoxidation purposes.

According to the model, by considering 75% recovery, the equilibrium mass % of aluminum is 0.066 % and equilibrium oxygen content in the bath is 3.66 ppm. Therefore, it can be concluded that the process has achieved near thermodynamic equilibrium.

(b) Calculation of Recovery of Al charged at SRU:

Heat No: 2494

Date: 10/4/2004

Venue: SMS-II, Bokaro Steel Plant

After arrival at SRU:

Initial oxygen content of bath $[O]_i$ = 12.2 ppm (measured by Celox)

Initial Al content of bath $[Al]_i$ = 0.006 %

Al Charged = 180 kg

After arcing and purging at SRU (Ladle furnace):

Final Oxygen in the bath $[O]_f$: = 4.3 ppm (measured by Celox)

Final Al in the bath $[Al]_f$ = 0.016 %

Calculations:

$$[O] \text{ reduced by Al} = \frac{(0.00122 - 0.00043) \times 2.893 \times 10^5}{100} \text{ kg [O]}$$

=2.285 kg [O]

$$\text{Aluminum used} = \left(\frac{2 \times 27}{3 \times 16}\right) \times 2.285 \text{ kg}$$

= 2.571 kg

Again, in the bath %Al increases to 0.016% from 0.006%

$$\text{Hence Al dissolved into the bath} = \frac{(0.016 - 0.006) \times 3 \times 10^5}{100} \text{ kg [Al]}$$

= 30 kg [Al]

Total Al used in metal bath = (2.285+30) kg = 32.285 kg

Hence, % recovery = $\frac{32.285}{180} \times 100 = 17.94\ \%$

The recovery of aluminum at ladle furnace is small because a large proportion of aluminum, added in the form of aluminum shots, melts at surface and reacts with ambient atmosphere. Argon stirring also helps in oxygen pickup from atmosphere. The aluminum wire injector is not used at Bokaro steel plant. If aluminum wire is practiced then recovery will improve.

According to the model, by considering 18% recovery, the equilibrium mass % of aluminum is 0.0165 % and equilibrium oxygen content in the bath is 9.26 ppm.

3.5.4 Calculation of initial size of nucleus and its growth by mass transfer

The initial conditions assumed for calculating the size of the nucleus (from Eqn 3.55) and its subsequent growth (from Eqns 3.61-3.65) are summarized in Table. 3.5.

(a) Calculation of super-saturation value and critical radius

The super saturation, Π, can be calculated from Eqn (3.45)

$$\Pi = \frac{C_t}{C_e}$$

The values of C_e and C_t can be obtained by calculating equilibrium constant for the deoxidation reaction from Eqn (3.33)

$$\log(K_e) = \frac{58473}{TK} - 17.74 = \frac{58473}{1923} - 17.74$$

$$= 12.66718$$

Table 3.5: Data used for the calculation

Symbol	Meaning	Unit	Numerical Value used
Al_i	Initial Al addition into the bath	kg	400
d_{Fe}	Average density of iron	kg/m^3	7000
d_{in}	Average density of inclusions	kg/m^3	3000
H	Height of liquid bath of the ladle	m	3.5
K_{Al}	Average diffusivity of [Al] in molten steel	m^2/s	2.5×10^{-5}
Ko	Average diffusivity of [O] in molten steel	m^2/s	2.5×10^{-5}
No	Initial no of particles		1.0×10^{-12}
$[O]_i$	Initial Oxygen level	ppm	800
R	Universal gas constant	J/K	8.314
t_n	Total number of moles present in the bath	mole	5357.14
T	Temperature of steel in Kelvin	K	1923
V_m	Volume of metal	m^3	42.86
W_m	Weight of metal	kg	3×10^5
η_{Al}	Aluminum recovery	%	100
μ_{Fe}	Average viscosity of iron	kg/m.s	0.005
σ_{s-i}	Surface tension at steel and inclusion interface	N/m^2	2.3

Or, $K_e = 10^{12.66718} = 4.64704 \times 10^{12}$

By using Eqn (3.34 – 3.36), the values of $[Al]_e$ and $[O]_e$ are 0.04395 % and 0.00048 %, respectively. Hence

$C_e = [Al]_e^2 [O]_e^3 = 2.15 \times 10^{-13}$

The values of $[Al]_i$ and $[O]_i$ are 0.13333 % and 0.07 %, respectively, for the first time step. Thus,

$C_t = [Al]_i^2 [O]_i^3 = 9.102223 \times 10^{-6}$

The super-saturation of the bath is,

$\log (C_t / C_e) = 7.62639$

The critical radius of nucleus can be calculated from Eqn (3.47)

$$r_c = \frac{2\sigma V m}{RT \log\left(\frac{C_t}{C_e}\right)}$$

$$= \frac{2 \times 2.3 \times 3.4 \times 10^{-5}}{8.314 \times 1923 \times 7.626391}$$

$= 0.1283 \times 10^{-8}$ m

Critical radius is approximately 0.13 Å

The calculated value of the critical radius calculated from classical homogeneous nucleation theory is less than the size of atom. This is primarily due to large super saturation assumed. For further calculation the value of critical radius is assumed to be 8 Å, which would be approximately the value when Ct is only slightly greater than Ce (for example $\log\left(\frac{C_t}{C_e}\right) \approx 0.1$)

(b) Growth of nucleus by mass transfer

When the deoxidation achieves equilibrium then the for a small time step, Δt the increase in radius, Δr, can be calculated from Eqn (3.59)

$$\Delta r = 0.01275\, k_{Al} \left(C^{b}_{Al} - C^{i}_{Al} \right) \Delta t$$

Here, the values of C^{b}_{Al} and C^{i}_{Al} can be calculated from Eqns (3.55) and (3.56).

From Eqn (3.55),

$$C^{b}_{Al} = [\text{mass\%Al}^{b}] \frac{\rho_{Fe}}{100 \times M_{Al}}$$

Where, M_{Al} is the molecular weight of aluminum, and ρ_{Fe} is density of iron.

$$\text{Hence, } C^{b}_{Al} = \left[\frac{400}{300000} \times 100 \right] \times \frac{7000}{100 \times 27}$$

$$= 0.3457 \text{ kmole/m}^3$$

The bulk concentration of oxygen can be calculated from Eqn (3.57)

$$C^{b}_{O} = [\text{mass\%O}^{b}] \frac{\rho_{Fe}}{100 \times M_{O}}$$

Where, M_o is the molecular weight of oxygen and is equal to 16.

$$\text{Hence, } C^{b}_{O} = 0.07 \times \frac{7000}{100 \times 16} = 0.30626 \text{ kmole/m}^3$$

The value of C^{i}_{Al} has been calculated by iteration method from Eqn (3.55), the value of C^{i}_{Al} for the first time step is 0.1429 Kmoles/m^3.

Now, the value of interfacial concentration of oxygen can be calculated from Eqn (3.50)

$$C^i_{O} = \left(\frac{\rho_{Fe}}{100 \times M_O}\right) \times \sqrt[3]{\frac{1}{K_e\left[C^i_{Al} \times \left(\frac{\rho_{Al}}{\rho_{Fe}}\right)\right]}}$$

$$= \left(\frac{7000}{100 \times 16}\right) \times \sqrt[3]{\frac{1}{4.64704 \times 10^{12} \times \left[0.1429 \times \left(\frac{2700}{7000}\right)\right]^2}}$$

$$= 0.00181 \text{ kmole/m}^3$$

Thus, increase in the radius during a small time step Δt is

$$\Delta r = 0.01275\, k_{Al} (C^b_{Al} - C^i_{Al})\, \Delta t$$

$$= 0.01275 \times 2.5 \times 10^{-5} (0.3457 \times 10^{-3} - 0.1429 \times 10^{-3}) \times 0.1$$

$$= 6.464 \times 10^{-12} \text{ m (or, } 6.464 \times 10^{-6} \mu\text{m)}$$

Corresponding increase in mass of alumina in the bath after deoxidation can be calculated from Eqn (3.60)

$$d[Al_2O_3] = N_0 \frac{4}{3}\pi\{[r + dr]^3 - r^3\}\rho_{Al2O3}$$

Where, No is the initial number of inclusions formed in the bath and assumed to be equal to 10^{12}. Now by putting in the values of No, r ,dr and ρ_{Al2O3}, we get

$$d[Al_2O_3] = 10^{12} \times \frac{4}{3}\pi\{[8 \times 10^{-8} + 6.464 \times 10^{-12}]^3 - [8 \times 10^{-8}]^3\} \times 3000$$

$$= 1.56 \times 10^{-9} \text{ kg}$$

Change in mass percent of aluminum in bulk can be calculated from the Eqn (3.61)

$$d[\text{mass}\%Al] = \frac{2 \times d[Al_2O_3]}{W_m} \times 100$$

$$= \frac{2 \times 1.56 \times 10^{-9}}{300000} \times 100\% = 1.04 \times 10^{-12}\%$$

Change in mass percent of oxygen in bulk can be calculated from the Eqn (3.62)

$$d[\text{mass\%O}] = \frac{3 \times d[Al_2O_3]}{W_m} \times 100$$

$$= \frac{3 \times 1.56 \times 10^{-9}}{300000} \times 100$$

$$= 1.56 \times 10^{-12} \%$$

The radius of inclusion is plotted as a function of time in Fig. 3.11(a) and the concentration of dissolved oxygen and aluminum are plotted as a function of time in Fig. 3.11(b). It is clear from Fig. 3.11(a) and 3.11(b) that the system attains chemical equilibrium after approximately 5 minutes of aluminum addition and the minimum radius of inclusions present at equilibrium is approximately 2.4 microns. The final size would increase if number of nuclei is assumed to be less.

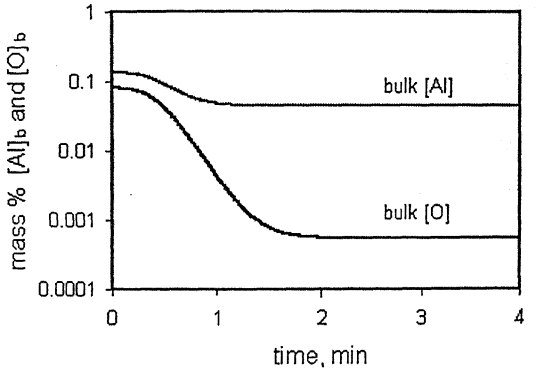

Fig 3.11(a): Decrease of mass % [Al] and [O] before equilibrium

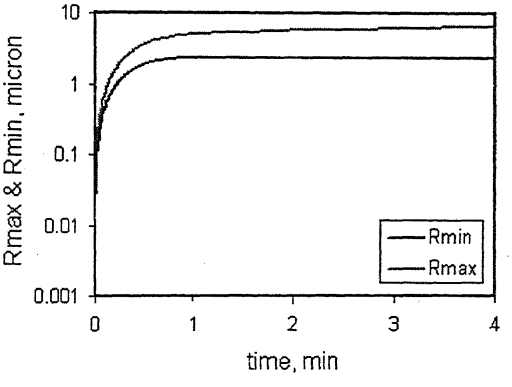

Fig 3.11(b): Increase of inclusion radius before the system achieves equilibrium

3.5.5 Calculation of change in the size range and number of inclusions by collision and assimilation by top slag

The equations to be used for calculating the change in size and number of inclusions due to collision and assimilation by top slag have been described in section 3.4. The simplifying assumptions made in the calculation procedure adopted in this work, are

- Deoxidizers dissolved uniformly in the melt soon after addition.
- The inclusions formed are also homogeneously distributed through out the steel melt.
- A certain initial number of nuclei are assumed to be formed in the bath
- After attainment of thermodynamic equilibrium, the inclusions grow only by collision mechanisms and not by mass transfer because system has already achieved equilibrium

Table 3.5 summarizes the data used in the kinetic model for the prediction. The sample calculations are given below.

Table 3.5: Data used in the kinetic model

Symbol	Meaning	Unit	Numerical Value used
Al_i	Initial Al addition into the bath	kg	400
d_{Fe}	Average density of iron	kg/m^3	7000
d_{in}	Average density of inclusions	kg/m^3	3000
H	Bath Height	m	3.5
K	Boltzmann constant	J/K	$1.38\ 10^{-23}$
K_{Al}	Average diffusivity of [Al] in molten steel	m^2/s	2.5×10^{-5}
Ko	Average diffusivity of [O] in molten steel	m^2/s	2.5×10^{-5}
No	Initial no of particle		1.0×10^{-12}
$[O]_i$	Initial Oxygen level	ppm	800
R	Universal gas constant	J/K	8.314
T	Temperature of steel in centigrade	°C	1650
TK	Temperature of steel in Kelvin	K	1923
Vm	Volume of metal	m^3/mol	3.4×10^{-5}
Wm	Weight of metal	kg	3×10^5
α	Collision efficiency		0.5
η_{Al}	Aluminum recovery	%	100
μ_{Fe}	Average viscosity of iron	kg/m.s	0.005
σ_{s-i}	Surface tension at steel and inclusion interface	N/m^2	2.3

The calculation is done over a small time step, $\Delta t = 0.1$ sec. The collision volumes of different mechanisms can be calculated from the Eqns (3.63-3.65) A sample calculation for the first time step is given below.

From the calculation of equilibrium radius of inclusions, the minimum size of inclusion present in the bath after attainment of equilibrium, r_{eqlm}, is approximately equals to 2.4 μm. The time required for attainment of equilibrium, t^{eqlm}, is approximately 4 minutes and the total number of inclusions present in the bath, N_0 ,is assumed to 10^{12}.

at $t = 0$,

$N_i = N_0 = 10^{12}$, if $i = 1$

$Ni = 0$ if $i = 2, 3, 4.....$

Now, at $t = 0 + \Delta t$

The collision volume due to Brownian motion can be calculated from Eqn (3.63)

$$W_{ij}^{B} = \frac{2KT}{3\mu_{Fe}}\left(\frac{1}{r_i} + \frac{1}{r_j}\right)(r_i + r_j)$$

$$= \frac{2\times 1.38\times 10^{-23}\times 1923}{3\times 0.005}\left(\frac{1}{r_0} + \frac{1}{r_0}\right)(r_0 + r_0)$$

$$= \frac{21.3810^{-23}\times 1923}{3\times 0.005}$$

$$= 3.53832 \text{ x } 10^{-18}$$

The collision volume due to Stokes collision can be calculated from Eqn (3.64)

$$W_{ij}^{s} = \frac{2\pi g(\rho_{Fe} - \rho_i)}{9\mu_{Fe}}(r_i + r_j)^3 \,|\, r_i - r_j \,|$$

As here, $i = j = 1$ [Only one size range particle exists at $t = 0$]

Hence, $r_i = r_j = r_1 = r_0$

$\therefore, W^{S}_{11} = 0$

So, no Stokes collision takes place during the first time step.

Calculation of decrease in the number of inclusions by collision mechanisms, as described by Eqn (3.67), is

$\therefore, dN_i\ (i = 1) = -\ (W_{11}^{S} + W_{11}^{B}) \times N_1 \times N_1 \times dt$

$= -\ [0 + 3.53832 \times 10^{-18}\ ] \times 10^{12} \times 10^{12} \times 1$

$= -\ 3.53832 \times 10^{-18} \times 10^{12} \times 10^{12}$

$= -\ 3538320$

$dN_j\ (j = 1) = -\ (W_{11}^{S} + W_{11}^{B}) \times N_1 \times N_1 \times dt$

$= -\ 3538320$

$dN_{[1+1]} = N_2 = +\ (W_{11}^{S} + W_{11}^{B}) \times N_1 \times N_1 \times dt$

$= 3538320$

Therefore, $N_1^{*} = N_1 + 2 \times dN_1 = 10^{12} - 2 \times 3538320 = 99999292340$

$N_2^{*} = N_2 + 2 \times dN_2 = 0 + 2 \times 3538320 = 7076640$

Hence for the first step the decrease in number of inclusions due to collision between particles is $= dN_1 + dN_1 - dN_2$

$= 2 \times 3538320 - 3538320$

$= 3538320$

Now, in the same time step some of the r_2 particles will collide with both r_1 and r_2 sized particles and they will form inclusions of size r_3 and r_4, respectively, and so on.

The decrease in number of inclusions removed by assimilation by top slag can be calculated from Eqn (3.68)

$$\frac{dN_i}{dt} = \frac{2g}{9\mu}(\rho_{Fe} - \rho_i) r_i^{2} \frac{N_i}{H}$$

For i =1,

$$\frac{dN_1}{dt} = \frac{2g}{9\mu}(\rho_{Fe} - \rho_i)r_1^2 \frac{N_1}{H}$$

Or, $$dN_1 = \frac{2g}{9\mu}(\rho_{Fe} - \rho_i)r_1^2 \frac{N_1}{H} dt$$

$$= \frac{2 \times 9.81}{9 \times 0.005}(7000 - 3000)(2.37772088 \times 10^{-6})^2 \frac{999962509312}{3.5} \times 1$$

$$= 281698$$

Similarly $dN_2 = 8$, $dN_3 = 0$, $dN_4 = 0$ and so on, for the first time step.

Hence the total removal to the slag = $dN_1 + dN_2 + dN_3 + dN_4$ .....

$$= 281698 + 8 + 0 + 0 ....$$

$$= 281706$$

Result obtained after a time step, Δt, is

$N_1 = 999962509312 - 281698 = 999962227614$

$N_2 = 18736086 - 8 = 18736078$

$N_3 = 0$, $N_4 = 0$ and so on.

These values are to be used in the calculation during the next time step, Δt.

The logarithmic distribution of inclusions of different sizes, which are present in the liquid bath after different ladle holding times, is plotted in Fig. 3.12. As seen from the Fig. 3.12, the range of inclusion sizes present in the bath widens with increase in the holding time. The concentration of small sized inclusions in the bath decreases with holding time, and the concentration of bigger size inclusions increases at the expense of the smaller inclusions. The total number of inclusions continuously decreases (Table 3.6 and Fig. 3.13).

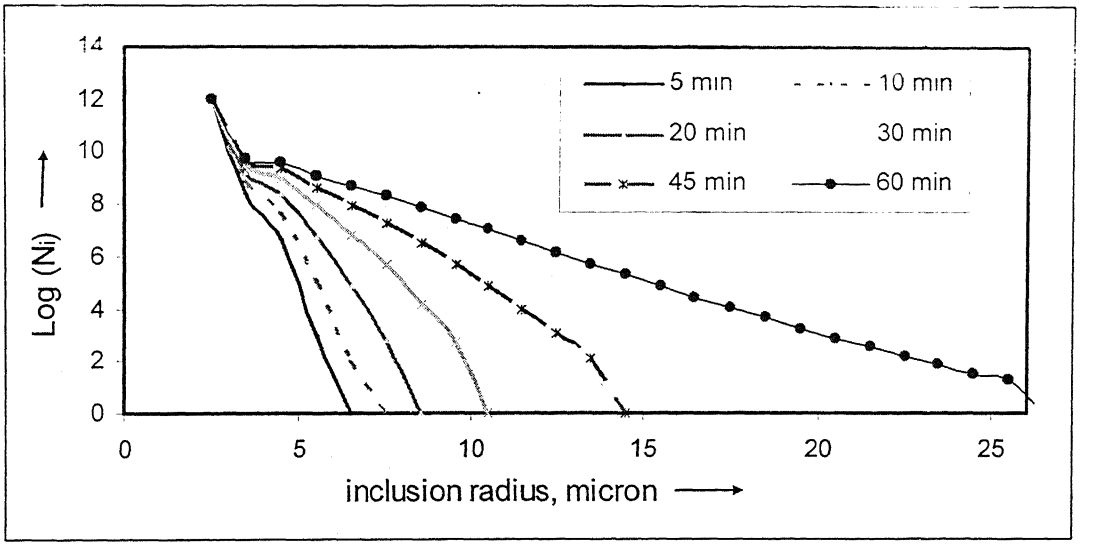

Fig. 3.12: Plot of logarithmic inclusion distribution for different holding times

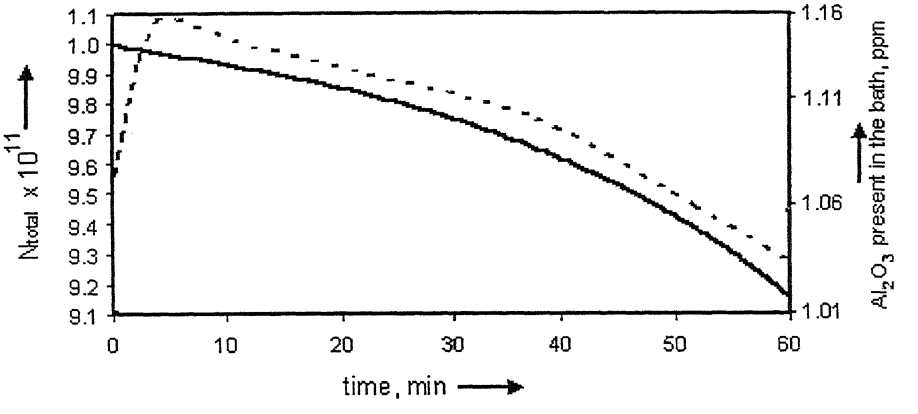

Fig. 3.13: Predicted number of inclusions and mass of inclusions present after different holding times

Table 3.6: Inclusion size distribution in the bath after different holding times

Range(μm)	5 min	10 min	20 min	30 min	45 min	60 min
2 - 3	9.00×10^{11}	9.92×10^{11}	9.85×10^{11}	9.72×10^{11}	9.514×10^{11}	9.087×10^{11}
3 - 4	2.33×10^{8}	6.56×10^{8}	1.61×10^{9}	3.04×10^{9}	4.5×10^{9}	5508048384
4 - 5	4788148	39889460	2.5×10^{8}	9.52×10^{8}	2.167×10^{9}	3597425664
5 - 6	981	111649	5709985	86377520	436471136	1206495616
6 - 7		87	76555	6673791	89937752	444622976
7 - 8			630	452026	19684498	190102880
8 - 9				16176	3153790	68448688
9 - 10				472	497124	26183152
10 - 11				10	70916	10014960
11 - 12					8706	3607955
12 - 13					1083	1385015
13 - 14					121	515376
14 - 15						191154
15 - 16						71870
16 - 17						28210
17 - 18						10941
18 - 19						4434
19 - 20						1800
20 - 21						755
21 - 22						335
22 - 23						149
23 - 24						70
24 - 25						34
25 - 26						19
Total	9.96×10^{11}	9.93×10^{11}	9.87×10^{11}	9.76×10^{11}	9.59×10^{11}	9.20×10^{11}

The total number of inclusions and the mass of inclusions present in the bath is shown for different holding times in Fig. 3.13. It is assumed here that turbulent stirring is absent during the time of transportation of the ladle to SRU. According to Fig. 3.13 in absence of stirring only 2% of the inclusion formed by the deoxidation reaction are likely to be removed within first 20 minutes of ladle holding time, and 7% in 45 minutes of ladle holding time. For higher ladle holding times the chances of formation of bigger particles increase (Fig. 3.14) due to the contribution of stokes collision. Also, the chances of removal of inclusions by flotation increase as the size increases. The largest size inclusion formed in the bath is plotted as a function of time in Fig. 3.14; after approximately 5 minutes of holding time, there is a change in slope of the curve. This is due to the assumption that the contribution of Stokes' collision begins only after the inclusions attains a size of 5μm. It has been reported that for the case of Stokes collision the collision volume decreases rapidly in the size range of 2-4 microns [3.14]. Hence, during the first 5-6 minutes Brownian motion is, perhaps, the dominant growth mechanism. After 5-6 minutes, there is a sufficient number of inclusions in size range of 4-6 microns, and therefore the Stokes collision mechanism becomes the dominant growth mechanism. This is also evident from Fig. 3.15. According to the model, it is possible to form inclusions of size of 15 μm in the metal bath by holding but without purging. It can be seen from Table 3.6, the number of bigger inclusions is less, but the number of inclusions of size 5-10 μm is high. A sample of Bokaro steel plant (BSP), collected before purging (approximately 45 minute holding time) may confirm this. A SEM study of sample collected at SRU just before purging is shown in Fig. 3.16. The diameter of a typical inclusion, in Fig. 3.16, is approximately 15 μm.

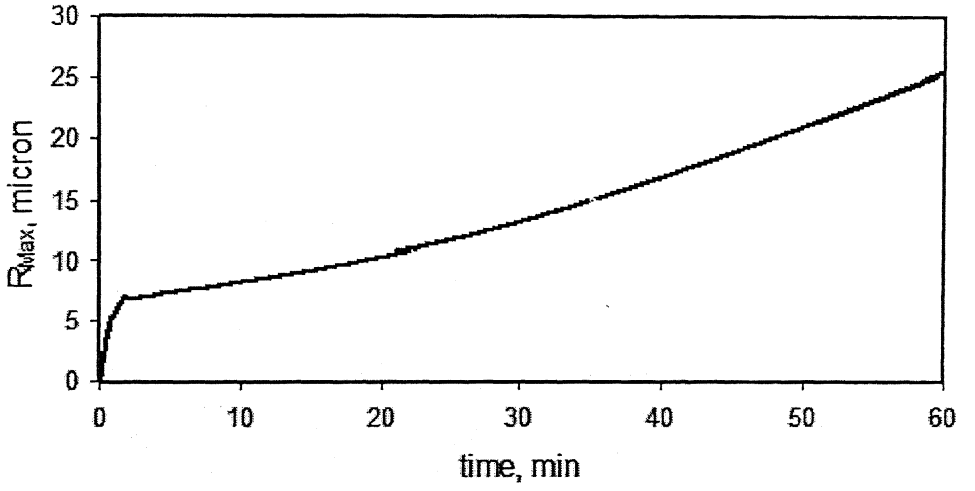

Fig. 3.14: Prediction of the largest sized inclusion in the bath for different holding times

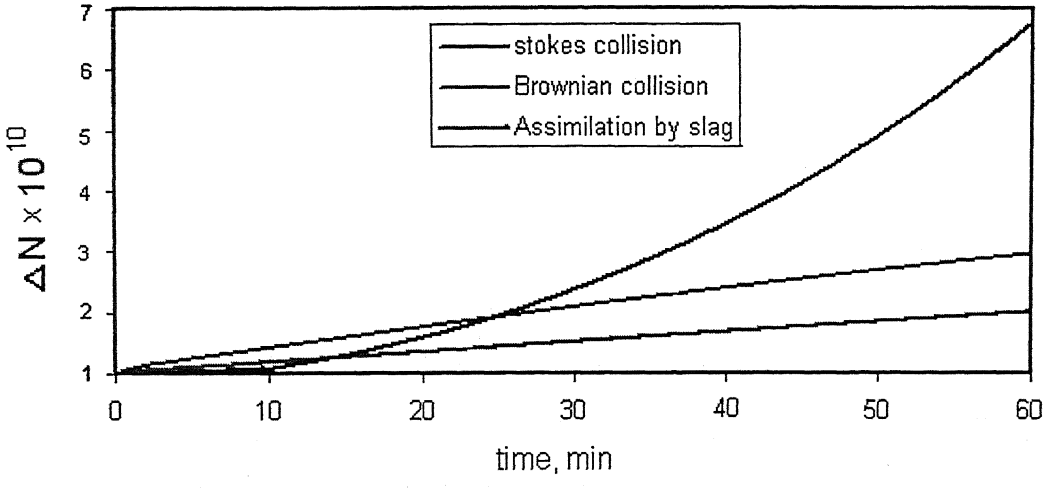

Fig. 3.15: Contribution of different mechanisms to the total removal of inclusion

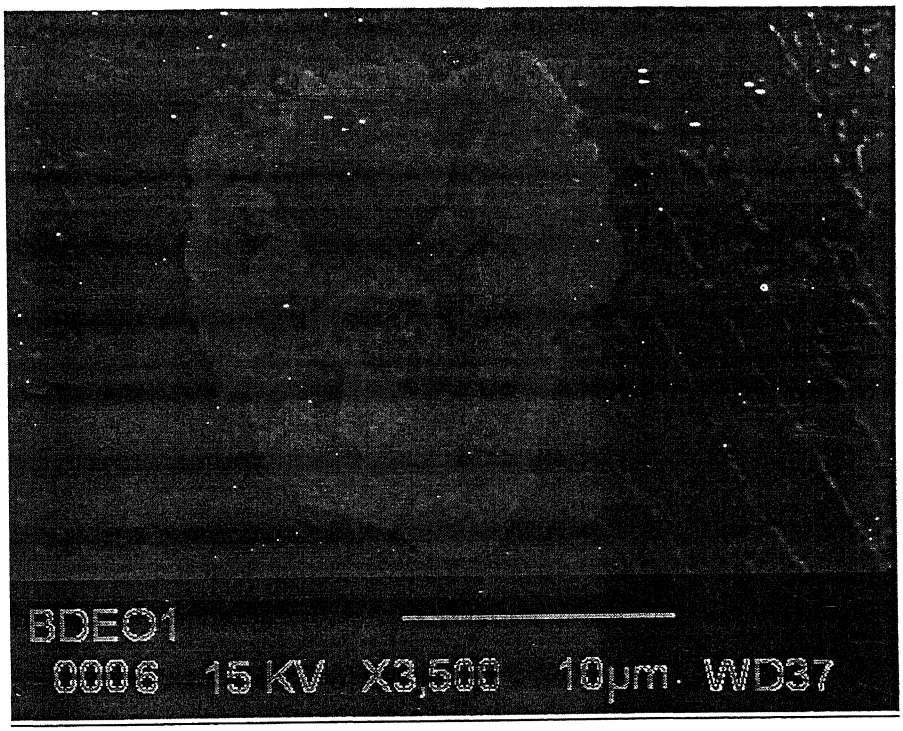

Fig. 3.16: SEM micrograph of a sample (before purging) collected from BSP showing a typical alumina inclusion of approximately 15 µm size.

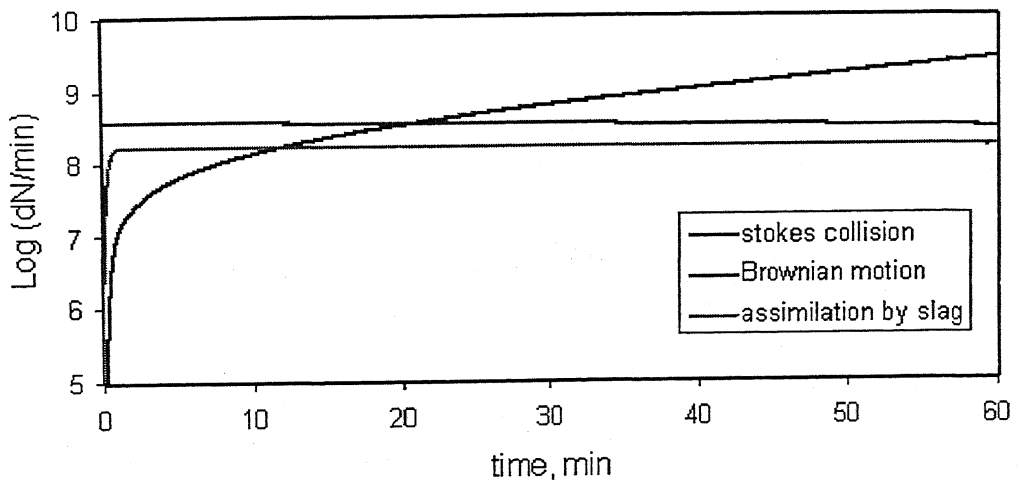

Fig. 3.17: Rate of change of different inclusion removal mechanisms with time

Fig. 3.15 compares the contribution of different mechanisms to inclusion removal. It can be seen that in the beginning, the contribution of Brownian motion dominates, but later on Stokes collision becomes a more dominant mechanism of inclusion removal. The rate of inclusion removal by the collision caused by Brownian motion is nearly constant (infact, it decreases at a slow rate within the 45 minutes of holding time), as shown in Fig. 3.17. It may be due to the fact that the decrease of smallest sized inclusion is only 8.3% of the initial concentration within a 45 minute holding time. The rate of assimilation of inclusion by the top slag slowly increases with time. After 5 minutes of holding time the rate of inclusion removal rate by Stokes' collision increases rapidly from a very low value.

3.5.6 Effect of gas purging on the total removal of inclusions

A study of the relative contribution of different collision mechanisms on total removal of alumina inclusions in the presence of gas purging is presented in this section. The comparison of contribution of mass transfer and other mechanisms to inclusion growth, before the bath attains equilibrium, is shown in Fig. 3.18. It can be seen from Fig. 3.18 that the largest size inclusion formed in the bath by mass transfer mechanism gradually increases with time, whereas, by introducing other collision mechanisms R_{Max} increases rapidly (with sudden jumps). The reason for sodden jumps is due to the formation of bigger particles as a result of collision at discrete time steps, as assumed in the calculation procedure in this work.

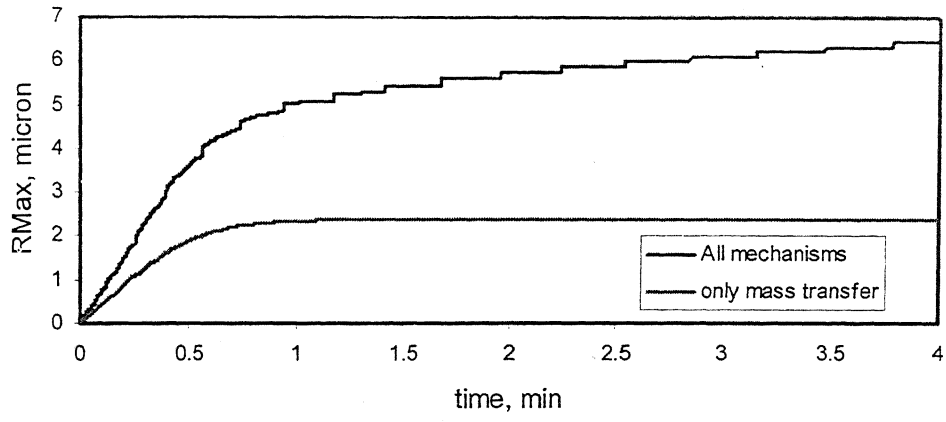

Fig. 3.18: Comparison of increase in R_{Max} when mass transfer mechanism and when all mechanisms are acting in the first 4 minutes of deoxidation

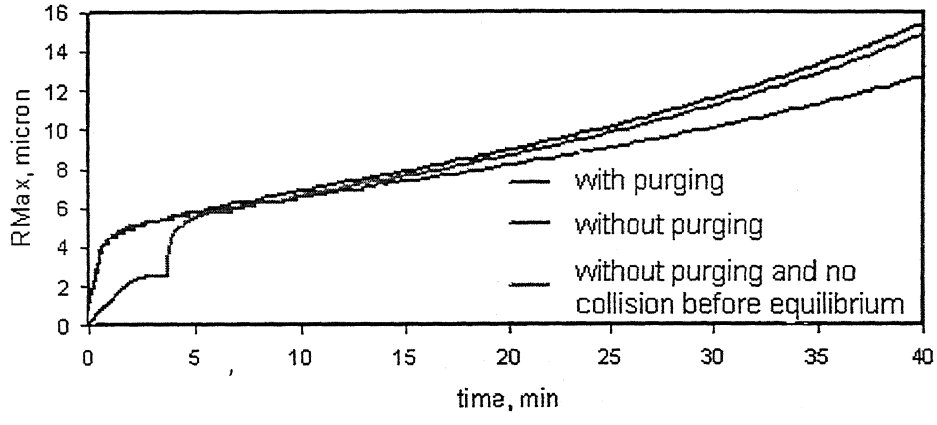

Fig. 3.19: Comparison of increase in R_{max} due to only mass transfer, due to mass transfer and collisions (without purging), and due to all mechanisms act before the bath attains equilibrium

It can be seen from Fig. 3.19 that the effect of purging (of 2 lit/ton min gas) on R_{Max} is only limited. But the presence of collision mechanisms before equilibrium affects the value of R_{Max} significantly. This may be due to the contribution of turbulence in the bath by purging of gas. Stirring enhances the chance of collision and hence the chance of formation of bigger particle. Therefore, the contribution of other mechanisms also increases (Figs. 3.20(a) and (b)).

The effect of gas purging on the rate of removal by stokes and Brownian motion is shown in Fig. 3.20(a) and (b). It can be seen from Fig. 3.20(a), that due to introduction of turbulence into the bath (2 lit/min/ton of metal), the rate of inclusion removal by stokes collision increases by a factor of 10 compared to the case when no purging is used. It can also be seen from Fig. 3.20(b), that the effect of purging on the removal rate of inclusions by Brownian motion in not significant, which is expected. The comparison of total inclusion removal from the bath, with or without purging is plotted in Fig. 3.21. Purging with a gas flow rate, Q, of 2 lit/min/ton of metal is capable of reducing inclusions by approximately 50% (of the initial number of inclusions) in less than an hour of holding time.

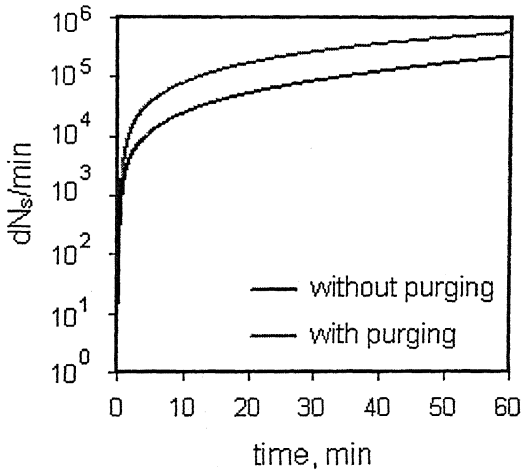

Fig. 3.20(a): Effect of purging on Stokes collision

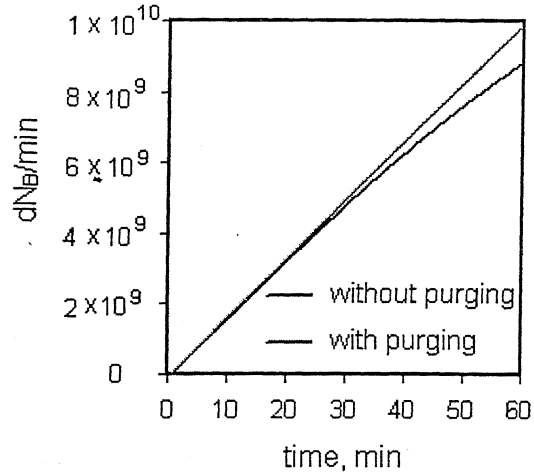

Fig. 3.20(b): Effect of purging on Brownian motion

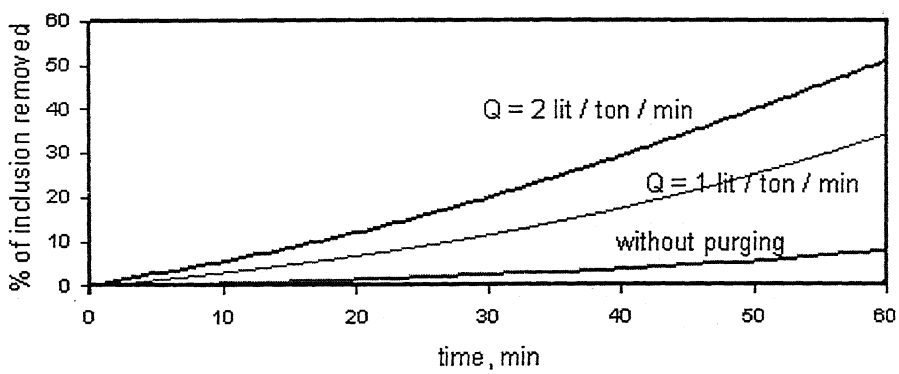

Fig. 3.21: The effect of turbulence collision on total removal of inclusions

3.6 User friendly model for prediction of size distribution and amount of alumina inclusion for aluminum killed steels

A prediction model, incorporating the kinetics of aluminum deoxidation, various collision mechanisms and assimilation by the top slag, has been developed. The sequence of steps executed in the model is shown in Fig. 3.22

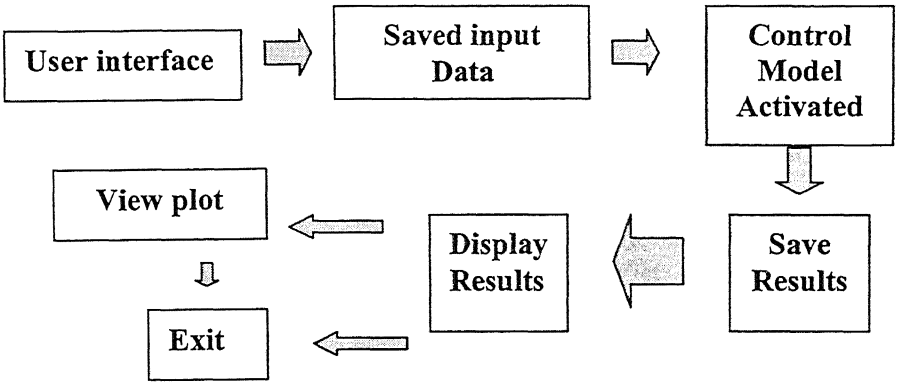

Fig. 3.22: The sequence of steps executed in the user friendly model

It may be noted that in the initial stages of deoxidation (say during the first four minutes) the inclusion size range is small, owing to assumption made that all nuclei are of the same size to start with. Due to this reason the time needed for computation of inclusion growth and coalescence by different mechanisms is also small. The computation time, however, increases almost exponentially for large holding times. A special optimization procedure based on genetic algorithm (described in Appendix 3.A) has been incorporated in the present work, for the first time, to reduce the

computation time, for example by nearly 70%, for holding time of 60 minutes or more.

The user friendly interface of this prediction model is shown in Fig.3.24. The features of the user friendly interface are as follows:

- **Input window**: This facility helps the user to key-in the initial conditions, including the dissolved oxygen measured in the ladle at the time of sampling, estimated nitrogen content, amount of aluminum added for deoxidation, tapping time, holding time, temperature, etc.
- **Output window:** Displays the results of inclusion size and amount, dissolved oxygen, nitrogen and aluminum, and maximum size of inclusion.
- **Storage facility:** Stores data in input and output folders which can later be retrieved for further analysis and verification.
- **Graph:** Model provides online graph facility. The plot of inclusion distribution immediately after the calculation can be obtained.

3.6.1 Steps to be followed for Using the Model:

Step 1: Double click on the desktop icon 'Collision.exe'.

Step 2: The "input window" will open. The inputs can be changed by typing-in a new value in the corresponding text box. Click 'ENTER' and the out put window (Fig.3.25) will appear.

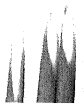

Step 3: For viewing the plot of inclusion size distribution click on the "PLOT" button. It will generate the plot of size range vs. logarithm of number of inclusions (see Fig. 3.26).

Step 4: For details of results and further access see following output files created by the program (inside the installed folder). The output of different output files are as follows

- **Absorption.txt:** Gives the predicted amount of oxygen and nitrogen absorbed by the liquid steel during tapping
- **B4Eqlm.txt:** Gives the increase in inclusion radius, decrease in dissolved aluminum and oxygen content before attainment of equilibrium in the bath
- **SizeCaL.txt:** Gives the predicted amount of inclusion of different sizes after total holding time
- **MaxR.txt:** Gives predicted maximum radius for different times
- **Removed.txt:** Gives the predicted amount of inclusion removal by different mechanisms
- **Output.txt:** Gives the predicted amount of inclusion of different size ranges after total holding time

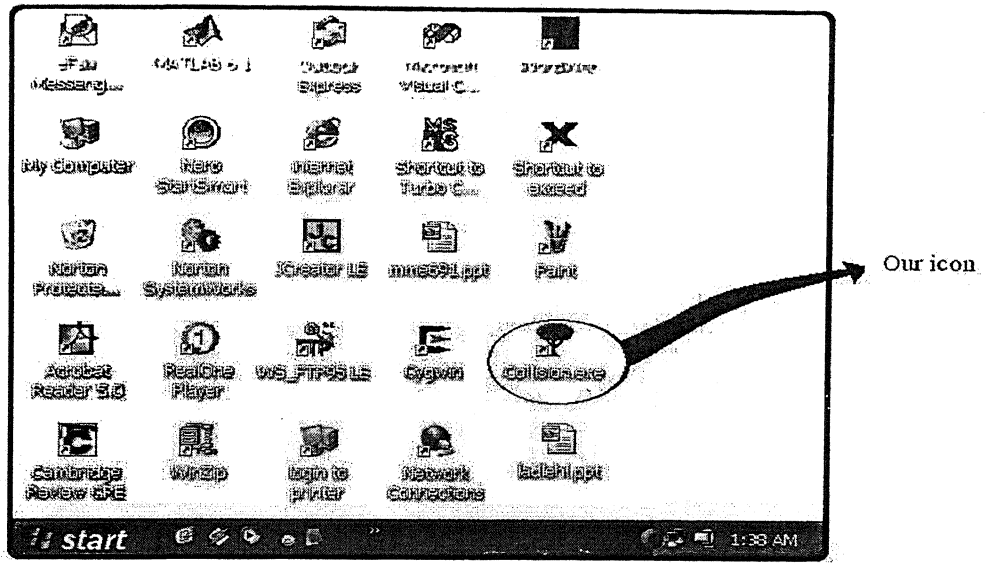

Fig. 3.23: Desktop icon of the user friendly model

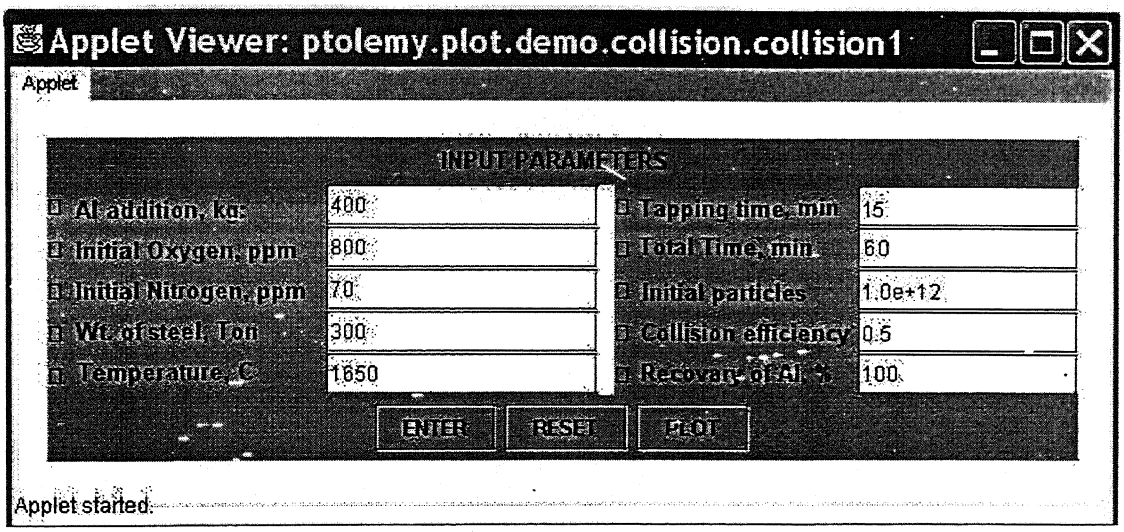

Fig. 3.24: User friendly input window of the model

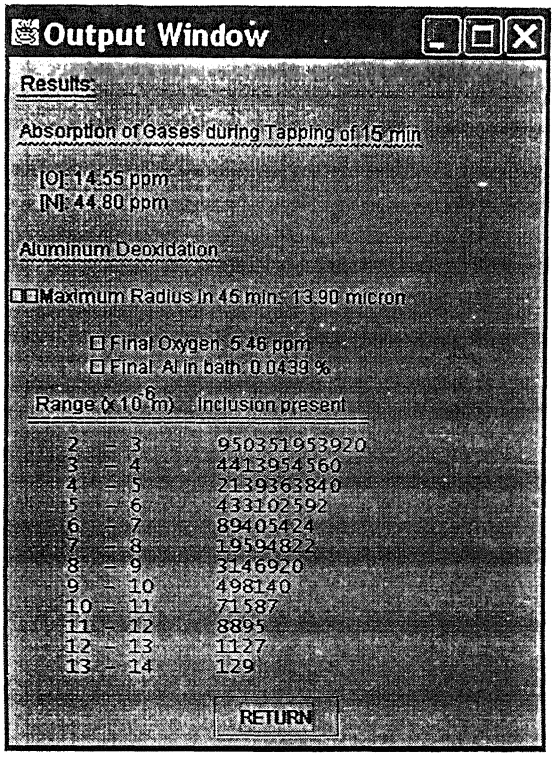

Fig. 3.25: Output window of the model

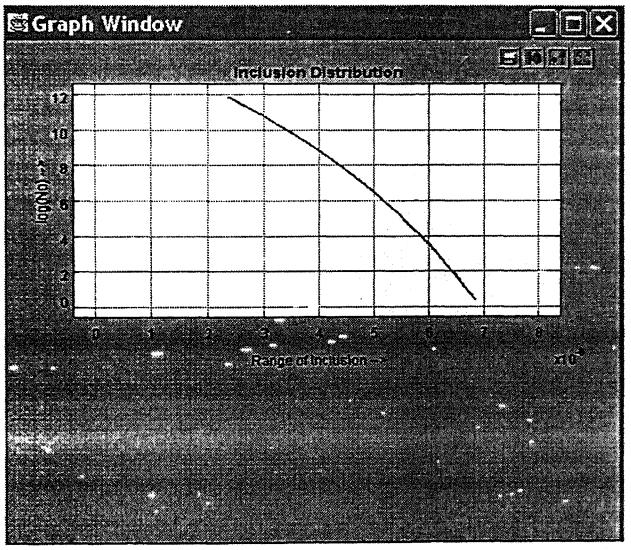

Fig. 3.26: The plot of amount of inclusion vs. range of inclusions in the output window of the model

4. Conclusions

4.1 Conclusions for chapter 2

A good strategy, after having obtained the operational data, is to do statistical analysis of the data in terms of normal distribution, clustering, covariance, etc. and then do multiple linear regression analysis to develop regression models. Simultaneously, kinetic model based on first fundamentals should be developed so as to understand the process well. This will eventually help in deciding the direction of any technical improvement/modification. The next step should be to optimize the kinetic model by GA, develop ANN model as a back-up support, and finally, if needed, develop FRBES model for predictions to be made only in very specific process operation ranges. The results of different models, when analyzed together, help in cross checking the performance of models in different regions of operation. In a plant environment, one should not base all decisions on the basis of one model only but rather narrow down to the possible decision range and then take an optimal decision [2.22].

4.2 Conclusions for chapter 3

For 300 ton liquid steel, having initial dissolved oxygen of 800 ppm and nitrogen of 50 ppm, and deoxidized with 400 kg aluminum

1. Absorption of [O] and [N] through the surface of the falling stream may contribute approximately 7-8 % of the total pickup of [O] and [N]. The entrained gas bubbles contribute approximately to 90 % of the total pickup of [O] and {N].

2. In order to obtain a final oxygen content of bath below 5 ppm the optimum aluminum to be added lies between 350 to 500 kg, depending on percentage recovery of aluminum addition.
3. In the case of non-stirred bath, the concentration of inclusion decreases with time at a low rate. A 45 minute holding time is capable of removing only 7% of the initial inclusions present. Approximately 10% of the initial concentration of the smallest inclusion, R_{min}, can be removed within 45 minute holding time.
4. The contribution of Stokes' collision rapidly increases with time as the availability of the big inclusions also increases with time. Similarly, the contribution of assimilation of inclusion by top slag also increases with time because the big inclusions have high upward velocity.
5. During holding of steel in a non stirred-bath, the collision mechanism plays the most significant role for removal of inclusions. For a 45 minute holding period the inclusion removal by collision mechanism is more than 15 times than that by assimilation of inclusions by slag.
6. In case the bath is stirred by gas or induction current turbulent, collision plays a significant role on the inclusion removal process. For example, if the bath isstirred with a gas flow rate of 2 lit/ton/min, approximately 50% of the initial inclusions may be removed in 45 minutes.
7. Inclusion removal process is a dynamic process hence the time step for calculation should be small (0.15). Results obtained by using high Δt value may lead to higher error level.

5 References

2.1. Robinson, S.W.; Bartram, R.W.; Houghton, G.M. In Kinetic model for predicting hot metal desulphurizer consumption. In *Steel making conference proceedings*, ISS, 1989; 457-461.

2.2. Deo, B.; Grieveson, P. Desulphurization of molten pig iron containing aluminum by powder injection. Steel Research **1988**, *59*, 263-268.

2.3. Deo, B.; Grieveson, P. Kinetics of desulphurization of molten pig iron. Steel Research **1986**, *57*, 514-519.

2.4. Ohguchi, S.; Robertson, D.G.C.; Deo, Brahma; Grieveson, P.; Jeffes J.H.E. Simultaneous desulphurization and dephosphorisation of molten pig iron, Ironmaking and Steelmaking **1984**, *11*, 2O2-213.

2.5. Deo, B.; Boom, R. Injection metallurgy (Chapter 8), In *Fundamentals of steelmaking metallurgy*, Prentice Hall: London, 1992; 254-261.

2.6. Seshadri, V.; Silva, C.A.; Silva, I.A.; Kruger, P.V. A Kinetic model applied to the molten Pig iron desulphurization by Injection of Lime based powders. ISIJ international **1997**, *37* (1), 21-30.

2.7. Lingamaneni, R.K. Kinetic, Statistical, Fuzzy Logic and Artificial Intelligence Models of Hot Metal Desulphurization in Torpedoes. M.Tech Thesis, Dept. of Materials & Metallurgical Engineering, IIT Kanpur, India, July, 1999.

2.8. Sandburg, H. Desulphurization of hot metal. Iron and Steel making **1977**, *4* (5), 280-284.

2.9. Ohguchi, S.; Deo, B.; Robertson, D.G.C. Theoretical and laboratory studies on injection phenomena, In *Ladle Metallurgy Principles and Practices*, Fruehan, R.J., Ed., TMS-AIME , U.S.A., 1986; 67-78.

2.10. Dutta, A.; Hareesh, M.; Kalra, P.M.; Deo, B.; Boom, R. Adaptive neural net (ANN) models for desulphurization of hot metal and steel. Steel research **1994**, *65* (11), 466-471.

2.11. Rastogi, R.; Deb, K.; Deo, B.; Boom, R. Genetic adaptive search model of hot metal desulphurization. Steel research **1994**, *65* (11), 472-478.

2.12. Deo, B.; Bose, P.K.; Mehrotra, K.K. Models for predicting sulfur and phosphorous distribution ratios in oxygen steelmaking. Trans. IIM **1988**, *41*, 475-479.

2.13. Deo, B. Some observations on the use of exotic diluents for hot metal desulphurization. Trans. IIM **1988**, *41*, 99-1O1.

2.14. Deo, B. Desulphurization of high silicon molten pig iron with lime based fluxes. Trans. IIM, **1988**, *41*, 6O1-6O9.

2.15. Jongejans, R.A.V.; Deo, B.; Unen, van G.; Boom, R.; Kinetics of permanent and transitory reactions during desulphurization in 300 ton torpedoes at

Hoogovens IJmuiden. Proc. Int. Steel Ninetees symposium, Jamshedpur, 1991; IIM Calcutta Pub., 1991; 3-10.

2.16. Deo, B.; Gandhi, S.; Rastogi, R.; Unen van G.; Boom, R. Theoretical and practical aspects of desulphurization in 400 ton torpedoes. Trans. IIM **1995**, *48,* 441-446.

2.17. Deo, B.; Singh, S.; Chandra, P.; Fluid flow and mass transfer in simultaneous mixing separation and teeming (SIMSET) reactor. Steel Research **1989**, *60*, 12-18.

2.18. Wei, J.-H.; Zhu S.-J.;Yu, N.-W. A Kinetic model of desulphurization by powder injection and blowing in RH Refining of molten Steel. In *Materials Processing in the Computer Age III,* TMS Annual Meeting & Exhibition, Nashville, Tennessee, March 12-March 15, 2000, *Voller, V. R.., Henein H.* Eds.; TMS Publications: 2000, pp. 135-146.

2.19. Gitterle, W.; Hot metal desulphurization – an important step in the production of high quality steel. In *Asia Steel International Conference – 2003*, Jamshedpur, India, April 9-April 12, 2003, Mukherjee, T, Dhillon A. S. Eds.; 2003, pp: 1.h.2.1-1.h.2.4.

2.20. Lischka, H.; Features of high efficient hot metal desulphurization. In *Asia Steel International Conference – 2003*, Jamshedpur, India, April 9-April 12, 2003, Mukherjee, T, Dhillon A. S. Eds.; 2003, pp: 1.h.3.1-1.h.3.3.

2.21. Alfred, E.; Heinz, V. B.; Recent progress in internal hot metal desulphurization. In *Asia Steel International Conference – 2003*, Jamshedpur, India, April 9-April 12, 2003, Mukherjee, T, Dhillon A. S. Eds.; 2003, pp: 1.h.4.1-1.h.4.7.

2.22. Deb, K. *Multi-objective Optimization Using Evolutionary Algorithms*; John Wiley & Sons: New York, 2001.

3.1. Choh, T., Inouye, M. "The Rate of Oxygen Absorption of Liquid Iron". ISIJ, **1980**, Vol. 20, pp. 768-775.

3.2. Iwata, K., Choh, T., Inouye, M. "A Model Experiment on the Gas Entrainment with Pouring Liquid Steel Stream". ISIJ, **1983**, Vol. 23, pp. 218-227.

3.3. Choh, T., Iwata, K., Inouye, M. "Estimation of Oxygen and Nitrogen Absorption of Liquid Steel during Tapping from Converter". ISIJ, **1983**, Vol. 23, pp. 680-689.

3.4. Ghosh, A., Gas Absorption during Tapping and Teeming from Surrounding Atmosphere (Chapter 8), In *Secondary Steelmaking Principles and Applications*, CRC Press, New York, 2001; pp. 225-229.

3.5. Deo, B.; Boom, Kinetics of Oxidation of Disolved Aluminum by Carried Over Slag in an Argon-Stirred Ladle (Chapter 7), In *Fundamentals of steelmaking metallurgy*, Prentice Hall: London, 1992; 254-261.

3.6. Misra, S, Fruehan, R. J. "Nitrogen Pickup during Tapping of Liquid Steel", AISTech Proceedings, **2004**, Vol. I, pp. 1057-1069.

3.7. Lindborg U., Torssell K. "A Collision Model for the Growth and Seperation of Deoxidation Products". Transactions of the Metallurgical Society of AMIE, **1968**, Vol. 242, pp. 94–242.

3.8. Iyengar R. K., Philbrook W. O. "A Mathematical Model to Predict the Growth and Elimination of Inclusions in Liquid steel Stirred by Natural Convection". Metallurgical Transactions, **1972**, Vol. 3, pp. 1823–1830.

3.9. Smoluchoski, M. V., Physik Z., **1916**, Vol. 17, pp. 585 – 599.

3.10. Saffman P. G., Turner J. S. "On the Collision of drops in Turbulent Clouds". J. Fluid Mech., **1956**, Vol. 1, pp. 16 – 30.

3.11. Langmuir I.: J. Meteorol., **1948**, Vol. 5, pp. 172 -192.

3.12. Fuchs N. A. "The Mechanics of Aerosols". Pergamon Press, New York, 1964.

3.13. Engh T. A., Lindskog N. "A Fluid Mechanical Model of Inclusion Removal", Scandinavian Journal of Metallurgy, **1975**, Vol. 4, pp. 49 – 58.

3.14. Söder M. "Growth and Removal of Inclusions During Ladle Stirring", Licentiate Thesis, 2001, Dept. of Materials Science and Engineering, Royal Institute of Technology, Stockholm.

3.15. Miki Y., Thomas B. G. "Modelling of Incluson Removal in Tundish". Metallurgical and Materials Transactions, **1999**, Vol. 30B, pp. 639 – 654.

3.16. Zhang L., Tanighuchi S., Cai K. "Fluid Flow and Inclusion Removal in Continuous Casting Tundish". Metallurgical and Materials Transactions, **2000**, Vol. 31B, pp. 253 – 266.

Appendix-A

Optimization of computation time by genetic algorithm

The usability a model in an industry is depends on the computation time required for execution of the model. It has been found, in this study, that at the beginning (say for time less than 20 minutes) the total number size of inclusions are less, and for higher holding time (say more than 45 minutes) that is large. The size range and the corresponding number of inclusions present in the bath for different holding times, as predicted by the model, are presented in Table 3.7.

Table 3.7: Number of size range present at different time

Time, min	No. of sizes (n)
2	8
5	12
10	19
20	37
30	70
45	200
60	751

If a large size range is assumed from the beginning of the calculation, the computation is extremely slow, even for 20 minutes holding time. To reduce the computation time linear regression and genetic algorithm has been applied separately. A linear regression model has very high R^2 value (R^2= 0.99). It can be seen from Fig. 3.27, linear regression gives a closer result to the data shown in Table 3.7. The linear regression model, for some time step, predicting lesser size range than that of the model (for example 2nd minute, 30th minute) as shown in the Fig. 3.27. Therefore, it

introduces computational errors at different time steps as the predictions may lesser than that of the model. Optimization by genetic algorithm (G.A.) gives better result. The optimization technique with respect to the data, given at the Table 3.7, is described below

It is assumed that the size range is follows a 3rd degree polynomial function

$F(x) = A\,t^3 + B\,t^2 + C\,t + D.$

Where, A, B, C, D are the constants and needed to be find out by G.A, t is time, and n is the number of sizes at different time steps as calculated by the model. Predicted F(x) should be maintain the tolerance with the data given by the model, n,

i.e.; $F(x) > n$

For providing sufficient room over n, the constraint has been redefined as

$F(x) > n + \sqrt{5}\,t$

Therefore, the single objective optimization problem is as follows

Minimize $F(x) = A\,t^3 + B\,t^2 + C\,t + D$

Subjected to: $F(x) > n + \sqrt{5}\,t$

Optimization of the function F(x) by genetic algorithm has been done by using a GA code available at the website of Kanpur Genetic Algorithm Laboratory (KANGAL). The different GA parameters are given below

Number of generations is 5000, population size is 300, cross over probability is 0.8, mutation probability is 0.2, distribution index for SBX is 2, and distribution index for mutation is 100

The values of the constants as given by GA are A = 0.01, B = - 0.57, C = 12.25, D = 5.317. The prediction of number of size ranges of inclusions is shown in Fig. 3.27.

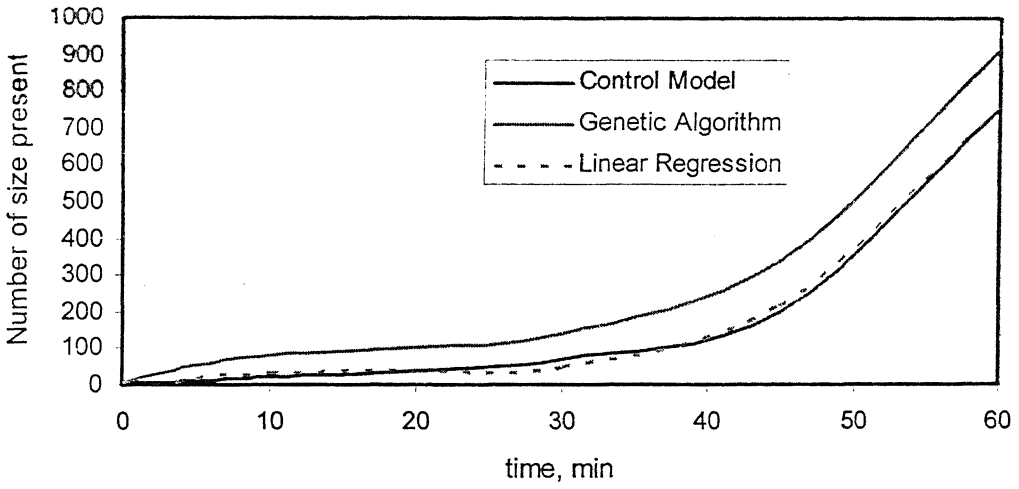

Fig 3.27: Comparison of predictions by both linear regression and genetic algorithm for the prediction of number of size range of inclusions

The comparison of predictions by both linear regression and genetic algorithm is shown in Fig. 3.27. From Fig. 3.27, it can be seen that by using genetic algorithm the number of size range is always above the required number of size range, predicted by the model, at different time steps. For the first 20 minutes of holding time, the number of size range is small, so if GA predicts 50 more size ranges then it will not affect the computation time much. Linear regression, sometimes, predicts lesser number of size ranges, and as discussed earlier that introduces calculation error. Thus, it can be concluded that by introducing some tolerance, the chances of error is reduced.